SISSA
Scuola Internazionale Superiore di Studi Avanzati

Neuroscience Area – PhD course in Neurobiology

Functional Profiling of Olfactory Sensory Neurons: Electrophysiological Characterization of Human Olfactory Epithelium and Maturation-Dependent Changes in Mouse Neuronal Excitability

Candidate: Chiara Ricci

Supervisor: Prof. Anna Menini

Academic Year 2025-26

TABLE OF CONTENTS

ABSTRACT

The olfactory system is crucial for the detection of chemical cues from the environment, allowing species survival. Olfactory sensory neurons (OSNs) within the olfactory epithelium (OE) are responsible for odorant detection and signal transmission to the brain. To investigate olfaction, rodents, along with other species such as amphibians and fishes, have been extensively used as laboratory models.

In the first part of this thesis, we provided the first electrophysiological characterization of human OSNs. Current knowledge about human OE is primarily confined to its morphology and molecular profile. However, little is known about the functional properties of human OSNs and supporting cells. We obtained acute slices of human OE from nasal biopsies and demonstrated their viability for whole-cell patch-clamp recordings. We measured voltage-gated currents from both OSNs and supporting cells in voltage-clamp configuration. Current-clamp protocols allowed us to assess the excitability of OSNs, which exhibited diverse firing patterns. Moreover, we demonstrated that these acute slices are also feasible for studying olfactory transduction, as we obtained the first electrophysiological responses of human OSNs upon odorant stimulation. Stimulation with a phosphodiesterase inhibitor elicited neuronal inward currents and action potentials, providing evidence that cyclic adenosine monophosphate (cAMP) is involved in the transduction pathway of human olfaction.

In the second part of the thesis, we investigated immature OSNs from the mouse OE. The OE has the capability to continuously regenerate throughout life. To better characterize epithelial regeneration, a deeper knowledge of immature OSNs is required. While gene remodelling and morphological rearrangements are well established, changes in electrophysiological properties across maturation, remain largely unexplored. Using an electrophysiological approach, we explored the intrinsic properties of immature OSNs. Through loose-patch recordings, we demonstrated that immature OSNs are already endowed with a spontaneous activity. Current-clamp experiments showed that these neurons are excitable, although displaying lower excitability and slower action potential kinetics compared to mature OSNs. Both electrophysiological and transcriptomic analyses revealed differences in voltage-gated currents along development. Focusing on voltage-gated Na^+ and K^+ channels, we found the emergence of tetrodotoxin-resistant Na^+ currents and transient A-type K^+ currents when neurons become mature, likely influencing changes in firing behaviour.

Altogether, these findings provide a comprehensive electrophysiological characterization of human OSNs, contributing to a deeper understanding of olfactory mechanisms in humans, and

expand the current knowledge of OSN functional maturation through the functional description of immature OSNs in a mouse model.

LIST OF ABBREVIATIONS

4-AP	4-aminopyridine
ACIII	Adenylyl cyclase III
AOB	Accessory olfactory bulb
AP	Action potential
Ascl1	Achaete-scute homolog 1
ATP	Adenosine triphosphate
CaM	Calmodulin
CaMKII	Ca^{2+}/calmodulin-dependent protein kinase II
cAMP	Cyclic adenosine monophosphate
Ca_v	Voltage-gated calcium channel
CNG	Cyclic nucleotide–gated ion channel
CNS	Central nervous system
Cxcr4	C-X-C chemokine receptor type 4
EOG	Electro-olfactogram
Gap43	Growth-associated protein 43
GBC	Globose basal cell
GFP	Green fluorescent protein
GPCR	G protein coupled receptor
Gγ8	G protein γ-subunit 8
HBC	Horizontal basal cell
INP	Immediate neuronal precursor
KO	Knockout
K_v	Voltage-gated potassium channel
MOB	Main olfactory bulb
MuHV-4	Murid Herpesvirus-4
Na_v	Voltage-gated sodium channel
NCKX4	Na^+-Ca^{2+} exchanger 4
Neurog1	Neurogenin1
NKCC1	Na^+-K^+-Cl^- cotransporter 1
OB	Olfactory bulb
OE	Olfactory epithelium
OMP	Olfactory marker protein
OR	Olfactory receptor

OSN	Olfactory sensory neuron
PDE1C2	Phosphodiesterase 1C isoform 2
PKA	Protein kinase A
PKC	Protein kinase C
RE	Respiratory epithelium
RT-PCR	Real Time PCR
SARS-CoV-2	Severe Acute Respiratory Syndrome Coronavirus 2
scRNA-seq	single-cell RNA-sequencing
TEA	Tetraethylammonium
TMEM16B	Transmembrane protein member 16B (or anoctamin-2)
TTX	Tetrodotoxin
VNO	Vomeronasal organ

1. INTRODUCTION

1.1 The olfactory system

Gaining information from the external environment is crucial for species survival: the detection of chemical cues supports essential functions such as locating food, identifying mates for reproduction, and avoiding threats like predators and toxic substances (Mombaerts, 2004; Su *et al.*, 2009; Manzini *et al.*, 2022). To perform these tasks, terrestrial animals have evolved highly sophisticated chemo-sensory systems, primarily divided into gustatory and olfactory systems. The gustatory system is responsible for detecting chemicals with nutritive values or avoiding poisonous bitter-tasting compounds (Gutierrez & Simon, 2021); whereas the olfactory system is specialized in the selective recognition of two major classes of stimuli: odorants and pheromones (Mombaerts, 2004; Manzini *et al.*, 2022).

Odorants are volatile, low molecular weight molecules with a highly heterogenous chemical repertoire. These include aliphatic and aromatic structures with diverse functional groups, such as aldehydes, esters, alcohols, amines and thiols (Firestein, 2001; Touhara & Vosshall, 2009). On the other hand, pheromones are defined as molecules secreted by an individual, capable of eliciting a reaction in another individual of the same species (Tirindelli *et al.*, 2009). Given the vast diversity of detectable compounds, the olfactory system is endowed with a remarkable discriminatory power, being capable of distinguishing even between different pairs of enantiomers (Laska & Shepherd, 2007). It also exhibits a great sensitivity across a wide range of concentrations, from nanomolar to millimolar levels (Mombaerts, 2004; Manzini *et al.*, 2022).

In rodents, two primary olfactory substructures are located within the nasal cavity: the olfactory epithelium (OE), for detecting odorants and the vomeronasal organ (VNO), responsible for pheromone detection (Ferrero & Liberles, 2010) (Figure 1). In addition, two other spatially segregated sensory regions have been identified: the septal organ and the Grueneberg ganglion. The septal organ is also known as organ of Masera, since it was first described in detail by Rodolfo-Masera in 1943 (Rodolfo-Masera, 1943). It is located at the ventral base of the nasal septum, and it is thought to support odorant detection with high sensitivity, although its function is still debated (Munger *et al.*, 2009; Enomoto *et al.*, 2021). The Grueneberg ganglion is organized in a cluster of neurons at the dorsal tip of the nasal cavity. It serves as a dual sensory organ, sensing alarm pheromones and predator-related odorants, but also responding to cool temperatures (Fleischer, 2021). The presence of multiple olfactory subsystems offers a great advantage by enhancing the overall detection capacity of the vast array of environmental stimuli.

Peripheral information is conveyed to the olfactory bulb (OB), which represents the first relay station within the central nervous system (CNS). Neurons from the OE, septal organ and Grueneberg ganglion project to the main olfactory bulb (MOB), while axons from the VNO target the accessory olfactory bulb (AOB), which lies dorsally to the MOB (Munger *et al.*, 2009; Manzini *et al.*, 2022) (Figure 1).

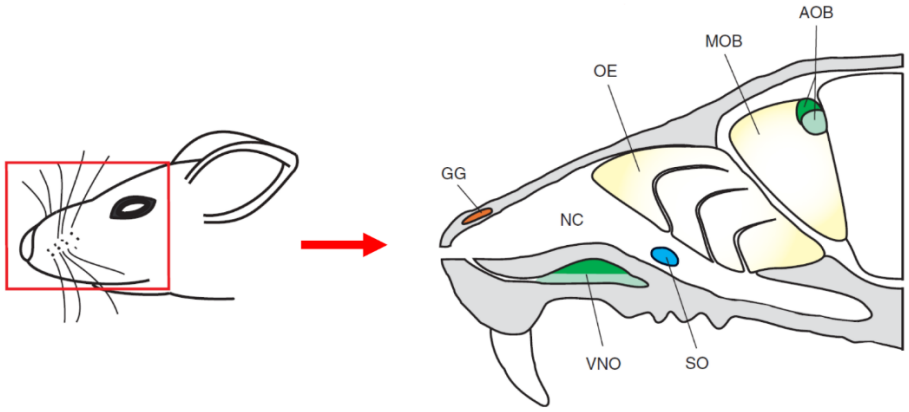

Figure 1. Anatomical organization of mouse olfactory system.
The nasal cavity (NC) of the mouse hosts the principal elements of the olfactory system: the OE lining turbinates, cartilagineous structures that increase the surface area; the VNO on the palate roof; the septal organ (SO) and the Grueneberg ganglion (GG) on the dorsal tip. Sensory neurons from the OE, SO and GG project to the MOB; whereas the AOB receives inputs from the VNO (Adapted from Ferrero & Liberles, 2010).

Chemosensory information is then decoded in higher brain centers, which are highly interconnected. The OB sends axons to the olfactory cortex, which includes regions of the anterior olfactory nucleus, the olfactory tubercle, the piriform cortex and entorhinal cortex. In addition, the OB directly innervates the amygdala. Further cognitive processing occurs through indirect connections with the hippocampus, involved in memory and learning, and hypothalamus, which regulates behavioural responses (Ma, 2007; Manzini *et al.*, 2022).

1.2 The olfactory epithelium (OE)

The OE is the primary site for the initial odorant detection, necessary for translating chemical signals into electrical ones that ultimately give rise to perception. In rodents, the OE covers the majority of the nasal cavity, lining the septum in the most dorso-caudal region (Alvites *et al.*, 2018); while the respiratory epithelium (RE) occupies almost 46% of the nasal surface, in the antero-rostral part of the nostrils. The ciliated cells of the RE are responsible for purifying and heating the air rich in odorants directed towards the OE. The boundary between the two epithelia is not strictly defined: a transition zone lies between the two, with a mosaic of mixed cell types.

The OE can be histologically identified by its greater thickness and the presence of Bowman's glands, which produce mucous secretions (Alvites *et al.*, 2018) (Figure 2A, B).

The first accurate description of the vertebrate OE was provided by Schultze in 1856 (Doty, 2003), who identified its main cellular components: olfactory sensory neurons (OSNs), basal cells, sustentacular and microvillar cells (Figure 2B). OSNs are the primary functional element of the tissue, since they are responsible for odorant detection and signal transmission. These are bipolar neurons with a single dendrite that reaches the epithelial surface and terminates in a knob-like structure from which cilia protrude (Schild & Restrepo, 1998). These cilia are the site of olfactory receptors (ORs) that directly interact with odorants dissolved in the lumen, and of the protein machinery involved in transduction of the odour signal. On the basal side, a single unbranched axon penetrates the basal lamina and projects to the OB in spherical structures called glomeruli (Figure 2B, C). Each OSN expresses only one type of OR and cells expressing the same receptor project to the same glomerulus. The concepts of 'one neuron-one receptor' and 'one glomerulus-one OR' represent the central dogma of olfaction (Mombaerts *et al.*, 1996; Axel, 2005; Buck, 2005; Fang & Yu, 2024) (Figure 2C). However, the one axon-one glomerulus wiring logic is not conserved across all vertebrates. In amphibians, for example, axons of OSNs regularly bifurcate and innervate multiple glomeruli, independently on the developmental stage of the animal (Weiss *et al.*, 2020).

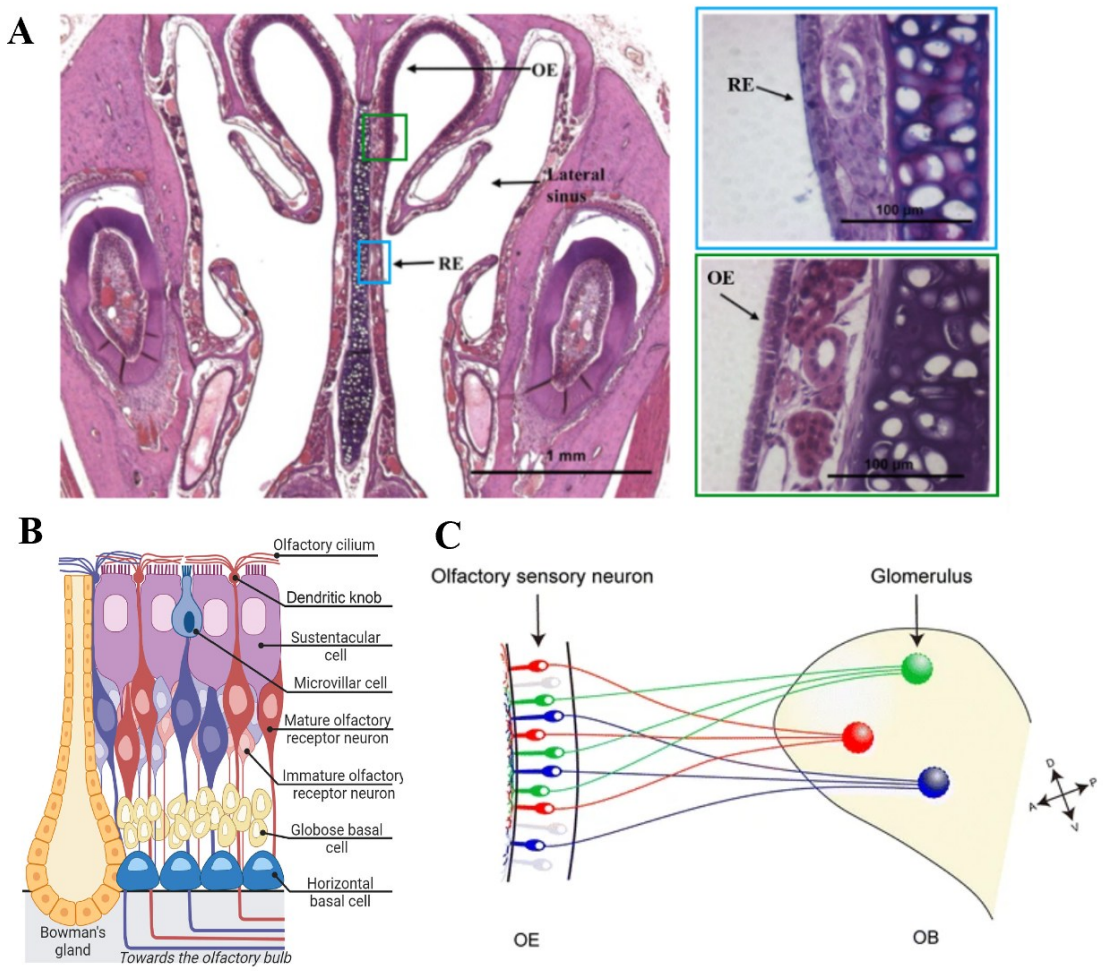

Figure 2. Structural and functional organization of the OE.

(A) Coronal section of the mouse nasal cavity stained with hematoxylin and eosin, showing the OE in the dorsal part and the RE in the ventral region. Insets on the right highlight the increased thickness of OE (green square, bottom) compared to the RE (blue square, top). **(B)** Schematic representation of the cellular organization within the OE. The Bowman's gland, which produces mucus, serves as landmark for OE recognition. OSNs originate from basal cells and form a pseudostratified layer, progressing from immature to mature stages. Mature OSNs face the mucus layer with their olfactory cilia for accessing odorants, while their axons project towards the olfactory bulb. Sustentacular and microvillar cells constitute the non-neuronal epithelial components. **(C)** Each OSN expresses a single OR in a monoallelic manner (represented by different colours). Neurons expressing the same receptor type converge their axons onto a common glomerulus within the OB. (Adapted from Hilliard *et al.*, 2008; Takeuchi & Sakano, 2014; Dibattista *et al.*, 2021).

Direct exposure of OSNs to the external environment, while necessary for accessing odorants, also renders them more vulnerable to damage than any other neuron. However, OSNs can regenerate throughout life, a distinctive feature that makes them almost unique among neurons (McClintock *et al.*, 2020). The process of neurogenesis is driven by basal cells, stem cells located at the very base of the lamina that can differentiate into neurons even during adulthood. The pseudostratified architecture reflects this continuous turnover with less mature cells located basally and the most mature neurons found more apically (Figure 2B) (McClintock *et al.*, 2020).

The maintenance of the tissue is also guaranteed by the other cellular components. Supporting cells, also named sustentacular, are glial-like columnar cells that form a monolayer at the apical surface of the epithelium, facing the mucus with several microvilli, while their basal processes anchor to the basal lamina (Doty, 2003). These cells share functional features of both epithelial and glial cells (Hegg *et al.*, 2009). Surrounding neurons, they maintain the structural integrity of the neuroepithelium: loss of supporting cells may indeed cause desquamation or malfunctioning of the entire epithelium, leading to complete anosmia, as demonstrated in cases of infection from SARS-CoV-2 in humans (Fodoulian *et al.*, 2020) and hamsters (Bryche *et al.*, 2020) or Murid Herpesvirus-4 (MuHV-4) in mice (Milho *et al.*, 2012). Moreover, sustentacular cells provide metabolic support: they control water and salt balance of the mucus (Breipohl *et al.*, 1974; Menco *et al.*, 1998), contribute to the detoxification of xenobiotic compounds (Bannister & Dodson, 1992) and participate in the phagocytosis of dead OSNs (Suzuki *et al.*, 1996). Additionally, they secrete neurotrophins and neuromodulators such as insulin and ATP, participating in the epithelial physiology (Lacroix *et al.*, 2008; Hayoz *et al.*, 2012).

Microvillar cells constitute a minor population of cells characterized by the presence of apical microvilli thicker than those of supporting cells (Carr *et al.*, 1991). These cells present high heterogeneity in microvillar thickness, length and diameter (Menco & Jackson, 1997). Microvillar cells contribute to the regulation of detoxification processes by detecting xenobiotic substances and activating neighbouring cells (Lin *et al.*, 2008; Genovese & Tizzano, 2018). Moreover, they can act as modulators of neuronal proliferation through the release of neuropeptide Y (Montani *et al.*, 2006).

1.3 Postnatal neurogenesis of olfactory sensory neurons

Neurogenesis has been long believed to occur only during embryonal development. However, in 1960s it was demonstrated that new neurons can be generated postnatally in both rat hippocampus and OB (Altman & Das, 1965; Altman, 1969). The first evidence of adult neurogenesis in rat and mouse OE came in the late 1970s (Harding *et al.*, 1977; Graziadei & Monti Graziadei, 1978). If adult neurogenesis within the CNS mainly serves the neural plasticity function, for the olfactory system it becomes fundamental in guaranteeing robust regeneration and repair due to the vulnerability of the tissue (McClintock *et al.*, 2020).

The majority of OSNs typically has a 1-3 month lifespan (Mackay-Sim & Kittel, 1991; Holl, 2018; Liberia *et al.*, 2019). However, their lifespan can vary considerably, depending on both extrinsic and intrinsic factors. The external environment can introduce stressful agents but also provide sensory stimuli. Indeed, odorant stimulation has been shown to enhance the survival of

OSNs expressing the cognate OR (Watt *et al.*, 2004; Santoro & Dulac, 2012). Age is another key determinant: both survival likelihood and proliferation rate are higher in young postnatal mice and gradually decline with aging (Loo *et al.*, 1996; Gaun *et al.*, 2022).

1.3.1 Maturation of OSNs within the OE

In the healthy OE, neurogenesis is sustained by globose basal cells (GBCs), multipotent progenitors that undergo continuous mitotic division to generate Achaete-scute homolog 1 (Ascl1)-expressing cells, committed to become neurons. Following injury, epithelial regeneration is instead driven by horizontal basal cells (HBCs), a quiescent population located in the most basal region. Under normal conditions, they serve as a reserve pool of stem cells and contribute only minimally to OSN production (McClintock *et al.*, 2020). Neurally fated cells transit through an immediate neuronal precursor (INP) stage, marked by neurogenin1 (Neurog1), before differentiating into nascent OSNs (Fletcher *et al.*, 2017) (Figures 2B, 3A).
After the last mitotic division, OSNs require approximately 7-10 days to complete the maturation process (Rodriguez-Gil *et al.*, 2015; Liberia *et al.*, 2019). Throughout lineage progression, cells within the OE undergo apical migration accompanied by dynamic changes in phenotype and gene expression, reflecting the intrinsic program of OSN differentiation (Liberia *et al.*, 2019) (Figure 3B). Nascent OSNs initially extend a basal process and a short apical neurite, a process mediated by the gene C-X-C chemokine receptor type 4 (Cxcr4). As differentiation proceeds, these neurons reach the state of immature OSN, becoming $Cxcr4^-$ and expressing both the G protein γ-subunit 8 (Gγ8), involved in signal transduction (Ryba & Tirindelli, 1995; Tirindelli & Ryba, 1996), and the growth-associated protein 43 (Gap43), implicated in axonal growth (Verhaagen *et al.*, 1989; Liberia *et al.*, 2019). Immature OSNs develop a primordial axon and form exuberant synapses within the OB (Marcucci *et al.*, 2011). On the other side of the cell, short dendrites reach the apical surface forming a knob with incompletely elongated cilia. This stage constitutes the longest phase of maturation, as it involves extensive genetic reprogramming and morphological remodeling before terminal differentiation (McClintock *et al.*, 2020). As genes are gradually refined, intermediate states arise in which cells co-express markers of both immature and mature phenotypes. During this transition, a subset of OSNs begins to express olfactory marker protein (OMP) while still expressing Gap43 and Gγ8 (Cheetham *et al.*, 2016; Huang *et al.*, 2022). Gap43 and Gγ8 are subsequently downregulated, and OSNs reach maturity, characterized by an OMP^+, and $Gap43^-$ and $G\gamma8^-$ profile (Miragall & Graziadei, 1982; Rodriguez-Gil *et al.*, 2015; Hanchate *et al.*, 2015; Liberia *et al.*, 2019) (Figure 3A, B).

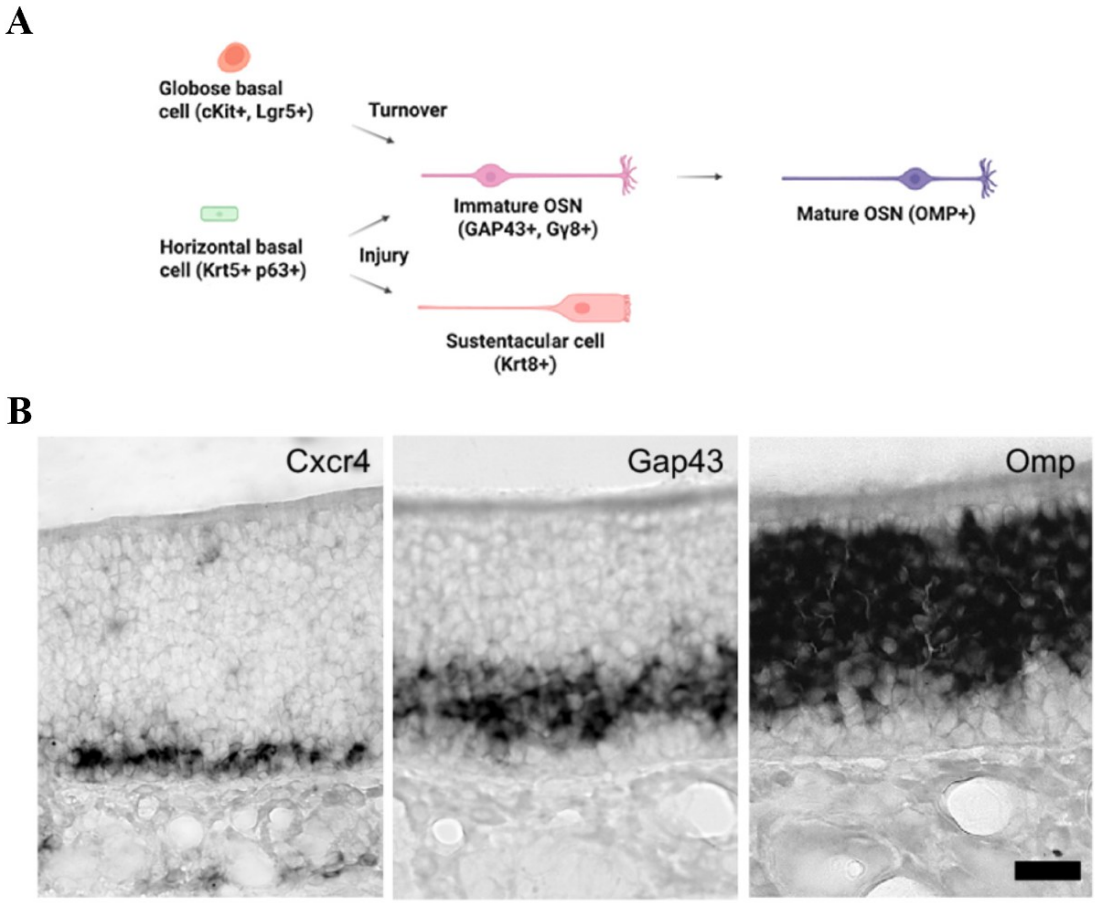

Figure 3. Trajectory of OSNs differentiation.

(A) Developmental lineage of OSNs. Globose basal cells sustain neuronal turnover by generating new OSNs that progress through a prolonged immature stage before reaching maturity. Horizontal basal cells are generally quiescent but can undergo differentiation upon injuries to replace both OSNs and sustentacular cells. Representative stage-specific marker genes are indicated below each cell type. cKit, Type III receptor tyrosine kinase; Lgr5, Leucine-rich repeat-containing G protein coupled receptor 5; Krt, Keratin. **(B)** In situ hybridization for Cxcr4, Gap43, and Omp mRNAs shows the location within the epithelium of nascent, immature and mature OSNs respectively. Scale bar: 20 µm (Adapted from McClintock *et al.*, 2020; Gregory *et al.*, 2025).

The crucial step in the transition from immature to mature OSNs is the stochastic selection of a single OR gene: low levels of multiple OR transcripts are detected in immature OSNs until one single receptor is chosen from the available pool (Hanchate *et al.*, 2015; Tan *et al.*, 2015; Saraiva *et al.*, 2015; Yusuf & Monahan, 2024) (Figure 4). OSNs that fail to stably express a single OR do not reach maturity. Conversely, OSNs that successfully stabilize OR expression achieve maturity, completing ciliogenesis, assembling the entire odorant transduction machinery and establishing synaptic connections within the OB (McClintock *et al.*, 2020).

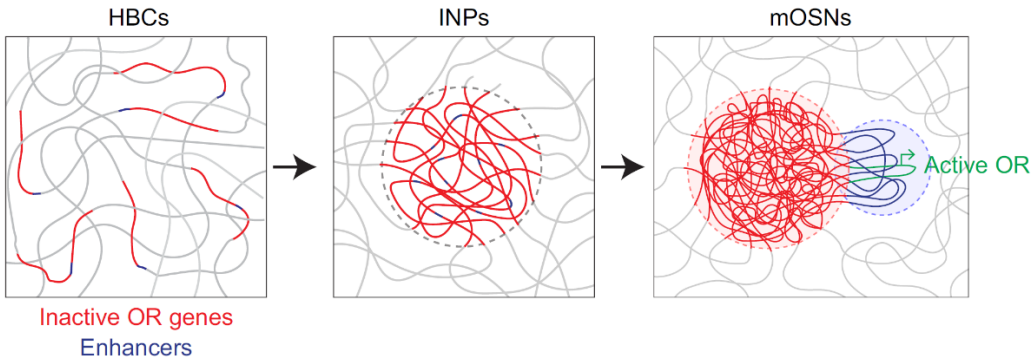

Figure 4. Rearrangement of OR genes.

An epigenetic program remodels OR gene organization within the nucleus. OR gene expression is regulated through interactions between gene clusters and enhancers (blue lines). These interactions are absent in the HBCs but begin to emerge during differentiation into INPs, although still weak. Transition to single expression of OR in mature OSNs (mOSNs) likely corresponds to the stochastic assembly of enhancers into an activating structure, the 'enhancer hub' (blue area), which drives the transcription of the selected OR gene (green), extruded from the heterochromatin compartment. Non-chosen OR genes are, in turn, transcriptionally silenced (Yusuf & Monahan, 2024).

1.3.2 Glomerular map formation within the olfactory bulb (OB)

During development, OSNs must establish a sensory map. Their axons segregate into distinct glomeruli according to the specific OR they express, thereby conveying odour information through distinct glomerular activation patterns (Ressler *et al.*, 1993; Vassar *et al.*, 1993; Sakano, 2020). Glomeruli are spherical structures within the OB where olfactory sensory afferents form excitatory synapses primarily with mitral and tufted cells (Mombaerts, 2004; Nagayama *et al.*, 2014; Redolfi & Lodovichi, 2021). In mice, the formation and refinement of the glomerular map occurs during embryogenesis and early postnatal days (Gogos *et al.*, 2000), although timings vary depending on the identity of expressed OR (Cheetham & Belluscio, 2014; Redolfi & Lodovichi, 2021). The initial glomerular positioning along the antero-posterior axis is mainly driven by agonist-independent receptor activity. Specifically, it relies on molecular gradients regulated by cyclic adenosine monophosphate (cAMP) levels generated through the activation of the G_s protein coupled to the receptors (Dibattista *et al.*, 2021; Fang & Yu, 2024) (Figure 5A). Glomerular segregation is then refined by the OR-driven neuronal activity: OSNs expressing different ORs exhibit specific firing patterns (Reisert, 2010; Connelly *et al.*, 2013; Nakashima *et al.*, 2019), which, in turn, regulate the expression of axon guidance molecules. These molecules promote either attractive or repulsive interactions among axons expressing the same or different OR, respectively (Nakashima *et al.*, 2019; Sakano, 2020; Fang & Yu, 2024) (Figure 5B).

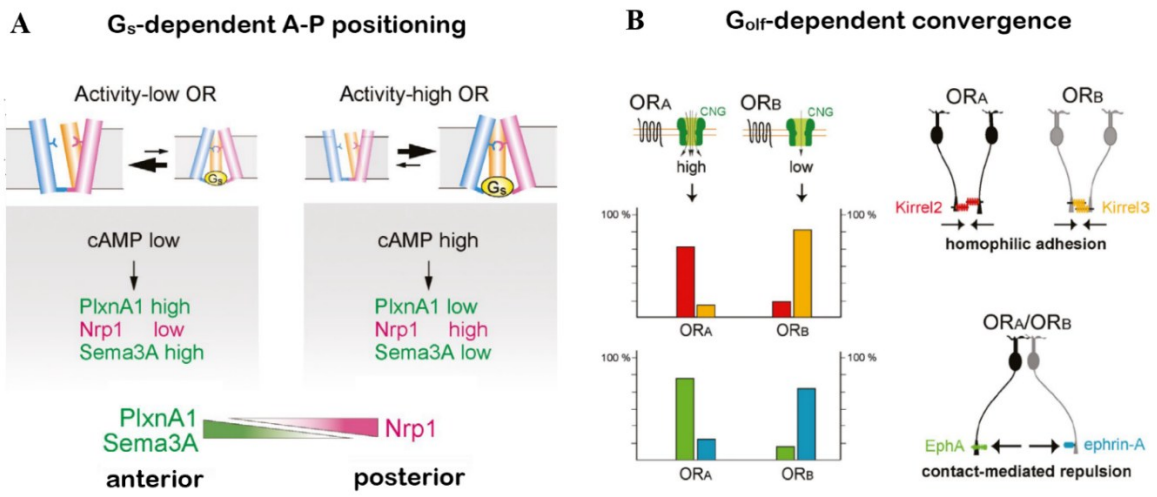

Figure 5. Glomerular segregation is regulated by OR-specific activity.

(A) When neurons are still immature, they express ORs coupled to the G_s protein. ORs undergo conformational changes among active and inactive forms. Activation of G_s induces cAMP production, that will act as a second messenger for transcription of targeting molecules, such as Plexin Al (PlxnA1) and Semaphorin 3A (Sema3A) that drive the anterior positioning and Neuropilin 1 (Nrp1), whose expression is higher in the posterior OSNs. **(B)** In mature OSNs the baseline activity of ORs is coupled to the G_{olf}-dependent signaling, which results in cyclic nucleotide–gated (CNG) ion channel activation. High-activity ORs (OR_A) promote expression of Kirrel2 (red) and EphA (green), whereas in OSN with low-activity ORs (OR_B), Kirrel3 (yellow) and ephrin-A (blue) are highly expressed. Kirrel2/3 are responsible for homophilic adhesion, whereas EphA/ephrin-A mediate heterotypic repulsion among OSNs expressing different receptors. (Adapted from Sakano, 2020).

While OR identity provides cues for glomerular formation, spontaneous activity is essential for the refinement and maintenance of the circuitry. This has been demonstrated using Kir2.1 transgenic mice, in which overexpression of the inward rectifying potassium channel Kir2.1 causes membrane hyperpolarization and reduced spontaneous firing. These mice exhibit broader and heterogeneous glomeruli innervation (Yu *et al.*, 2004; Lorenzon *et al.*, 2015), confirming the role of spontaneous activity in stabilizing synaptic connections.

The first postnatal week in mice is considered a critical period, characterized by heightened plasticity. Perturbations within this time window can disrupt axonal convergence but the system can recover. By contrast, alterations persisting beyond the critical period will result in permanent changes (Cheetham & Belluscio, 2014; Ma *et al.*, 2014; Redolfi & Lodovichi, 2021; Fang & Yu, 2024).

Once established, the projection patterns remain unchanged throughout life, despite the continuous neuronal turnover. Newborn OSNs are capable of targeting the right glomeruli preserving the fidelity of the glomerular map (Gogos *et al.*, 2000).

1.4 Characteristics of mature OSNs

Morphological and functional features of mature OSNs are delineated by complete formation of the two ends: the apical cilia, which contain all the proteins required for odorant detection and signal transduction, and the axonal compartment which is enriched in proteins that regulate ion flux, generate electrical responses and mediate signal transmission (McClintock *et al.*, 2020).

1.4.1 Odorant detection and transduction cascade

1.4.1.1 Odorant receptors (ORs)

The first identification of ORs was achieved in 1991, when Linda Buck and Richard Axel cloned for the first time 18 different members of this family (Buck & Axel, 1991); a discovery that earned them the Nobel Prize in 2004. ORs belong to one of the largest family within the G protein coupled receptors (GPCRs), encoded by a vast gene repertoire that varies across species: ~1,000 functional genes in mice and ~390 in humans (Malnic *et al.*, 2010; Barnes *et al.*, 2020). Each mature OSN exhibits monoallelic expression of a specific OR, ensuring production of only one type of OR protein. This mechanism increases the signal-to-noise ratio in odorant detection by preventing the expression of polymorphic alleles that encode ORs with differing specificities (Mombaerts, 2004). However, ORs transcripts are present even in immature OSNs, when Gap43 is expressed and OMP is still absent. In this immature stage, low levels of mRNA from multiple ORs can be detected (Iwema & Schwob, 2003; Nickell *et al.*, 2012; Rodriguez-Gil *et al.*, 2015; Hanchate *et al.*, 2015; Tan *et al.*, 2015), suggesting that immature OSNs may already be capable of odorant detection.

All the ORs share a seven-transmembrane domains structure. However, the transmembrane regions are relatively variable, with sequence similarity ranging from 40% to over 90% (Figure 6A). This variability likely contributes to the formation of diverse odorant-binding pockets, allowing the discrimination across the enormous repertoire of olfactory ligands (Firestein, 2001; Touhara & Vosshall, 2009). To maximize the detection capacity, ORs employ a combinatorial coding strategy: each odorant can be detected by more than one OR and, conversely, each OR can recognize several odorants. ORs capable of detecting a wide range of ligands are referred to as broadly tuned, while those selective for specific compounds are defined as narrowly tuned (Touhara & Vosshall, 2009).

Within the OE, ORs are expressed across different broad zones in a continuous and overlapping manner (Figure 6B). Within each zone, OSNs expressing a determined OR are randomly interspersed (Zapiec & Mombaerts, 2020). The spatial distribution correlates with the mucus solubility of the ligands, further optimizing odorant detection (Ruiz Tejada Segura *et al.*, 2022).

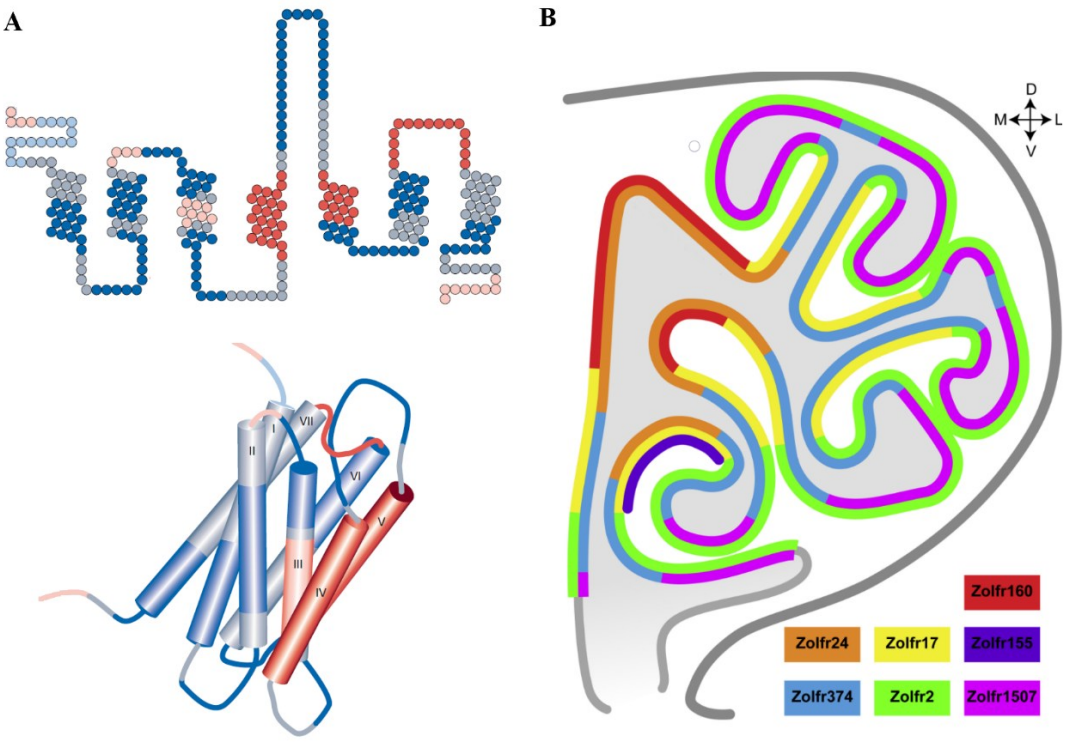

Figure 6. Schematic representation of OR structure and distribution.

(A) 2D (top) and 3D (bottom) schematic view of an OR. ORs are GPCRs composed by seven α-helical regions connected to each other by intracellular and extracellular loops. Comparison among ORs revealed many regions of variability, represented by the colour code (in blue the most conserved regions, in red the most variable ones). Numbers in the 3D model indicate the respective transmembrane regions. **(B)** Coronal section of OE with OR expression areas. Seven out of nine zones found by Zapiec and Mombaerts (2020) are represented by different colours. Zones listed below refer as Zolfr zones, with Z for zone and olfr number of a representative OR gene (e.g. Zolfr24 means that is the zone where the OR gene 24 (olfr24) is one of the most expressed). Importantly, Zolfr zones are not mutually exclusive, but highly overlapping (Adapted from Firestein, 2001; Zapiec & Mombaerts, 2020).

In mature OSNs, ORs couple to a heterotrimeric G-protein composed of an α-subunit G_{olf}, essential for mediating odorant signalling, together with the subunits β_1 and γ-13. Binding of an odorant to its receptor activates G_{olf}, which in turns initiates the adenylyl cyclase III (ACIII) pathway (Jones & Reed, 1989; Belluscio *et al.*, 1998; Li *et al.*, 2013; Boccaccio *et al.*, 2021) (Figure 7).

At earlier time points, when the neuron is still immature, the α-subunit G_s is expressed instead of G_{olf} (Jones & Reed, 1989; Nakashima *et al.*, 2013; Hanchate *et al.*, 2015). Similarly to G_{olf}, G_s mediates ORs signals and cAMP production, but its role has been related to axonal guidance and glomerular positioning rather than olfactory signalling (Nakashima *et al.*, 2013; Fang & Yu, 2024).

1.4.1.2 Transduction pathway

Activation of the protein G_{olf} triggers ACIII to convert adenosine triphosphate (ATP) in cAMP. The resulting increase in intracellular cAMP concentration causes the opening of cyclic nucleotide–gated (CNG) ion channels (Nakamura & Gold, 1987; Zufall *et al.*, 1994; Pifferi *et al.*, 2006). CNG channels are non-selective cation channels composed of two CNGA2 subunits, one CNGA4 and one CNGB1 subunit. Each subunit has six transmembrane domains with a binding site near the cytoplasmatic C-terminal, providing a total of four binding sites per channel. Channel opening occurs through an allosteric mechanism (Pifferi *et al.*, 2010). Lack of CNGA2 in knockout (KO) models results in complete anosmia, underlying the pivotal role of this protein for signal transduction (Brunet *et al.*, 1996; Kleene, 2008; Boccaccio *et al.*, 2021). Activation of CNG channels allows the conversion of the chemical signal to the electrical one: when open, CNG channels permit the flow of Na^+ and Ca^{2+} ions into the ciliary lumen resulting in membrane depolarization (Lowe & Gold, 1995; Pifferi *et al.*, 2006; Boccaccio *et al.*, 2021) (Figure 7).

Ca^{2+} entry through CNG channels further activates the Ca^{2+}-activated Cl^- channel TMEM16B (or anoctamin 2). TMEM16B belongs to the TMEM16 (transmembrane protein 16)/anoctamin family; it is a homodimer with ten transmembrane domains containing Ca^{2+}-binding sites and it is selectively permeable to anions (Stephan *et al.*, 2009; Pifferi *et al.*, 2009; Cenedese *et al.*, 2012; Pifferi, 2017; Dibattista *et al.*, 2024). TMEM16B was first localized within mature OSNs cilia and only later functionally characterized (Pifferi *et al.*, 2012; Dibattista *et al.*, 2017). Due to the activity of the Na^+-K^+-$2Cl^-$ (NKCC1) cotransporter, OSNs maintain an unusually high intracellular Cl^- concentration (Kaneko *et al.*, 2004; Reisert *et al.*, 2005). Therefore, TMEM16B activation causes Cl^- efflux, further depolarizing the membrane and triggering action potentials (APs) (Figure 7). Several studies have shown TMEM16B's role in amplifying the CNG response, since the Cl^- conductance accounts for more than the 80% of the total transduction current (Lowe & Gold, 1995; Reisert *et al.*, 2005; Boccaccio & Menini, 2007). Although TMEM16B KO mice are not completely anosmic (Billig *et al.*, 2011), they present impaired olfactory ability (Pietra *et al.*, 2016; Neureither *et al.*, 2017; Zak *et al.*, 2018). This channel is, therefore, fundamental in tuning odour coding: beyond amplification, TMEM16B limits odorant-evoked firing and shapes the response kinetics (Pietra *et al.*, 2016; Guarneri *et al.*, 2023; Reisert *et al.*, 2024).

Termination of the response depends on the closure of both CNG and TMEM16B channels, with Ca^{2+} serving as the central regulator of feedback inhibition. Formation of the Ca^{2+}-calmodulin (CaM) complex inhibits ACIII via the Ca^{2+}/calmodulin-dependent protein kinase II (CaMKII)

and activates the ciliary phosphodiesterase PDE1C, accelerating cAMP degradation (Boccaccio *et al.*, 2006). Additional buffering of cAMP is mediated by OMP (Nakashima *et al.*, 2020). On the other hand, closure of the TMEM16B channel is ensured by Ca^{2+} clearance through the K^+-dependent Na^+-Ca^{2+} exchanger 4 (NCKX4) (Stephan *et al.*, 2012) and mitochondrial uptake within the knob (Fluegge *et al.*, 2012) (Figure 7).

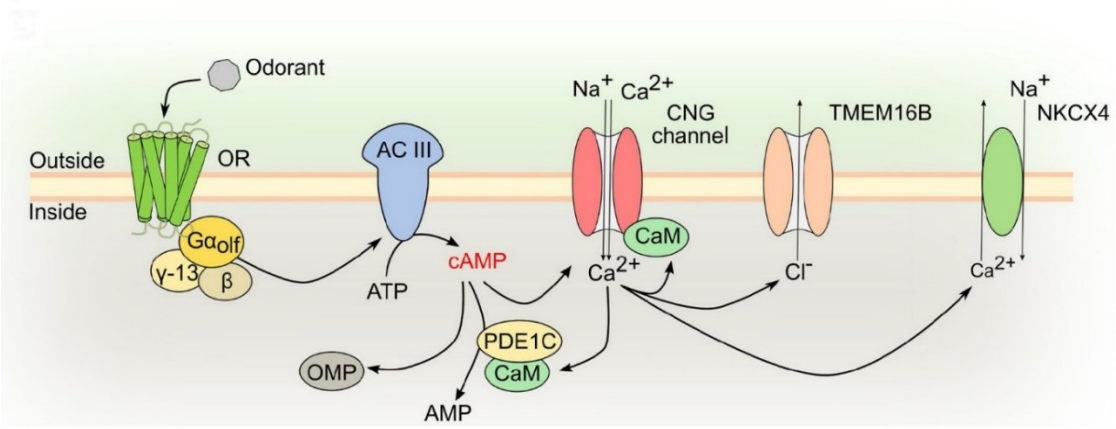

Figure 7. Transduction pathway in mature OSNs.

The transduction pathway is activated when an odorant binds to its specific receptor (OR). Activation of the coupled G-protein (G_{olf}) stimulates ACIII to produce cAMP. In response, CNG channels open, allowing Na^{2+} and Ca^{2+} influx. Ca^{2+} further activates the TMEM16B channel that permits Cl^- efflux. This cascade of events leads to action potential generation. The response is terminated by a series of negative feedbacks that will restore the initial ionic equilibrium (cAMP hydrolyzation by PDE1C, cAMP buffering by OMP and Ca^{2+} clearance through the NCKX4) (Boccaccio *et al.*, 2021).

Ca^{2+}-CaM modulation of CNG channels is thought to be the principal mechanism underlying fast adaptation in response to prolonged stimulation (Kurahashi & Menini, 1997), although recent evidence highlight a significant contribution from TMEM16B to this process (Guarneri *et al.*, 2023; Reisert *et al.*, 2024).

Several studies use elements of the transduction pathway, together with OMP expression, as markers to define mature OSNs (Nickell *et al.*, 2012; Hanchate *et al.*, 2015; Fletcher *et al.*, 2017). Whether immature OSNs rely on the same mechanisms remains unsolved. However, evidence shows that immature OSNs at later stages start to express components of the transduction cascade alongside ORs (Hanchate *et al.*, 2015). Furthermore, a recent study demonstrates that $G\gamma8^+$ OSNs can generate Ca^{2+} responses upon odorant stimulation and convey behaviourally relevant inputs to the OB (Huang *et al.*, 2022), suggesting that elements of a functional transduction cascade may already be present before completing maturation.

1.4.1.3 The olfactory marker protein (OMP)

The OMP is a cytoplasmatic protein expressed throughout OSNs, from the cilia to axonal endings. It was first described in 1972 by Margolis and later exclusively associated with mature OSNs, becoming widely used as a specific marker for maturation (Dibattista *et al.*, 2021). The first KO model was generated in 1996 (Buiakova *et al.*, 1996); followed by the OMP-GFP mouse strain in which OMP is replaced by the green fluorescent protein (GFP), enabling visualization of mature OSNs (Potter *et al.*, 2001). Electro-olfactogram (EOG) recordings from OMP-KO mice revealed that odorant responses display slower kinetics and impaired ability to respond to a second stimulus (Buiakova *et al.*, 1996). In agreement with this, subsequent works confirmed that absence of OMP prolongs both the onset and termination of the response (Reisert *et al.*, 2007; Dibattista & Reisert, 2016). Moreover, OMP-KO OSNs exhibit a reduced ability to generate reliable APs in response to high-frequency repetitive stimuli that mimic breathing (2 Hz) or sniffing (5 Hz). This deficit might arise from the delayed recovery of the response to the first stimulus, which prevents firing upon subsequent stimulations (Dibattista & Reisert, 2016; Nakashima *et al.*, 2020). Collectively, these findings highlight the relevance of OMP in sharpening OSNs sensitivity and contributing to the short-term protection against repetitive stimuli (Nakashima *et al.*, 2020).

Nakashima and colleagues (2020) showed that OMP modulates odorant responses by buffering intracellular cAMP. Upon odorant stimulation, OMP captures excess cAMP, preventing excessive overload of CNG channels (Figure 7). In this way, OMP acts as a low-pass filter, finely tuning the dynamic range of odorant responses (Nakashima *et al.*, 2020).

Spontaneous firing is also partially influenced by OMP through its modulation of cAMP levels. Although OMP knockout and heterozygous mice exhibit similar mean firing rates, they differ in the distributions of their firing patterns (Nakashima *et al.*, 2020). In particular, OSNs expressing high basal activity ORs, such as M71, show reduced firing in OMP-KO mice; whereas weaker effects are detectable in low basal activity ORs, such as mOR-EG (Dibattista & Reisert, 2016). Since cAMP is also critical for refinement of neuronal circuits (Sakano, 2020; Fang & Yu, 2024), OMP may also participate in proper glomerular targeting. Consistent with this, OMP-KO mice display a higher ratio of heterogeneous glomeruli, targeted by OSNs expressing different ORs, although the macrostructure is relatively unperturbed (Albeanu *et al.*, 2018).

1.4.2 Passive electrical properties and spontaneous firing

Rodent OSNs are very small cells and, therefore, exhibit a small membrane capacitance of few pF (2-4 pF) (Liman & Corey, 1996; Schild & Restrepo, 1998; Vogalis *et al.*, 2005). Another

peculiar feature of these neurons is the high resting membrane resistance. Because seal and membrane resistances in patch-clamp recordings often fall in the same range (from 1 to 40 GΩ), accurate determination of the real membrane values is challenging. Therefore, authors usually refer to input resistance (R_{input}) values, typically exceeding 1 GΩ (2-6 GΩ) (Lynch & Barry, 1989; Liman & Corey, 1996; Schild & Restrepo, 1998; Ma *et al.*, 1999; Vogalis *et al.*, 2005).
Measurements of resting membrane potential in mouse OSNs also show considerable variability, ranging from -90 mV to -45 mV. Despite this wide distribution, results are consistent across groups employing different recording techniques: from the cell-attached (Maue & Dionne, 1987) to the perforated-patch (Ma *et al.*, 1999) and the whole-cell configuration (Lagostena & Menini, 2003). However, as for the R_{input}, the resting membrane potential is also subject to underestimation due to technical limitations, and the real membrane potential is likely closer to negative values ranging from -70 to -90 mV (Lynch & Barry, 1989; Schild & Restrepo, 1998; Lagostena & Menini, 2003).
The high R_{input} makes OSNs highly sensitive cells and small depolarizations (on the order of a few pA) are sufficient to trigger APs (Liman & Corey, 1996; Madrid *et al.*, 2003) (Figure 8A). OSNs generally display heterogeneous firing behaviours in response to current injections. Some neurons exhibit repetitive firing (tonic firing), whereas others can only generate one or a few spikes followed by a sustained depolarization (phasic firing) (Liman & Corey, 1996; Madrid *et al.*, 2003; Kawai, 2024) (Figure 8A). This feature is conserved across species, having been observed also in frogs, salamanders and flies (Kawai, 2024). Madrid and colleagues (2003) found that intrinsic passive properties (mainly R_{input} and resting potential) can govern the firing pattern of individual OSNs (Madrid *et al.*, 2003). Moreover, adaptation in phasic firing OSNs is thought to optimize detection of changes in the environment (Liman & Corey, 1996).
Mouse OSNs are capable of spontaneous firing even in absence of stimulating molecules. Evidence suggests that this spontaneous activity is influenced by ORs (Reisert, 2010; Connelly *et al.*, 2013; Nakashima *et al.*, 2013). Like other GPCRs, ORs can assume both active and inactive conformations. In the absence of agonists, ORs keep spontaneously flipping between the two states, driving basal production of cAMP. This results in generation of spontaneous APs (Nakashima *et al.*, 2013). OSNs expressing different ORs show distinct levels of basal activity, with a wide range of spontaneous firing frequencies, from 0 to 12 Hz (Ma *et al.*, 1999; Reisert, 2010; Connelly *et al.*, 2013; Nakashima *et al.*, 2019). For example, OSNs expressing the OR-EG show lower firing mean rates (around 2 Hz) while I7-expressing neurons result more active with a mean rate of 4 Hz (Reisert, 2010; Connelly *et al.*, 2013; Nakashima *et al.*, 2019) (Figure 8B, C).

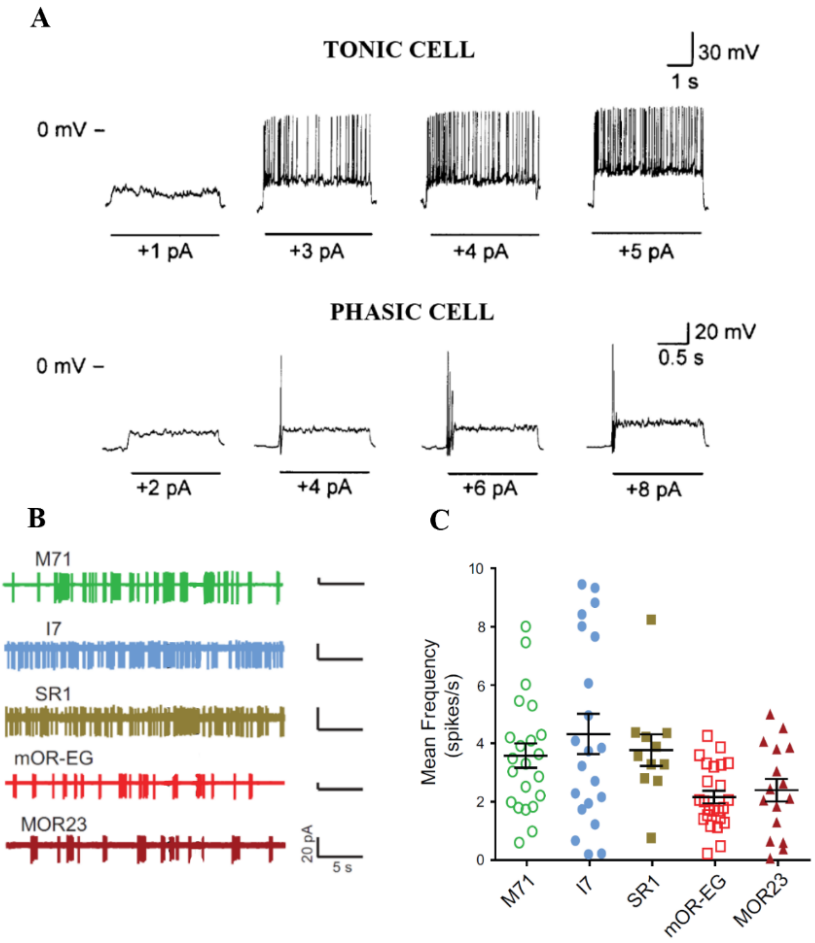

Figure 8. Evoked and spontaneous activity of OSNs.

(A) Whole-cell current clamp recordings from rat OSNs. Small current injections were sufficient for triggering action potentials. Tonic cell (top) displayed sustained repetitive firing, while the phasic cell (bottom) elicited only few action potentials. **(B)** Spontaneous activity recorded in cell-attached configuration from OSNs expressing M71, I7, SR1, mOR-EG and MOR23 receptors. **(C)** Mean firing frequencies of neurons shown in (B). I7 and M71 OSNs exhibit higher frequencies than mOR-EG and MOR23 neurons. Substantial variability can be observed even among OSNs expressing the same OR. (Adapted from Madrid *et al.*, 2003; Connelly *et al.*, 2013).

1.5 Voltage-gated ion channels in OSNs

1.5.1 Voltage-gated sodium channels

Voltage-gated sodium channels (Na_v) are responsible for initiation and propagation of APs (Bean, 2007). These channels consist of an α subunit interacting with auxiliary β subunits. The α subunit contains four domains (I-IV), each one composed of six transmembrane segments (S1-S6). The α subunit alone is sufficient to form a fully functional channel, as it contains all the essential elements (Yu & Catterall, 2003). In contrast, β subunits are characterized by a single transmembrane domain with extracellular immunoglobulin-like folds and modulate channel gating and kinetics (Catterall, 2000*a*; Yu & Catterall, 2003; Brackenbury & Isom, 2011) (Figure 9).

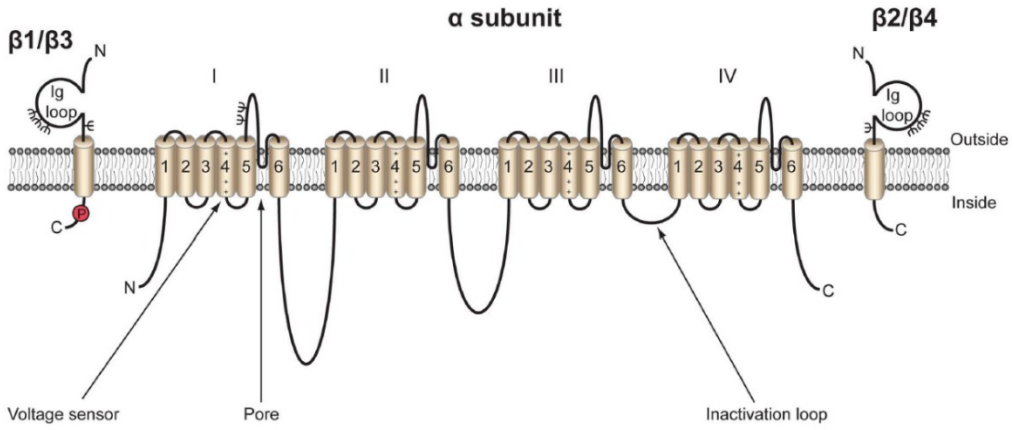

Figure 9. Structure of Na_v.

Schematic representation of a Na_v channel. Roman numbers indicate the four domains of the main α subunit (I-IV), while the Arabic numbers indicate the transmembrane segments (S1-S6). The extracellular loop between S5 and S6 forms the ion-selective pore, while the S4 acts as voltage sensor containing positively charged residues sensitive to the membrane depolarization. The intracellular loop between domains III and IV forms the inactivation gate. β subunits are formed by an intracellular C-terminal domain and an extracellular immunoglobulin (Ig) loop. Phosphorylation sites (P) contribute to channel modulation. α subunit extracellular loops interact with the extracellular domains of β subunits. Ψ, glycosylation sites. (Adapted from Brackenbury & Isom, 2011).

The neuronal Na_v family includes nine α subunits ($Na_v1.1$-$Na_v1.9$) and four β subunits (β1- β4) (Catterall, 2000*a*; Goldin *et al.*, 2000). Na_v isoforms differ in biophysical properties and pharmacological profiles. Based on their sensitivity to the specific blocker tetrodotoxin (TTX), Na_v are classified as TTX-sensitive ($Na_v1.1$, $Na_v1.2$, $Na_v1.3$, $Na_v1.4$, $Na_v1.6$, and $Na_v1.7$) or TTX-resistant ($Na_v1.5$, $Na_v1.8$, and $Na_v1.9$) channels (Wang *et al.*, 2017).

In OSNs, $Na_v1.7$ is considered the predominant channel (Weiss *et al.*, 2011; Ahn *et al.*, 2011; Bolz *et al.*, 2017). Its pivotal role in mammalian olfaction is highlighted by the fact that KO models for $Na_v1.7$ are anosmic. Although their OSNs can still generate APs in response to odorants, they fail to propagate signals to the glomeruli (Weiss *et al.*, 2011). Interestingly, TTX-resistant currents remain detectable in $Na_v1.7$-null OSNs, suggesting the presence of additional Na_v isoforms. Frenz and colleagues (2014) identified the presence of $Na_v1.5$ and suggested that this TTX-resistant channel contributes to the hyperpolarized shift in both activation and inactivation curves (Frenz *et al.*, 2014) (Figure 10A, B). mRNA profiling performed on OMP-GFP mice showed that $Na_v1.5$ is particularly expressed in mature, but not in immature OSNs (Sammeta *et al.*, 2007).

Further evidence from RT-PCR, *in situ* hybridization and immunostaining confirms that $Na_v1.7$ is the most abundant isoform, but $Na_v1.2$, $Na_v1.3$, $Na_v1.5$ and $Na_v1.6$ channels are also expressed at lower levels (Ahn *et al.*, 2011; Frenz *et al.*, 2014; Bolz *et al.*, 2017) (Figure 10C). Na_v

expression and subcellular localization undergo dynamical changes during the first postnatal week, coinciding with the critical period of the olfactory system development (Cheetham & Belluscio, 2014; Bolz *et al.*, 2017) (Figure 10D).

Electrophysiological recordings from rodent OSNs consistently show sodium currents with activation thresholds near -70 to -60 mV (Rajendra *et al.*, 1992; Liman & Corey, 1996; Ahn *et al.*, 2011) and a V_{half} around -45 mV (Rajendra *et al.*, 1992; Ahn *et al.*, 2011). Full activation occurs between -30 and -10 mV, with current amplitudes ranging from 0.5 to 1 nA (Trombley & Westbrook, 1991; Liman & Corey, 1996; Ma *et al.*, 1999; Lagostena & Menini, 2003; Ahn *et al.*, 2011). Larger Na^+ currents are observed when cells are held at more hyperpolarized potentials (Ma *et al.*, 1999; Lagostena & Menini, 2003).

Variability across studies is expected, given differences in experimental conditions such as animal species, age, recording techniques, solutions, and stimulation protocols.

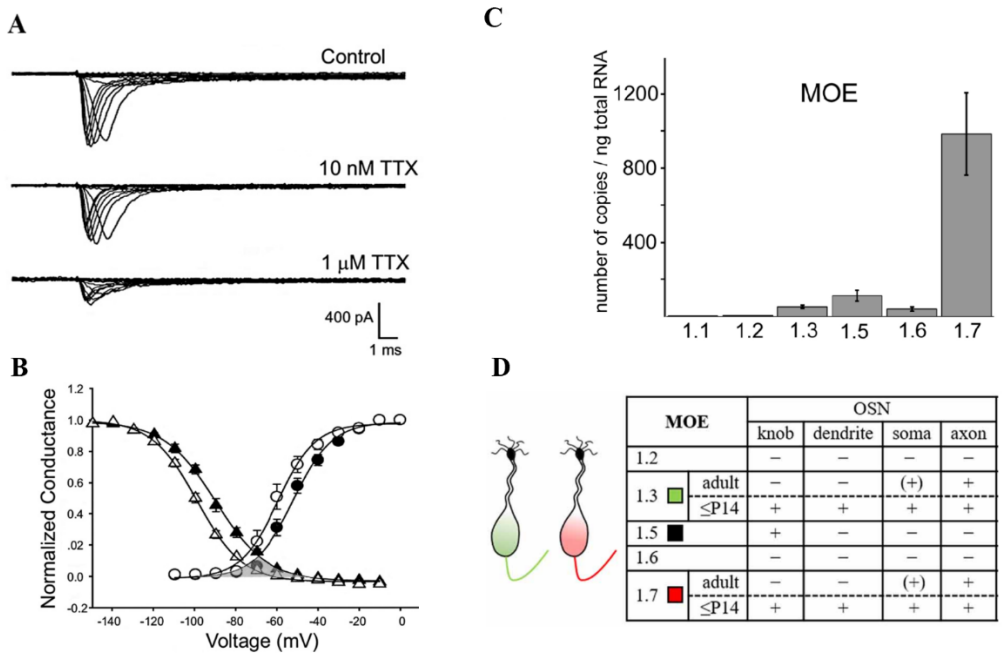

Figure 10. Na^+ currents in mouse OSNs.

(A) Whole-cell recordings of Na^+ currents elicited by depolarizing steps from -140 mV to 0 mV, starting from a holding potential of -150 mV. Application of tetrodotoxin (TTX) revealed both TTX-sensitive and TTX-resistant components: 10 nM TTX inhibited approximately the 25% of the maximal current, whereas 1 µM blocked the 75%. **(B)** Activation (circles) and inactivation (triangles) curves of Na^+ currents recorded in (A). 10 nM TTX treatment (open simbols) induced a hyperpolarizing shift in both curves. **(C)** Quantitative RT-PCR of Na_v isoforms shows that $Na_v1.7$ is the predominant channel. **(D)** Subcellular distribution of Na_v channels. Drawings on the left depict the localization of $Na_v1.7$ (red), $Na_v1.5$ (black) and $Na_v1.3$ (green) across OSNs compartments. + (present), − (absent), (+) (close to detection threshold). (Adapted from Frenz *et al.*, 2014; Bolz *et al.*, 2017).

1.5.2 Voltage-gated calcium channels

Voltage-gated calcium channels (Ca_v) are important for mediating Ca^{2+} influx for regulating AP firing patterns (Bean, 2007). All the Ca_v channels consist of a $Ca_v\alpha1$ subunit that determines the functionality of the channel. Like in Na_v, also this α subunit is organized in four domains (I-IV), each one with six transmembrane segments (S1-S6). In several subtypes, $Ca_v\alpha1$ associates with ancillary α2 and β subunits, which modulate trafficking, gating, and kinetics (Catterall, 2000*b*) (Figure 11).

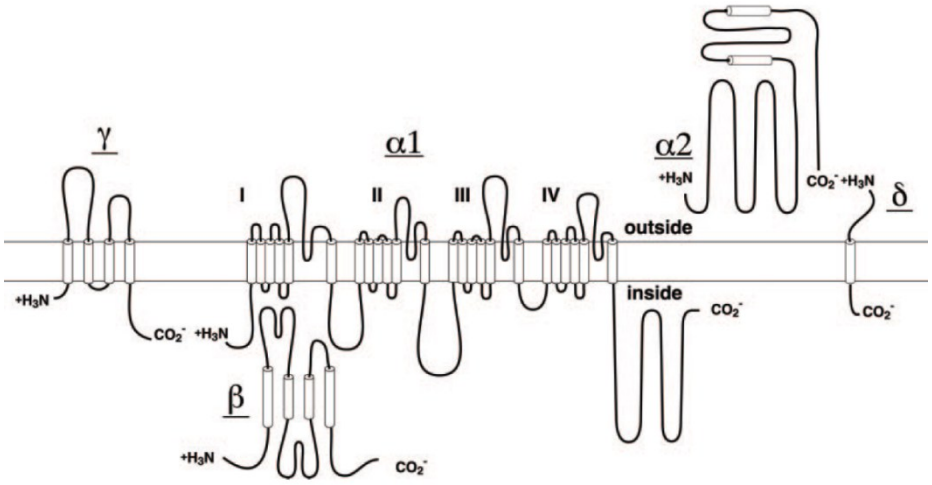

Figure 11. Structure of Ca_v.

Schematic model of $Ca_v\alpha1$ subunit, resembling the α subunit of Na_v channels. The four transmembrane domains (I-IV) are highlighted. Both intracellular and extracellular loops can interact with the auxiliary subunits α2, β and γ. (Catterall *et al.*, 2005).

Biophysical and pharmacological studies lead to the subdivision of Ca_v into three major families, primarily defined by the different $Ca_v\alpha1$ subunits: the Ca_v1, Ca_v2 and Ca_v3 channels (Catterall *et al.*, 2005). The Ca_v1 family encodes for the L-type channel, characterized by high voltage activation, large conductance and slow voltage-dependent inactivation, thus making the currents lasting for long (hence 'L-type'). These channels are specifically blocked by dihydropyridines, phenylalkylamines and benzothiazepines (Catterall *et al.*, 2005). Ca_v2 channels conduct P/Q-, N- or R-type currents, that also require strong depolarizations to activate but are inhibited by different toxins (ω-agatoxin IVA for P/Q-type; ω-Conotoxin-GVIA for N-type; SNX-482 for R-type) (Catterall *et al.*, 2005). The last family of Ca_v3 channels represents the T-type channels, low-voltage activated channels with transient kinetics. They are insensitive to the other blockers, while are preferentially inhibited by mibefradil (Lacinová, 2004; Catterall *et al.*, 2005) and relatively sensitive to zinc (Traboulsie *et al.*, 2007).

Ca_v have been described in OSNs from different species, although their current amplitude generally appears very small (Schild & Restrepo, 1998). In rodents, an L-type current has been

detected, displaying sustained activation around -30 mV and sensitivity to 100 µM Cd^{2+} and nifedipine (Trombley & Westbrook, 1991) (Figure 12). Modest evidence for Ca^{2+} currents was found in mouse OSNs using both cell-attached and excised-patches (Maue & Dionne, 1987); whereas Gautam and colleagues (2007) proposed that T-type channels contribute to propagation of odorant-induced Ca^{2+} transients in mammalian neurons, since mibefradil strongly reduced the Ca^{2+} signal recorded from the knob after stimulation (Gautam *et al.*, 2007).

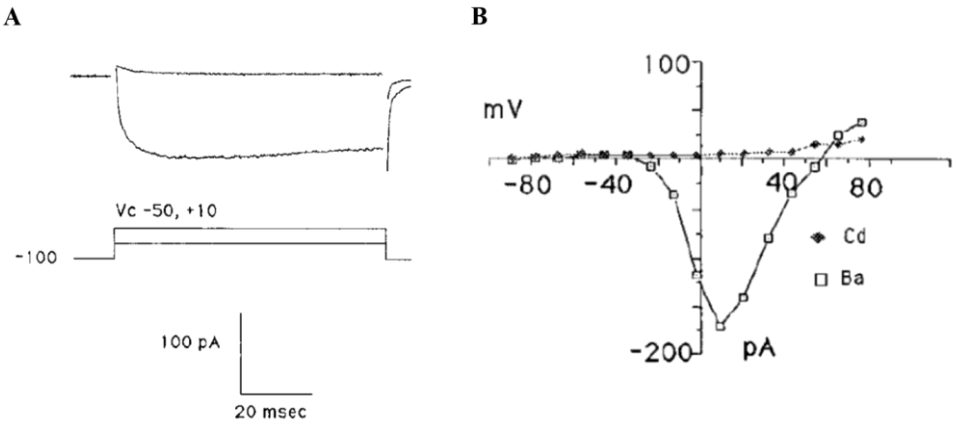

Figure 12. L-type Ca^{2+} current recorded in OSNs.
(A) A sustained inward current was elicited after depolarization to +10 mV as indicated by the voltage-clamp protocol on the bottom. **(B)** IV curve of the inward current shown in (A). The current is completely inhibited by 100 µM Cd^{2+}. (Adapted from Trombley & Westbrook, 1991).

1.5.3 Voltage-gated potassium channels

K^+ channels constitute one of the largest and most diverse classes of ion channels (Coetzee *et al.*, 1999). Voltage-gated potassium channels (K_v) play a critical role in the repolarization of the membrane following the rising phase of the AP, thereby determining the shape and duration of the AP (Bean, 2007). Functionally active K_v are tetramers of α subunits, each consisting of six transmembrane domains (S1-S6). Subunits can assemble as homotetramers if identical or heterotetramers when different, expanding the functional diversity of the channels (Coetzee *et al.*, 1999; González *et al.*, 2012; Attali *et al.*, 2023). Channel kinetics is further tuned by interactions with accessory β-subunits and other auxiliary proteins (González *et al.*, 2012) (Figure 13A, B).

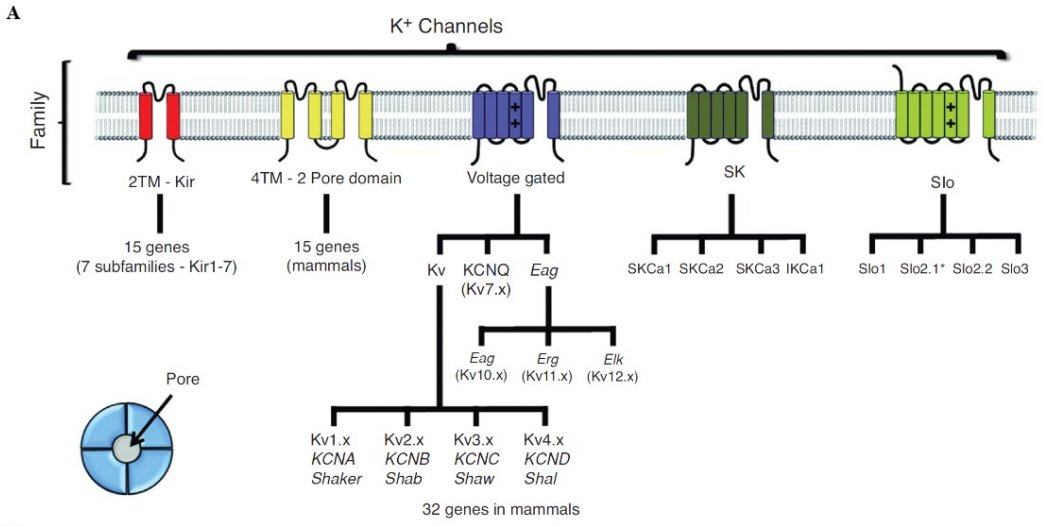

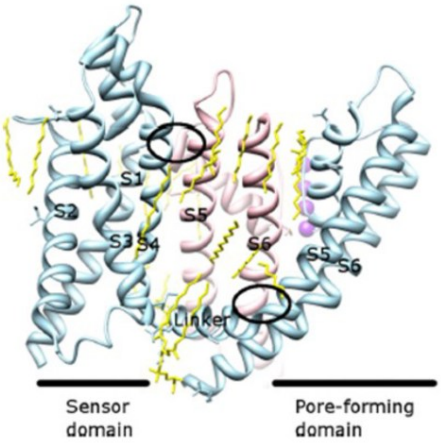

C

Principal α-subunits				
Channel Subfamily	**Alternative name**	**Channel subtype**	**Gene**	**Associated current**
Kv1.x	Shaker-like	Kv1.1	Kcna1	I_K
		Kv1.2	Kcna2	
		Kv1.3	Kcna3	
		Kv1.4	Kcna4	I_A
		Kv1.5	Kcna5	I_K
		Kv1.6	Kcna6	
		Kv1.7	Kcna7	
		Kv1.8	Kcna10	
Kv2.x	Shab-like	Kv2.1	Kcnb1	I_K
		Kv2.2	Kcnb2	
Kv3.x	Shaw-like	Kv3.1	Kcnc1	I_K
		Kv3.2	Kcnc2	
		Kv3.3	Kcnc3	I_A
		Kv3.4	Kcnc4	
Kv4.x	Shal-like	Kv4.1	Kcnd1	I_A
		Kv4.2	Kcnd2	
		Kv4.3	Kcnd3	

Figure 13. Functional-structural overview of K^+ channels.

(A) K^+ channel family grouped according to the subunit structure: the two transmembrane domains (2TM; Kir), the four transmembrane domains (4TM; 2 pore domain), the six transmembrane domains (voltage gated and SK) and the seven transmembrane domains (7TM; Slo). The voltage-gated family can be further divided into three classes: K_v (further subdivided into K_v1-K_v4), the KNCQ (composed by the K_v7 channels) and the ether-a-go-go (Eag), groups. For K_v also genes and alternative names are reported. **(B)** The six transmembrane domains (S1-S4) of one α subunit (light blue) interact with the neighbouring subunit (pink) in two sites of contact (circles). The extracellular loop between S5 and S6 forms the selectivity filter, constituting the pore-forming domain; while the first four segments form the voltage sensor domain (VSD), with the S4 acting as the main sensor, due to its positively charged residues (lysines or arginines). Lipids surrounding the channel are depicted in yellow. **(C)** Subfamilies of K_v, and corresponding genes, associated to delayed rectifier (I_K) or transient A-type (I_A) currents, the two major types identified in olfactory sensory neurons. (Adapted from González *et al.*, 2012; Attali *et al.*, 2023).

In OSNs, two major types of voltage-gated K^+ currents have been identified: delayed rectifier (I_K) currents and transient A-type (I_A) currents (Kawai, 2024).

Delayed rectifier currents slowly activate after depolarization and do not inactivate on the millisecond timescale. They were originally described by Hodgkin and Huxley as critical for terminating the AP and restoring the resting membrane potential (González *et al.*, 2012)

Members of the K_v1 (except $K_v1.4$), K_v2, and K_v3 (in particular $K_v3.1$ and $K_v3.2$) subfamilies typically generate I_K currents (Gutman *et al.*, 2005; González *et al.*, 2012; Ranjan *et al.*, 2019) (Figure 13C).

On the other hand, A-type currents are transient outward currents evoked by depolarization. They activate fast at subthreshold potentials and rapidly inactivate, within tens to hundreds of milliseconds, producing the characteristic 'A-shaped' profile (Connor & Stevens, 1971; Rogawski, 1985; Rudy, 1988; Sonner & Stern, 2007). Assigning the I_A current to specific K_v proved to be quite challenging since the biophysics and pharmacological profile can vary with the subunit composition; however K^+ currents with A-type properties are commonly associated to the $K_v1.4$, K_v3 (specifically $K_v3.3$ and $K_v3.4$) and K_v4 channels (Gutman *et al.*, 2005; González *et al.*, 2012; Ranjan *et al.*, 2019) (Figure 13C). I_A currents play a pivotal role into the repolarization of the AP, shaping the spike waveform, and regulation of neuronal firing frequency (Connor & Stevens, 1971; Rogawski, 1985; Rudy, 1988; Rudy *et al.*, 1999; Sonner & Stern, 2007).

I_K currents are generally blocked by millimolar concentrations of tetraethylammonium (TEA), whereas I_A currents are more sensitive to 4-aminopyridine (4-AP) (Rogawski, 1985; Gutman *et al.*, 2005; Johnston, 2021). Other compounds, such as catechol, have been reported to block I_A currents, similar to 4-AP (Ito & Maeno, 1986; Erdélyi & Such, 1988; Hess & El Manira, 2001). Inhibition of I_A prolongs AP duration, further emphasizing its importance in regulating AP dynamics (Erdélyi & Such, 1988; Sah & McLachlan, 1992; Hess & El Manira, 2001; Xiao *et al.*, 2021).

In OSNs, delayed rectifier currents are consistently observed across different studies: patch clamp recordings in rodents show that depolarizing steps elicit sustained outward currents that activate at around -30 mV and are strongly inhibited by high concentrations of TEA (20-25 mM) (Trombley & Westbrook, 1991; Ma *et al.*, 1999; Lagostena & Menini, 2003; Boccaccio, 2018) (Figure 14A-C). A current resembling the delayed rectifier has also been reported in cell-attached recordings (Maue & Dionne, 1987). The same depolarization protocols can also reveal the I_A type, that activates faster than the I_K (Lynch & Barry, 1991; Ma *et al.*, 1999; Lagostena & Menini, 2003; Han & Lucero, 2005) (Figure 14A-C). However, I_A current was not always detected. This might be explained by the steady-state inactivation of this current: when cells are held at more positive potentials, as for example -50 mV, this current may inactivate and thus remain hidden. Moving the holding to more hyperpolarized potentials can remove the inactivation, enhancing the I_A detection (Ma *et al.*, 1999; Lagostena & Menini, 2003). This principle has been exploited to isolate the I_A component. When both I_A and I_K are present, a pre-

pulse to highly positive voltages selectively inactivate I_A, leaving only the sustained component. Subtraction of this current from the total one reveals the pure I_A component (Ma *et al.*, 1999; Han & Lucero, 2005) (Figure 14D). Additionally, I_A current was completely inhibited by 5 mM 4AP (Lynch & Barry, 1991; Han & Lucero, 2005) (Figure 14E).

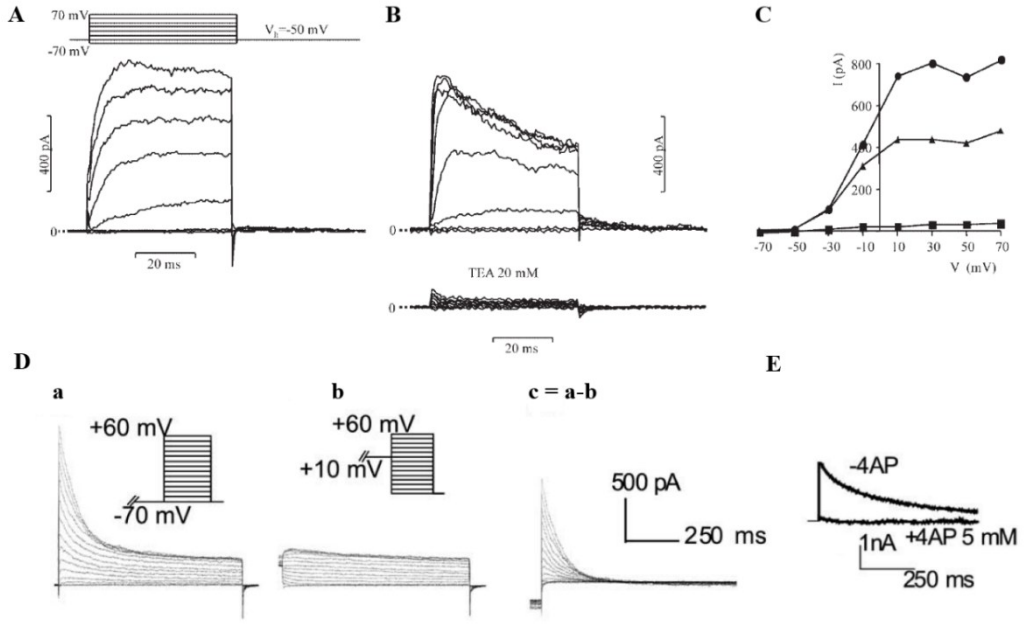

Figure 14. Voltage-gated K^+ currents in OSNs.

(A-B) Total outward currents recorded from mouse OSNs with the protocol shown. Some cells develop only a sustained current (A), whereas others show both the delayed and A-type currents (B). These currents are completely blocked by 20 mM tetraethylammonium (TEA) **(C)** IV curves for the currents measured in (B) at the peak (I_A, circles), at the end (sustained, triangles) and in presence of TEA (squares). **(D)** Transient and sustained currents in mouse OSNs activated with the protocols indicated on top. a, total current; b, sustained component obtained inactivating the I_A current with 1s pre-pulse at +10 mV; c, I_A component obtained subtracting a-b. Cells were held at -70 mV. **(E)** I_A current isolated from mouse OSNs with the protocol in (D) is completely blocked by 5 mM 4-aminopyridine (4-AP). (Adapted from Lagostena & Menini, 2003; Han & Lucero, 2005).

Molecular evidence from OSNs has identified some genes associated with A-type currents. In particular mRNA profiling of OMP-GFP mice revealed expression of $K_v3.4$ in mature but not in immature OSNs (Sammeta *et al.*, 2007). In contrast, Han and Lucero (2006) detected $K_v1.4$, $K_v4.2$ and $K_v4.3$ through both RT-PCR and immunohistochemistry (Han & Lucero, 2006).

1.6 Comparative overview of mouse and human olfactory systems

Rodents have been used for decades, along with other species (amphibians, fishes), as laboratory models to investigate olfaction. Therefore, they have been extensively studied. In contrast, less is known about human olfactory system, where most of the available information is limited to

anatomical and morphological features. While humans and rodents share several similarities, striking differences also exist.

Structurally, the human nasal cavity is relatively simpler compared to the mouse nose: humans are endowed with three nasal turbinates, whereas mice display highly complex foldings and branching turbinates that provide a much larger surface. Human OE covers a surface area of about 100-500 mm^2, varying among individuals, roughly corresponding to the 3% of the total nasal cavity, while in mice it extends over nearly the 50% of the surface (Morrison & Costanzo, 1990; Cheng *et al.*, 1996; Ménache *et al.*, 1997; Doty, 2003; Harkema *et al.*, 2006) (Figure 15). Both humans and mice show a transition zone between OE and RE (Alvites *et al.*, 2018; Hernandez-Clavijo *et al.*, 2022) (Figure 16A); however in humans patches of OE mixed with RE can be found (Morrison & Costanzo, 1990; Doty, 2003).

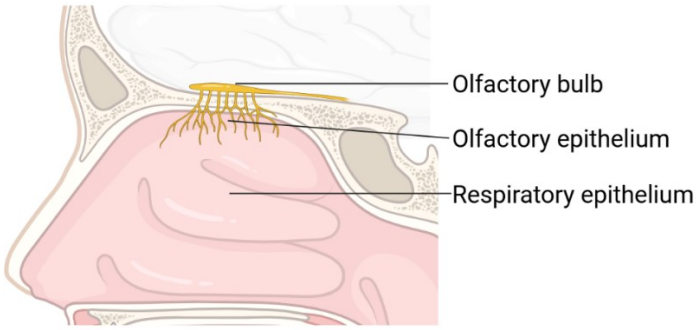

Figure 15. Structure of human olfactory system.

Schematic view of human olfactory system. The majority of the nasal cavity is occupied by the respiratory epithelium (pink), while the OE covers a very small area. Axons from the OSNs form nerve bundles that reach the OB (yellow).

From the histological point of view, the two systems are comparable: as in the mouse, human OE has a pseudostratified organization, with basal cells arranged in a necklace-like pattern close to the basal lamina and OSNs distributed across the layers according to their maturation state. Supporting cells span throughout the epithelium, with their microvilli intermingling among OSN cilia (Figure 16A), and microvillar cells localize near the mucosal surface (Morrison & Costanzo, 1990; Harkema *et al.*, 2006; Hernandez-Clavijo *et al.*, 2022).

Immunohistochemistry and scRNA-seq data revealed that the ratio of immature to mature OSNs is higher in OE from middle-aged humans than in adult mice (Durante *et al.*, 2020) (Figure 16B). Morphologically, human OSNs exhibit the typical bipolar structure, with dendrites bearing cilia facing the mucus and axons projecting to the OB, and their dimensions are comparable with those of mouse OSNs (Doty, 2003) (Figure 16A, B).

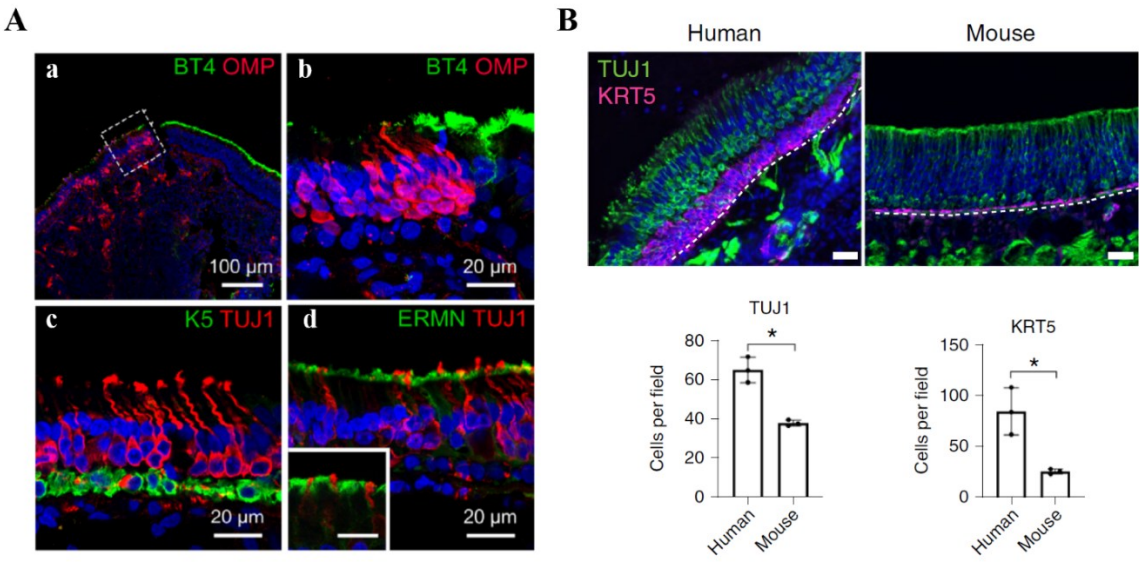

Figure 16. Histological organization of human OE.

(A) Immunohistochemistry of the human nasal epithelium. (a) Labelling of respiratory ciliated cells with β-tubulin IV (BT4) and mature OSNs with OMP, highlights the transition zone between respiratory and olfactory epithelia. (b) Magnification from the dashed square in (a). (c-d) Staining reveals the pseudostratified organization of the human OE: basal cells are labelled with Keratin 5 (K5), neurons with β-tubulin III (TUJ1) and the apical part of supporting cells with Ermin (ERMN). The inset in (d) shows a higher magnification. Scale bar: 10 µm. **(B)** Immunohistochemistry (top) shows a higher abundance of immature OSNs, labelled with β-tubulin III (TUJ1, green), and HBCs, marked with Keratin 5 (KRT5, magenta), in human OE compared with mouse OE. In humans, HBCs form a layered structure, whereas in mice they appear as a single flat layer. Nuclei are stained with DAPI (blue). The white dashed line indicates the basal lamina. Scale bar: 50 µm. Quantification of TUJ1- and KRT5-positive cells is shown below. (Adapted from Durante *et al.*, 2020; Hernandez-Clavijo *et al.*, 2022).

The ORs, located in the cilia, follow the 'one neuron-one receptor' rule, since only one type of OR was detected in each human mature OSNs (Durante *et al.*, 2020). The human genome accounts for ~900 OR genes, of which only ~390 are functional, while the remaining ~55% are pseudogenes. Compared with mice, the human OR repertoire is markedly reduced, not only in total gene number (~1500 in mice), but also in proportions of functional genes, with ~45% being protein-coding genes in humans *versus* ~75% in mice (Young *et al.*, 2002; Saraiva *et al.*, 2019; Sharma *et al.*, 2019; Barnes *et al.*, 2020). Interestingly, human ORs exhibit less conserved sequence motifs than mice, a feature proposed as a strategy to broaden receptor diversity and compensate for the smaller gene repertoire (Young *et al.*, 2002). Saraiva et al. (2019) compared the most abundantly expressed ORs in humans and mice to assess whether receptor expression reflects species-specific ecological needs. They found that humans are enriched for ORs detecting key food-related odorants, whereas mice are abundant in semiochemicals-detecting ORs (Saraiva *et al.*, 2019). Classifying the odorants activating ORs on the basis of their chemical structures, they found that both species share carboxylic acids (cheesy/sweaty odor) as the most represented class. Terpenes (green and minty) and azines (animalic and pungent) are detected

only by humans, while camphors exclusively by mice (Figure 17A). Looking at the odorant sensory profiles (defined by perceived human odour qualities), despite substantial overlap, humans show preferences for floral, spicy and sweaty/pungent odours, whereas mice are biased towards camphor/minty and sulforous/meaty odours (Saraiva *et al.*, 2019) (Figure 17B).

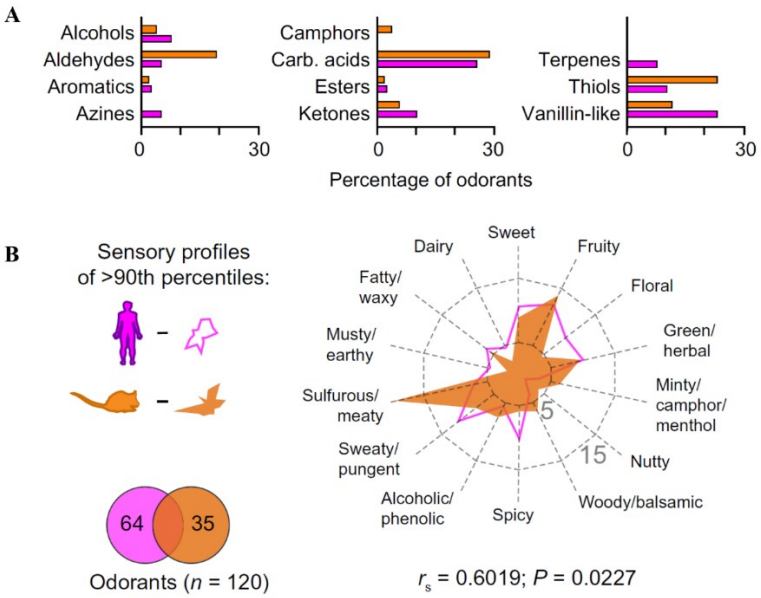

Figure 17. Profile of the most abundant ORs in humans and mice.

(A) Percentage of odorants, grouped by chemical class, that activate the most abundantly expressed ORs in humans (purple) and mice (orange). **(B)** Odorants activating the ORs above the 90th percentile of expression were analysed by Saraiva et al. (2019): 64 out of 120 were exclusively associated to human ORs (purple) and 35 out of 120 uniquely with mouse ORs (orange). Spider plots on Venn diagram show great overlap and strong correlation between sensory profiles of the two species; with minor preferences of humans for floral, spicy and sweaty/pungent perceived odorants (purple) and mice towards odorants associated to sulfurous/meaty and minty/camphor/menthol perception (orange). r_s, correlation index; P, p-value. (Adapted from Saraiva *et al.*, 2019).

Although challenging to quantify, several studies have attempted to estimate the total number of glomeruli in the human OB: early reports suggested ~3,000-9,000 glomeruli per OB (Maresh *et al.*, 2008), while recently it has been estimated an average of ~9,000-15,000 glomeruli per OB (Low *et al.*, 2024). These values are higher with respect to the ~2,850-3,600 glomeruli reported in the mouse OB (Richard *et al.*, 2010; Weng *et al.*, 2025). Comparing OSN innervation, mice appear to have roughly ten times more OSNs per glomerulus, potentially contributing to further species-specific qualitative differences in olfactory coding (Low *et al.*, 2024).

Transcriptomic studies show the expression of genes involved in the transduction pathway such as α and γ subunits of G proteins, CNG and TMEM16B channels (Durante *et al.*, 2020; Brann *et al.*, 2020; Fodoulian *et al.*, 2020), however functional evidence remain scarce. Odorant stimulation of dissociated human OSNs induced an increase in intracellular Ca^{2+}, probably

mediated by cAMP, although in some cells Ca^{2+} signal decreased upon odorant stimulation (Restrepo *et al.*, 1993*a*). Moreover, it has been shown that both protein kinase A (PKA), element of the cAMP-mediated pathway, and protein kinase C (PKC), downstream of the PLC pathway, are involved in odorant responses (Gomez *et al.*, 2000). Together, these findings suggest that both similarities and differences are present, although a clear functional transduction pathway is still not fully defined.

From the electrophysiological perspective, only a few groups have examined voltage-dependent conductances in human OSNs dissociated from nasal biopsies: sustained outward currents were typically observed, while transient inward current were detected only in a few cells (Restrepo *et al.*, 1993*a*; Tamari *et al.*, 2019) (Figure 18). Whether these differences reflect real species-specific properties or result from technical limitations associated with the cell dissociation process remains unclear.

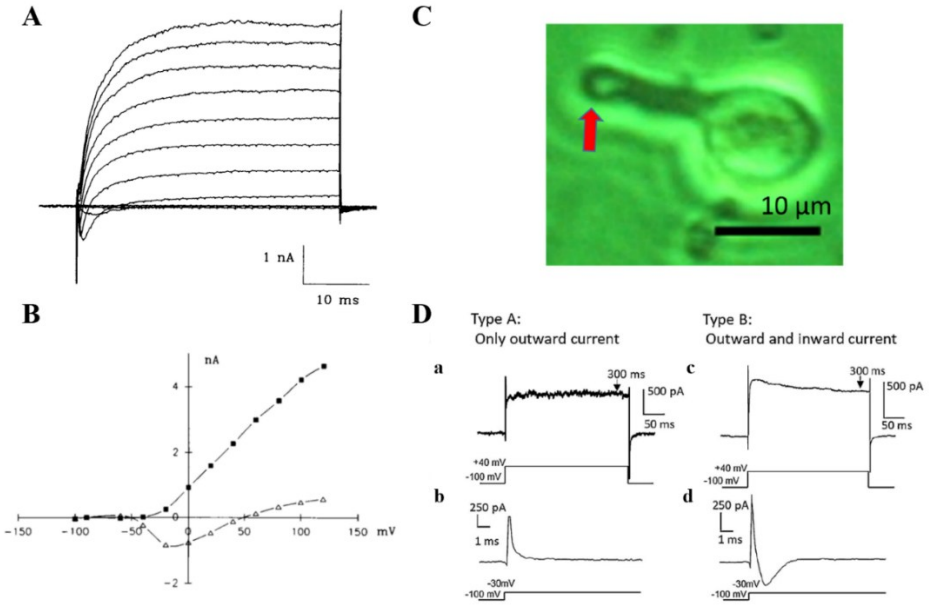

Figure 18. Voltage-gated currents measured from human dissociated OSNs.

(A-B) Representative traces of voltage-gated currents (A) and corresponding I-V plot (B) recorded from human dissociated OSNs by Restrepo et al. (1993). All cells displayed sustained outward currents (squares), while only one showed a transient inward current (triangles). Currents were evoked by voltage steps from -100 mV to +120 mV, starting from a holding of -80 mV. **(C)** Morphology of a human OSN isolated from a nasal biopsy by Tamari et al. (2019): a long dendrite extends from the soma and terminates in a knob structure (arrow). **(D)** Two human OSNs types identified by Tamari et al. (2019): type A, displaying only an outward current upon depolarization (a), while no inward currents were elicited (b), and type B OSNs showing both an outward current (c) and an inward current highlighted in (d). Voltage-step protocols are indicated below each representative trace. (Adapted from Restrepo *et al.*, 1993*b*; Tamari *et al.*, 2019).

2. AIMS

This work is focused on characterizing for the first time the electrophysiological features of the human olfactory epithelium and on investigating changes in the functional properties of OSNs during maturation in mouse olfactory epithelium.

In particular, the aims of the first part are:

- To analyse voltage-gated currents in human OSNs and supporting cells in acute slices obtained from nasal biopsies.
- To characterize firing activity in human OSNs using whole-cell current-clamp recordings.
- To investigate the transduction pathway in human OSNs through immunohistochemistry and electrophysiological stimulation with odorant mixtures.

The second part of this work aims to:

- Assess the spontaneous firing in immature OSNs in loose-patch configuration.
- Evaluate immature OSN excitability and analyse action potential parameters in comparison with mature OSNs.
- Characterize changes in voltage-gated currents and identify differential expression of voltage-gated channels across maturation.

3. RESULTS

3.1 Shedding light on human olfaction: Electrophysiological recordings from sensory neurons in acute slices of olfactory epithelium

Andres Hernandez-Clavijo,[1,4,6] Cesar Adolfo Sánchez Triviño,[1,4] Giorgia Guarneri,[1,4] **Chiara Ricci,[1]** Fabian A. Mantilla-Esparza,[1] Kevin Y. Gonzalez-Velandia,[1] Paolo Boscolo-Rizzo,[2] Margherita Tofanelli,[2] Pierluigi Bonini,[2] Michele Dibattista,[3,*] Giancarlo Tirelli,[2] and Anna Menini[1,5,*]

[1] Neuroscience Area, SISSA, Scuola Internazionale Superiore di Studi Avanzati, 34136 Trieste, Italy

[2] Department of Medical, Surgical and Health Sciences, Section of Otolaryngology, University of Trieste, 34149 Trieste, Italy

[3] Department of Translational Biomedicine and Neuroscience, University of Bari A. Moro, 70121 Bari, Italy

[4] These authors contributed equally

[5] Lead contact

[6]Present address: Department of Chemosensation, Institute for Biology II, RWTH Aachen University, Aachen, Germany

[*]Correspondence: michele.dibattista@uniba.it; anna.menini@sissa.it

iScience, Volume 26, Issue 7, 107186 July 21, 2023

DOI: https://doi.org/10.1016/j.isci.2023.107186

iScience

CellPress
OPEN ACCESS

Article

Shedding light on human olfaction: Electrophysiological recordings from sensory neurons in acute slices of olfactory epithelium

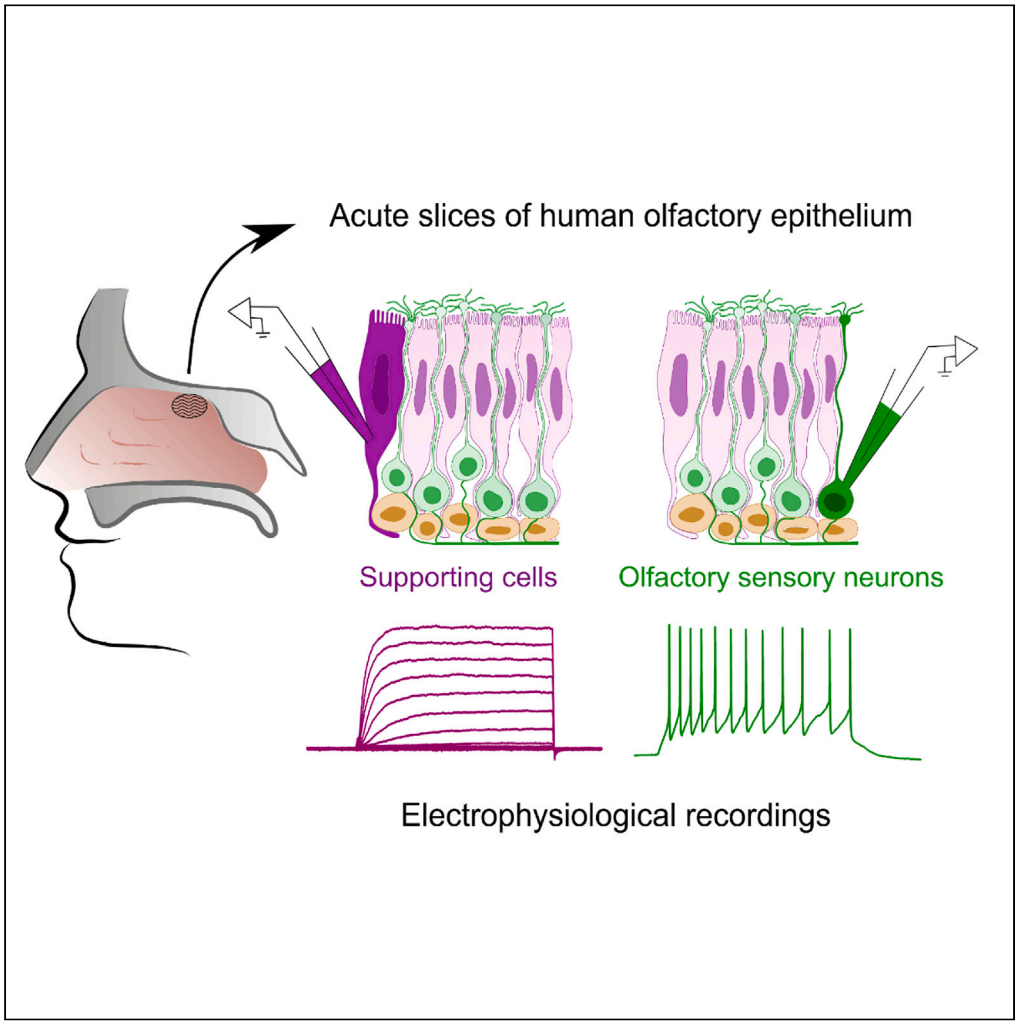

Andres Hernandez-Clavijo, Cesar Adolfo Sánchez Triviño, Giorgia Guarneri, ..., Michele Dibattista, Giancarlo Tirelli, Anna Menini

michele.dibattista@uniba.it (M.D.)
anna.menini@sissa.it (A.M.)

Highlights

Acute slices of human olfactory epithelium are viable for patch-clamp recordings

Supporting cells (non-neuronal) exhibit outward voltage-gated currents

Olfactory sensory neurons display diverse patterns of action potentials

Olfactory sensory neurons respond to odorants and other stimuli

Hernandez-Clavijo et al., iScience *26*, 107186
July 21, 2023
https://doi.org/10.1016/j.isci.2023.107186

iScience

CellPress
OPEN ACCESS

Article

Shedding light on human olfaction: Electrophysiological recordings from sensory neurons in acute slices of olfactory epithelium

Andres Hernandez-Clavijo,[1,4,6] Cesar Adolfo Sánchez Triviño,[1,4] Giorgia Guarneri,[1,4] Chiara Ricci,[1] Fabian A. Mantilla-Esparza,[1] Kevin Y. Gonzalez-Velandia,[1] Paolo Boscolo-Rizzo,[2] Margherita Tofanelli,[2] Pierluigi Bonini,[2] Michele Dibattista,[3,*] Giancarlo Tirelli,[2] and Anna Menini[1,5,*]

SUMMARY

The COVID-19 pandemic brought attention to our limited understanding of human olfactory physiology. While the cellular composition of the human olfactory epithelium is similar to that of other vertebrates, its functional properties are largely unknown. We prepared acute slices of human olfactory epithelium from nasal biopsies and used the whole-cell patch-clamp technique to record electrical properties of cells. We measured voltage-gated currents in human olfactory sensory neurons and supporting cells, and action potentials in neurons. Additionally, neuronal inward current and action potentials responses to a phosphodiesterase inhibitor suggested a transduction cascade involving cAMP as a second messenger. Furthermore, responses to odorant mixtures demonstrated that the transduction cascade was intact in this preparation. This study provides the first electrophysiological characterization of olfactory sensory neurons in acute slices of the human olfactory epithelium, paving the way for future research to expand our knowledge of human olfactory physiology.

INTRODUCTION

Human olfaction has long been considered a neglected sense and the recent COVID-19 pandemic has highlighted the scarce knowledge we have of human olfactory physiology. The sudden and widespread olfactory loss experienced during the pandemic caught us unprepared, with many individuals struggling to recover their sense of smell.[1–7] Indeed, although the morphology of the human olfactory epithelium was well known, there was limited knowledge about the molecular and functional landscape of different cell types within the human olfactory epithelium. Molecular data became soon available in the early phase of the pandemic[8–11] but the functional properties of the cells are still largely unknown.

The human olfactory epithelium is located in the upper posterior part of the nasal cavity, and it is found in patchy regions that alternate with non-sensory epithelium. Its cellular composition and organization are similar to that of most other vertebrates.[12–15] The epithelium consists of three main cell types: olfactory sensory neurons, supporting (or sustentacular) cells, and basal cells. Olfactory sensory neurons are bipolar neurons that have one dendrite ending with a knob from which several cilia originate at the surface of the epithelium, a soma, and a single axon reaching the olfactory bulb. Supporting cells, the "unsung heroes"[10] of the olfactory epithelium, are columnar in shape, extending from the basal to the apical portion of the epithelium. They provide structural support to olfactory sensory neurons, and bear microvilli on their apical side.[16] Basal cells are located at the basal part of the epithelium and have the ability to regenerate various cell types within the olfactory epithelium.[11,16,17]

Recent research during the COVID-19 pandemic has identified supporting cells as the primary target of SARS-CoV-2 in the olfactory epithelium.[8–10] Furthermore, the compromised functionality of supporting cells, along with inflammatory processes, can exacerbate olfactory loss.[18,19]

Olfactory transduction in rodents and amphibians has been extensively studied and it is well established that it occurs in the cilia of olfactory sensory neurons.[20–24] This process begins with the binding of odorant

[1]Neuroscience Area, SISSA, Scuola Internazionale Superiore di Studi Avanzati, 34136 Trieste, Italy

[2]Department of Medical, Surgical and Health Sciences, Section of Otolaryngology, University of Trieste, 34149 Trieste, Italy

[3]Department of Translational Biomedicine and Neuroscience, University of Bari A. Moro, 70121 Bari, Italy

[4]These authors contributed equally

[5]Lead contact

[6]Present address: Department of Chemosensation, Institute for Biology II, RWTH Aachen University, Aachen, Germany

*Correspondence: michele.dibattista@uniba.it (M.D.), anna.menini@sissa.it (A.M.)

https://doi.org/10.1016/j.isci.2023.107186

molecules to specific G protein-coupled odorant receptors, which activate a biochemical cascade that increases cAMP concentration within the cilia. As a result, the open probability of cyclic nucleotide-gated (CNG) channels increases, allowing the entry of Na^+ and Ca^{2+} and inducing neuron depolarization.[25–28] The increase in Ca^{2+} concentration within the cilia then activates the Ca^{2+}-activated Cl^- channel TMEM16B (also named ANO2) that contributes to regulate neuron depolarization.[29–35] When the depolarization reaches the threshold, action potentials are generated and transmitted to the olfactory bulb.[36–38] In combination with calmodulin, Ca^{2+} also contributes to response termination by enhancing the activity of the phosphodiesterase PDE1C2, which hydrolyzes cAMP, reducing the open probability of CNG channels.[39,40] The use of the PDE inhibitor 3-isobutyl-1-methylxanthine (IBMX) has unveiled the presence of a basal cAMP concentration, as upon IBMX application, inward currents were measured in the whole-cell voltage-clamp configuration in olfactory sensory neurons in amphibians and rodents.[41–43] Basal cAMP fluctuations (hence the IBMX response) are caused by the constitutive activity of odorant receptors that activate the transduction cascade, producing a depolarization followed by action potential generation. Different odorant receptors show different levels of constitutive activity.[44–46]

The mature olfactory sensory neurons, which express the olfactory marker protein (OMP)[47,48] and only one odorant receptor type among about 400–1000,[10,49] are the main functional units in the olfactory epithelium in most vertebrates, including humans. In human mature olfactory sensory neurons, some genes coding for proteins known to be involved in odorant signal transduction in rodents are expressed, such as several odorant receptor genes, G protein alpha and gamma subunits, adenylyl cyclase type 3, cyclic nucleotide-gated channel alpha2, and the calcium-activated chloride channel (*TMEM16B*/ANO2).[8–11,50] However, while immunohistochemistry data have confirmed expression of the G protein alpha and gamma subunits in human olfactory sensory neurons,[11,13] no data have been published for the other proteins potentially involved in the human olfactory transduction cascade.

From a functional point of view, a pioneering study by Restrepo et al.[51] reported that viable human olfactory sensory neurons could be dissociated from olfactory tissue biopsies, and showed, by using Ca^{2+} imaging, that some neurons responded to odorants with an increase in intracellular Ca^{2+} concentration. Further studies by the same laboratory[52,53] showed that some human olfactory neurons also responded to odorants with a decrease in intracellular Ca^{2+} concentration, a response never observed in neurons from other vertebrates,[51,54–56] suggesting that human olfactory neurons have unique properties compared to other vertebrates. Moreover, Gomez et al.[57] found that protein kinases A and C modulate odorant responses in different ways in human and rat olfactory neurons, indicating additional differences between the two species. Overall, these studies provided insight into the odorant-induced Ca^{2+} changes in human olfactory neurons revealing differences from other vertebrates.

In rodents and amphibians, electrophysiological techniques have been extensively used to study the functional properties of olfactory sensory neurons while only a few studies have been reported in humans.[51,58,59] One of these studies used the inside-out patch-clamp technique from the dendritic knob of dissociated human olfactory neurons to characterize activation of CNG channels by cAMP, providing evidence that these channels may be involved in olfactory transduction in humans.[58] Two other reports investigated the electrical properties of isolated human olfactory neurons with the whole-cell patch-clamp technique.[51,59] Both studies consistently measured outward voltage-gated currents in response to depolarizing voltage steps, while transient inward currents were rarely observed in human olfactory neurons. The absence of transient inward currents in most human olfactory neurons is surprising, as they are found in other vertebrates,[60] and this may be due either to a unique aspect of human olfactory transduction[59] or to neuron damage during the dissociation procedure.[51]

Knowledge of the initial electrical events in human olfactory neurons is crucial for understanding the signals transmitted from the periphery to the brain. To achieve this, it is essential to use a preparation that closely mimics the physiological environment of human olfactory sensory neurons. In our study, we developed a technique to obtain acute slices from biopsies of the human olfactory epithelium, which provides a more physiological setting for olfactory neurons than dissociated cells. Using this preparation, we employed the whole-cell patch-clamp technique to measure the basic biophysical properties and voltage-gated currents of olfactory sensory neurons and supporting cells, and recorded action potential generation in olfactory neurons. Moreover, we were able to record IBMX and odorant-induced

transduction currents, providing the first functional characterization of olfactory sensory neurons from acute slices of the human olfactory epithelium.

RESULTS

Immunohistochemistry of the human olfactory epithelium

We performed an immunohistochemical analysis of biopsies of human nasal tissues using specific markers to identify the presence of olfactory sensory neurons and supporting cells.

We used β-tubulin III (TUJ1) a known marker for neurons and the OMP to stain mature olfactory sensory neurons and clearly identified the typical bipolar morphology of olfactory sensory neurons (Figure 1A) with cell bodies within the epithelium and a dendrite extending until the apical side. Axon bundles were also distinguishable under the basal lamina. To identify supporting cells, we used ERMN as their marker[13,15] and observed a staining of the apical part of the epithelium, mutually exclusive with TUJ1 staining (Figure 1D).

Although it is well known that in rodents, several proteins of the transduction cascade are expressed in the apical dendritic knob and ciliary regions of olfactory sensory neurons, in humans, the expression and cellular localization of most of these proteins have not been investigated yet. Immunostaining with antibodies against adenylyl cyclase type 3 (AC3) and the Ca^{2+}-activated Cl^{-} channel TMEM16B revealed the expression of both proteins in the apical knob and ciliary region of the TUJ1-positive neurons (Figures 1B and 1C).

These results extend previous immunohistochemistry data showing that AC3 and TMEM16B are localized in the dendritic knob and cilia of human olfactory sensory neurons, where olfactory transduction takes place.

Voltage-gated currents in human olfactory sensory neurons and supporting cells

Since a very limited number of studies have attempted to measure the electrophysiological properties of human olfactory sensory neurons and these studies have been performed only on isolated neurons, we asked whether it is possible to record the electrical activity from cells in acute slices of the human olfactory epithelium. Slices may provide a more physiological environment to the olfactory neurons and better cell viability, important for obtaining long lasting and stable recordings.

We first established the viability of obtaining electrophysiological recordings by measuring basic electrical properties and voltage-gated currents in the whole-cell voltage-clamp configuration. To visually identify cells, we dissolved Alexa Fluor 594 in the intracellular solution filling the patch pipette and took fluorescence images after obtaining the whole-cell configuration and the diffusion of the fluorophore inside the cell (Figures 2A and 2D). A human olfactory sensory neuron, with its typical morphology comprising a cell body toward the basal part and a dendrite extending to the apical part of the epithelium, is shown in Figure 2A, demonstrating that it is possible to reach a whole-cell configuration and to visually identify neurons in acute slices of the human olfactory epithelium. We then evaluated the resting membrane potential in current clamp at I = 0 in neurons and calculated an average value of -52 ± 5 mV (range -76 to -24 mV, n = 13). The membrane input resistance, estimated in voltage clamp, had an average value of 4.2 ± 1.2 GΩ (range 1.0–9.7 GΩ, n = 12).

Next, we measured voltage-gated currents in human olfactory sensory neurons. Transient inward currents followed by outward currents were activated upon depolarization from a holding potential of -80 mV (Figure 2B). Current-voltage relations were measured at the peak of the inward currents or at the end of the sustained outward currents, averaged from several neurons and plotted in Figure 2C. The average current-voltage relations show that the transient inward current activated between -60 and -50 mV and reached a peak at -30 mV, with an average value of -0.7 ± 0.1 nA (n = 10) and then decreased toward 0 between 50 and 60 mV. Outward currents activated at about -30 mV and increased their amplitude with the depolarizing step potential reaching an average value of 1.1 ± 0.1 nA (n = 10) at +50 mV (Figure 2C).

We also recorded from supporting cells in the whole-cell voltage-clamp configuration. Fluorescence images of supporting cells showed their typical columnar shape with fine processes extending toward the

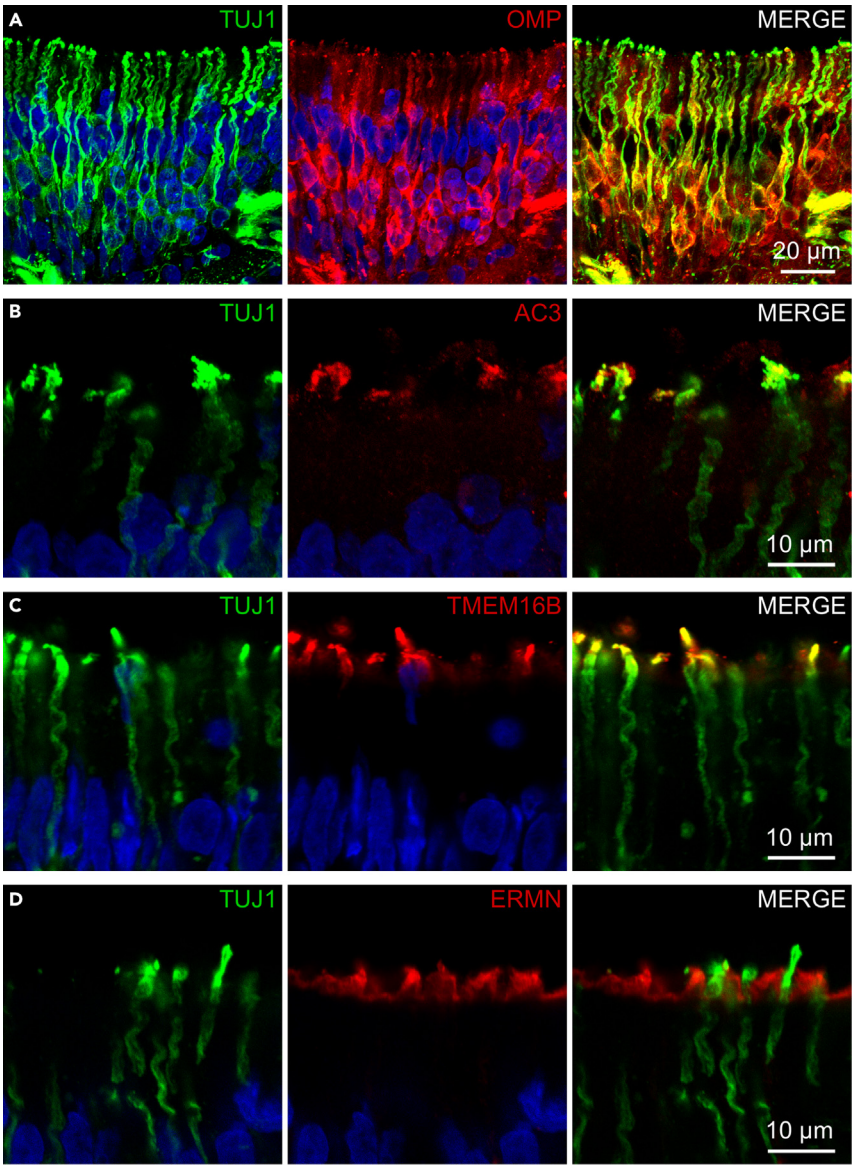

Figure 1. Olfactory sensory neurons from human olfactory epithelium express signal transduction proteins at the apical part

(A) Olfactory sensory neurons stained with the neuronal marker TUJ1 (green) and OMP (red).

(B) Co-expression of TUJ1 (green) and AC3 (red) at the apical part of olfactory sensory neurons.

(C) Co-expression of TUJ1 (green) and TMEM16B (red) at the apical part of olfactory sensory neurons. Note that AC3 and TMEM16B staining are present only in the dendritic knob and ciliary region of the neuron.

(D) Non-overlapping staining for the neuronal marker TUJ1 (green) and ERMN (red), a marker for the apical region of supporting cells. Cell nuclei were stained with DAPI (blue).

basal part of the epithelium (Figure 2D). The average membrane input resistance was 2.2 $\pm$ 0.6 GΩ (range 0.5–7.1 GΩ, n = 12). In a first set of experiments, we elicited voltage-gated currents with the same step protocol used for neurons from a holding potential of −80 mV and measured sustained outward currents (data not shown). As we and others have previously shown that supporting cells in mice also have voltage-activated transient inward currents,[61,62] in a second set of experiments, we lowered the holding potential to −120 mV before applying a depolarizing step protocol, also in this condition no transient inward currents were measured (Figure 2E). Outward currents activated at about −10 mV and increased with the depolarizing step potential (Figure 2F) reaching an average value of 0.7 $\pm$ 0.1 nA (n = 12) at +40 mV.

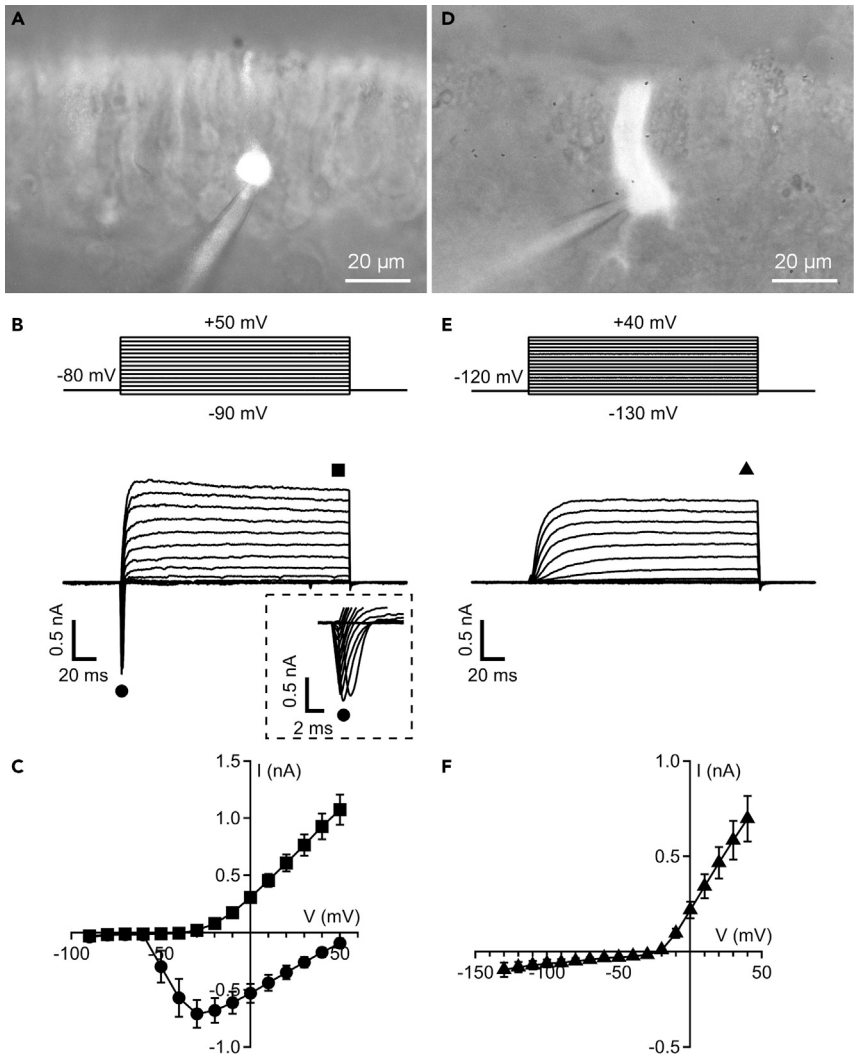

Figure 2. Voltage-gated currents in olfactory sensory neurons and supporting cells from acute slices of the human olfactory epithelium

(A and D) Fluorescence micrographs of an olfactory sensory neuron (A) and a supporting cell (D) filled with Alexa Fluor 594 through the patch pipette.

(B and E) Representative whole-cell currents recorded using the voltage protocols indicated at the top of the panels. The holding potential was −80 mV for olfactory sensory neurons (B) and −120 mV for supporting cells (E). Voltage steps in 10 mV increments were applied. The inset in (B) shows details of the inward currents on an expanded timescale.

(C and F) Plot of average ±SEM amplitudes of inward (black circles) and outward (black squares) currents in olfactory sensory neurons (C, n = 10) and outward (black triangles) currents in supporting cells (F, n = 12) versus the test potential.

These electrophysiological data show that voltage-gated currents in human olfactory sensory neurons have both transient inward currents and outward currents as in other vertebrate species. On the other side, human supporting cells displayed only outward voltage-gated currents, differently from mice, where also transient inward currents have been reported.

Firing patterns of human olfactory sensory neurons

To investigate the firing patterns of human olfactory sensory neurons in the acute slice preparation, we used whole-cell current-clamp recordings. The responses of three representative neurons to current injections from −2 to 10 pA of 2 s duration show the different types of spiking patterns we measured (Figure 3). The neuron at the top in Figure 3 generated a tonic firing consisting of sustained train of action potentials in response to current injection of 2 pA and displayed an increasing number of spikes up to 6 pA current steps.

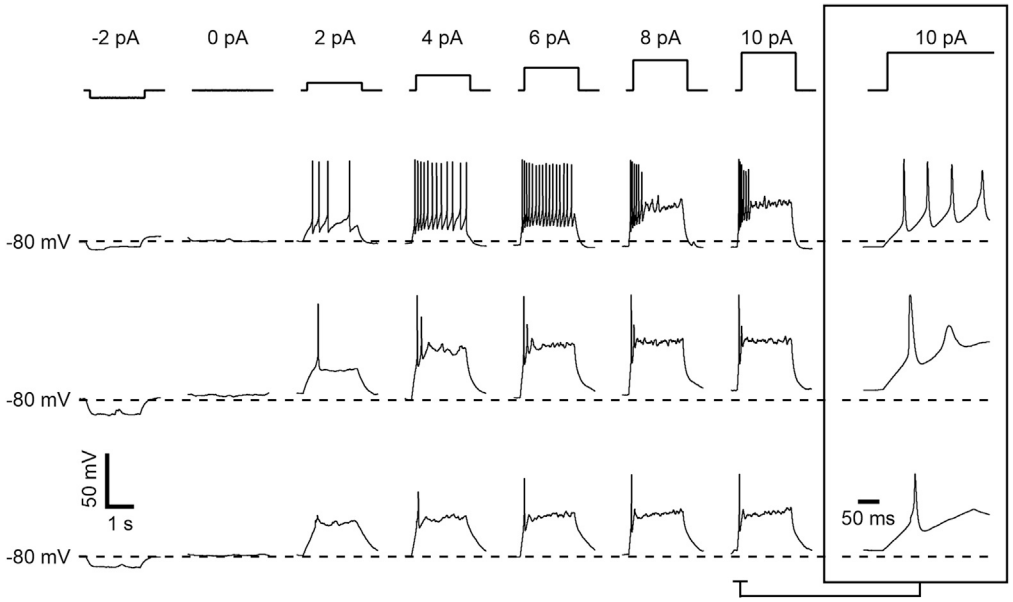

Figure 3. Firing patterns of olfactory sensory neurons recorded from acute slices of the human olfactory epithelium

Spiking activity of three different olfactory sensory neurons recorded in whole-cell current clamp in response to current steps of 2 s duration varying from −2 to 10 pA, with 2 pA increments, as indicated in the upper panel. Insets at the right show the details of firing activity generated with a 10 pA step and plotted on an expanded timescale for each cell.

At higher current injections of 8 and 10 pA, the same neuron generated a phasic firing with a brief train of action potential of decreasing amplitude followed by small oscillations around a voltage plateau. The other two neurons fired only one or two action potentials in response to current injections of 2–4 pA up to 10 pA, followed by a voltage plateau (middle and bottom recordings in Figure 3). Of eight neurons, two displayed tonic firing at current steps between 2 and 6 pA followed by phasic firing at 8 and 10 pA, while six fired only one or a few action potentials.

These experiments show that whole-cell current-clamp experiments in slices from human olfactory epithelium are able to capture the electrophysiological heterogeneity in firing behavior of different olfactory sensory neurons, a characteristic common to other vertebrate species.[36,63,64]

Responses to stimuli

To test if the olfactory transduction cascade is active in neurons of the human olfactory epithelium in acute slice preparation, we applied IBMX, a PDE inhibitor that acts on the transduction cascade by reducing the hydrolysis of cAMP. In the whole-cell voltage-clamp configuration at the holding potential of −80 mV, some neurons did not respond to stimulation with IBMX, although they generated an inward current when a solution containing high K^+ was applied to test the neuron viability (Figure 4A). Other neurons responded to 3 s stimulation of IBMX with an inward current that was slowly increasing its amplitude and then returning to baseline after IBMX removal (Figure 4B). We found that 33% (3 out of 9) of the neurons tested with IBMX displayed an inward current in response to IBMX with an average peak value of -37 ± 18 pA (n = 3), while the average value of the response to high K^+ of the same neurons was -200 ± 17 pA (n = 3). The remaining 67% (6 out of 9) did not respond to IBMX although they responded to high K^+.

We also recorded the spiking pattern in response to IBMX or high K^+ in the current-clamp configuration. The same neuron of Figure 4B displayed firing both in response to IBMX and to high K^+ (Figure 4C). We analyzed the first action potential by using phase plot analysis, in which changes of membrane potentials with time (dV/dt) are plotted as a function of membrane potential (Figure 4D). The action potential is represented by a loop, with the upper and lower parts representing the depolarization and repolarization phases, respectively. Phase plots were rather similar for the first action potential in both IBMX and high K^+ with the following values (Figure 4D): threshold −54 mV for IBMX and −55 mV for high K^+; peak amplitude

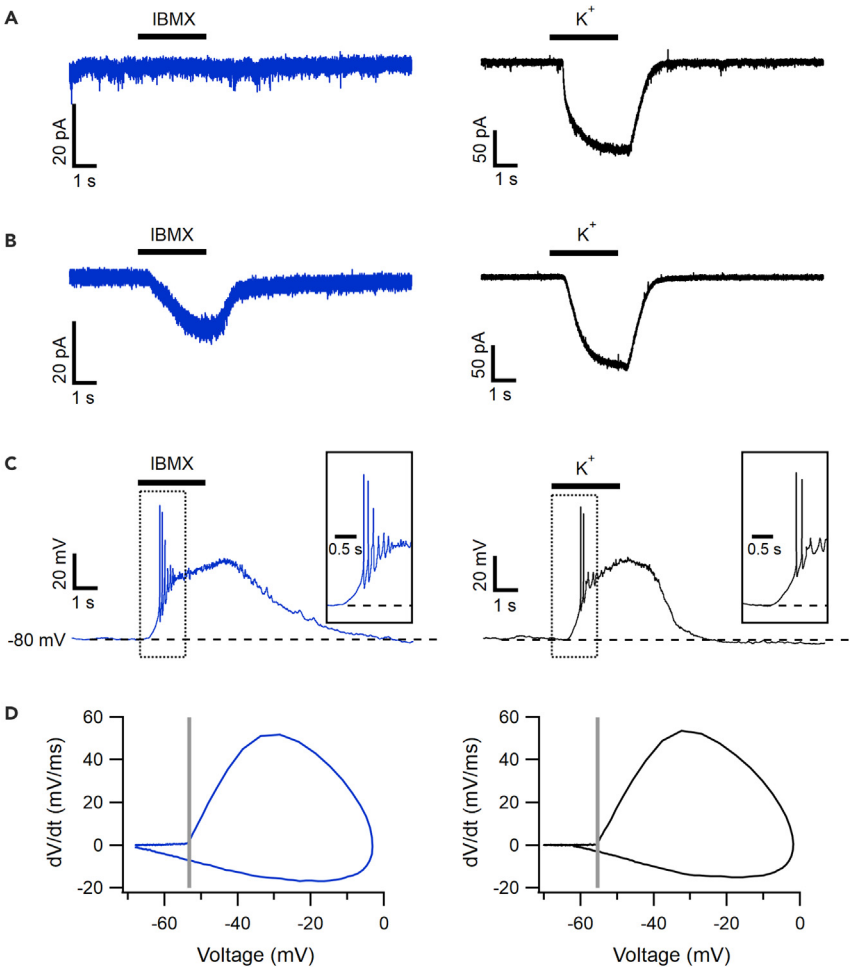

Figure 4. Responses of human olfactory sensory neurons to the phosphodiesterase inhibitor IBMX

(A) Example of an olfactory sensory neuron non-responding to 1 mM IBMX (blue trace; left) but responding to high K^+ with an inward current (black trace; right). Holding potential was −80 mV.

(B) Representative trace of an olfactory sensory neuron responding both to 1 mM IBMX and high K^+ with an inward current.

(C) Spiking activity measured in whole-cell current clamp in the same olfactory sensory neuron shown in (B) stimulated with 1 mM IBMX or high K^+. Insets show details of the spiking activity at the beginning of the stimulation on an expanded timescale.

(D) Phase plots of the first action potentials from the responses shown in (C). The crossing of vertical line with the upper loop indicates the voltage threshold for the first action potential. Stimulus duration for IBMX and high K^+ was 3 s.

−3 mV for IBMX and −2 mV for high K^+; the maximal slope of the depolarization phase was 52 mV/ms for IBMX and 54 mV/ms for high K^+; the maximal slope of the repolarization phase was −17 mV/ms for IBMX and −15 mV/ms for high K^+. Two other neurons responding to IBMX did not reach the voltage threshold for action potential generation.

To investigate if human olfactory sensory neurons in the slice preparation respond to odorants, we prepared two mixtures of odorants (mix 1 and mix 2, see STAR Methods) and recorded current responses under the voltage-clamp configuration at a holding potential of −80 mV. We found that two out of five neurons that we considered viable, as they responded to high K^+, responded to one of the two odorant mixtures with an inward transduction current. In one neuron, the peak amplitude of the current response was −18 pA with odorant mix 1 and -14 pA with IBMX, while mix 2 was not tested (Figure 5A). In another neuron, odorant mix 1 did not activate any current, while mix 2 elicited an inward current of −27 pA peak amplitude (Figure 5B).

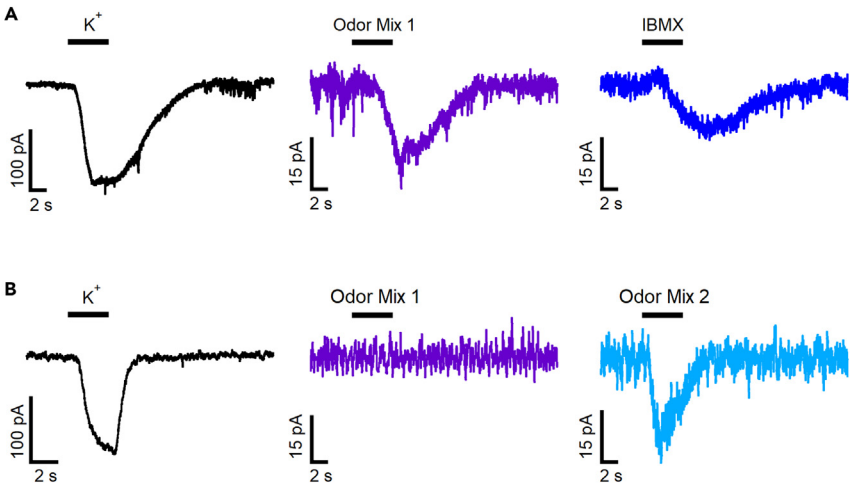

Figure 5. Responses of human olfactory sensory neurons to odorant mixtures

(A) One olfactory sensory neuron responding to high K^+, odorant mix 1, and 1 mM IBMX with inward currents.

(B) Another olfactory sensory neuron non-responding to odorant mix 1 but responding to high K^+ and to odorant mix 2 with an inward current. Holding potential was – 80 mV and stimulus duration was 5 s.

Altogether, these results show that human olfactory sensory neurons in acute slices of the olfactory epithelium have an intact transduction cascade and can respond differently to odorant mixtures. The transduction cascade involves PDE and cAMP which acts as a second messenger, since application of IBMX produces inward currents and elicits action potentials.

DISCUSSION

In this study, we have provided the first demonstration that it is possible to obtain acute slices of the human olfactory epithelium from biopsies that are viable for electrophysiological experiments, crucial to unveil the molecular logic of the very first events of human olfaction.

The resting electrical properties, input resistance, and resting membrane potential, that we measured from human olfactory sensory neurons in slices, were found to be similar to those reported by Restrepo et al.[51] from isolated human olfactory neurons and to those measured in other vertebrates.[60] However, in contrast to previous reports that recorded inward voltage-gated currents in only one out of eleven[51] or one out of fourteen[59] freshly dissociated human olfactory sensory neurons, we consistently recorded both voltage-gated transient inward currents and outward currents in olfactory neurons that were clearly visualized with a fluorescence dye. Our results suggest that avoiding enzymatic dissociation may be crucial for preserving the electrophysiological properties of these neurons. Therefore, recording from slices of the olfactory epithelium is a more suitable approach for studying the functionality of human olfactory sensory neurons.

In addition, we have also successfully recorded voltage-gated currents from human supporting cells and have found notable differences when compared with previous measurements taken in mice. Recordings from supporting cells in mouse acute slices showed the presence of very large leak currents, which could be reduced by using gap junction blockers, while we did not observe any large leak currents in our measurements from human slices. This observation may be due to species-specific differences in the density and/or composition of cellular gap junctions in the olfactory epithelium. Indeed, mouse supporting cells are electrically coupled by gap junctions composed at least by connexin 43 and 45,[65,66] while data about connexins in human supporting cells are still lacking. The composition of connexins within a gap junction can greatly influence its properties, such as sensitivity to changes in voltage and current density.[67] Diverse properties of gap junctions in olfactory supporting cells could lead to distinct electrophysiological properties and intercellular communication patterns, potentially contributing to the observed differences in leak currents between humans and mice.

Moreover, while mouse supporting cells displayed both voltage-gated transient inward currents and outward currents,[61,62] our measurements from human slices consistently showed only outward currents. Interestingly, TMEM16F is expressed in human supporting cells,[15] while in mice, it has only been found in the cilia of olfactory neurons.[68] These biophysical and molecular differences could have significant implications for our understanding of the contribution of supporting cells to the physiology in different species.

In human olfactory sensory neurons, we recorded action potential firing in the current-clamp configuration and observed that some human olfactory neurons responded to small depolarizing current steps of only 2–4 pA and 2 s duration with one or a few spikes, while others displayed a train of action potentials. Increasing current injections up to 10 pA, some neurons displayed tonic firing in the range from 2 to 6 pA, while at higher current injections (8 and 10 pA), the same neurons showed brief action potential trains followed by a voltage plateau. Our findings are consistent with previous measurements in amphibians or rodents, indicating that different firing properties can be displayed also by human olfactory sensory neurons.[36,63,64]

Although the olfactory epithelium from amphibians and rodents has provided insights into the olfactory transduction, the mechanisms underlying this process in human olfactory sensory neurons still need to be understood. While transcriptomic data from the human olfactory epithelium have confirmed the expression of several genes known to be involved in the transduction cascade in rodent olfactory sensory neurons,[8–11] the expression and localization of the proteins have only been confirmed for the alpha and gamma subunits of the G protein using immunostaining data.[11,13] Here, we used immunohistochemistry and showed that AC3, the protein responsible for cAMP production, is expressed in the dendritic knob and cilia of human olfactory neurons, indicating a potential role of cAMP as a second messenger in olfactory transduction in humans, similar to what has been observed in rodents and amphibians. Furthermore, we demonstrated the localization of Ca^{2+}-activated Cl^{-} channel TMEM16B in the dendritic knob and cilia, suggesting that it could have a significant role in human olfactory transduction, similar to previous findings in mice.[35]

By using patch-clamp recordings, we unveiled some crucial elements of the transduction in human olfactory sensory neurons. Specifically, we demonstrated that some olfactory neurons have a basal concentration of cAMP that is hydrolyzed by PDE in resting conditions. Indeed, when we applied the PDE inhibitor IBMX in whole-cell voltage clamp, we recorded an inward current in some viable neurons, but not all. Not only we found that a cAMP increase induced by PDE inhibition with IBMX produced inward currents in voltage clamp but it also elicited action potential firing as measured in the current-clamp configuration. This indicates that cAMP build-up in olfactory sensory neurons can generate transduction currents capable of driving action potential firing.

Previous studies in mice have revealed that the constitutive activity of some odorant receptors leads to spontaneous transduction events in olfactory neurons, while other odorant receptors have a lower activity and do not induce spontaneous events.[44–46] Our experiments with IBMX suggest that human olfactory neuron may also exhibit spontaneous activity, depending on the specific odorant receptor expressed. In rodents, it has been shown that the spontaneous activity of odorant receptors is important to define the glomerular map in the olfactory bulb.[69–71] Whether this also occurs in human is an important question, although difficult to answer.

Recording odorant responses in olfactory sensory neurons is a challenging task, as each neuron only expresses one type of odorant receptor, which is activated by a limited number of odorants. To increase the probability of eliciting a response, we prepared two odorant mixtures that contained compounds known to be ethologically relevant for humans, including some that have previously been shown to activate human odorant receptors *in vitro*.[72–74] In whole-cell voltage clamp, we recorded inward currents in response to each odorant mixture in different human neurons, thus showing that the transduction cascade initiated by odorant binding to specific receptor is fully functional in human olfactory sensory neurons in our slice preparation.

These recorded odorant responses, though not comprehensive, can pave the way for future experiments to understand human olfaction at the periphery by testing a large number of odorants, including food odorants.[74] In the future, calcium imaging from slices could increase the output of responding olfactory sensory neurons in a physiologically relevant context for odorant responses.

Acute slices of the human olfactory epithelium from biopsies are a valuable tool for investigating functional mechanisms behind olfactory dysfunctions, including those related to severe acute respiratory syndrome coronavirus 2 (SARS-CoV-2) infection and to long-term post-COVID-19.[7,19] Morphological changes in the olfactory epithelium of SARS-CoV-2-infected or long-term post-COVID-19 patients[10,18,19] and molecular data on cell types expressing proteins for viral entry[8,9,15] led to various hypotheses on smell loss pathogenesis. Electrophysiological recordings from human olfactory epithelium slices of hyposmic, anosmic, or parosmic patients could reveal changes in biophysical properties and odorant-evoked responses. Pharmacological manipulation would allow probing molecular pathways and characterizing various cell types' contributions. Since the SARS-CoV-2 virus primarily targets supporting cells in the olfactory epithelium, the use of ion-selective microelectrodes could help understand how the epithelial microenvironment changes with the loss of functionality of supporting cells. In addition, we have previously proposed that TMEM16F, which is expressed in human supporting cells,[15] may be involved in COVID-19 pathogenesis in the olfactory epithelium as it has been shown in the lung.[75] Thus, the use of TMEM16F blockers could identify and validate a potential target for treatment of COVID-19-related olfactory loss.

In summary, our data provide the first electrophysiological recordings of odorant responses in human olfactory sensory neurons from acute slices of the olfactory epithelium. We have demonstrated that the transduction mechanism involves PDE and that cAMP serves as a second messenger. Our findings lay the groundwork for future research using acute slices of the human olfactory epithelium, positioning humans as an ideal model for studying olfaction.

Limitations of the study

Data reported in this study are limited to recordings from acute slices of human olfactory epithelium from nasal biopsies of healthy patients. We could not use biopsies from patients with COVID-19 because the biosafety level of our electrophysiological laboratory was not considered sufficient for handling SARS-CoV-2-infected tissues. Another limitation of our study is the use of a limited number of odorants that were only tested in mixtures. Nonetheless, we proved that human olfactory sensory neurons in acute slices respond to odorants and paved the way for a more comprehensive future functional characterization.

STAR★METHODS

Detailed methods are provided in the online version of this paper and include the following:

- KEY RESOURCES TABLE
- RESOURCE AVAILABILITY
  - Lead contact
  - Materials availability
  - Data and code availability
- EXPERIMENTAL MODEL AND STUDY PARTICIPANT DETAILS
  - Human nasal tissue
- METHOD DETAILS
  - Immunohistochemistry
  - Preparation of acute slices of human nasal tissue
  - Electrophysiological recordings
  - Experiments were performed at room temperature (20–25°C)
- QUANTIFICATION AND STATISTICAL ANALYSIS

ACKNOWLEDGMENTS

We thank the patients who gave their consent for this study.

AUTHOR CONTRIBUTIONS

A.M., A.H.C., and M.D. conceptualized the project and designed experiments. A.H.C. and K.G.V. performed immunohistochemistry and confocal microscopy. A.H.C., C.A.S.T., G.G., C.R., and F.A.M. made slices, performed patch-clamp recordings and data analysis. P.B.R., M.T., P.B., and G.T. collected human biopsies. A.M., M.D., and A.H.C. wrote the manuscript with comments from all the other authors.

DECLARATION OF INTERESTS

The authors declare no competing financial interests.

INCLUSION AND DIVERSITY

We worked to ensure gender balance in the recruitment of human subjects.

Received: April 13, 2023
Revised: May 19, 2023
Accepted: June 16, 2023
Published: June 21, 2023

REFERENCES

1. Iannuzzi, L., Salzo, A.E., Angarano, G., Palmieri, V.O., Portincasa, P., Saracino, A., Gelardi, M., Dibattista, M., and Quaranta, N. (2020). Gaining Back What Is Lost: Recovering the Sense of Smell in Mild to Moderate Patients After COVID-19. Chem. Senses *45*, 875–881. https://doi.org/10.1093/chemse/bjaa066.

2. Parma, V., Ohla, K., Veldhuizen, M.G., Niv, M.Y., Kelly, C.E., Bakke, A.J., Cooper, K.W., Bouysset, C., Pirastu, N., Dibattista, M., et al. (2020). More Than Smell-COVID-19 Is Associated With Severe Impairment of Smell, Taste, and Chemesthesis. Chem. Senses *45*, 609–622. https://doi.org/10.1093/chemse/bjaa041.

3. Cecchetto, C., Di Pizio, A., Genovese, F., Calcinoni, O., Macchi, A., Dunkel, A., Ohla, K., Spinelli, S., Farruggia, M.C., Joseph, P.V., et al. (2021). Assessing the extent and timing of chemosensory impairments during COVID-19 pandemic. Sci. Rep. *11*, 17504. https://doi.org/10.1038/s41598-021-96987-0.

4. Gerkin, R.C., Ohla, K., Veldhuizen, M.G., Joseph, P.V., Kelly, C.E., Bakke, A.J., Steele, K.E., Farruggia, M.C., Pellegrino, R., Pepino, M.Y., et al. (2021). Recent Smell Loss Is the Best Predictor of COVID-19 Among Individuals With Recent Respiratory Symptoms. Chem. Senses *46*, bjaa081. https://doi.org/10.1093/chemse/bjaa081.

5. Boscolo-Rizzo, P., Hummel, T., Hopkins, C., D'Alessandro, A., Menini, A., Dibattista, M., and Tirelli, G. (2022). Comprehensive Chemosensory Psychophysical Evaluation of Self-reported Gustatory Dysfunction in Patients With Long-term COVID-19: A Cross-sectional Study. JAMA Otolaryngol. Neck Surg. *148*, 281–282. https://doi.org/10.1001/jamaoto.2021.3993.

6. Butowt, R., Bilinska, K., and von Bartheld, C.S. (2023). Olfactory dysfunction in COVID-19: new insights into the underlying mechanisms. Trends Neurosci. *46*, 75–90. https://doi.org/10.1016/j.tins.2022.11.003.

7. Boscolo-Rizzo, P., Hummel, T., Invitto, S., Spinato, G., Tomasoni, M., Emanuelli, E., Tofanelli, M., Cavicchia, A., Grill, V., Vaira, L.A., et al. (2023). Psychophysical assessment of olfactory and gustatory function in post-mild COVID-19 patients: A matched case-control study with 2-year follow-up. Int. Forum Allergy Rhinol. https://doi.org/10.1002/alr.23148.

8. Brann, D.H., Tsukahara, T., Weinreb, C., Lipovsek, M., Van den Berge, K., Gong, B., Chance, R., Macaulay, I.C., Chou, H.-J., Fletcher, R.B., et al. (2020). Non-neuronal expression of SARS-CoV-2 entry genes in the olfactory system suggests mechanisms underlying COVID-19-associated anosmia. Sci. Adv. *6*, eabc5801. https://doi.org/10.1126/sciadv.abc5801.

9. Fodoulian, L., Tuberosa, J., Rossier, D., Boillat, M., Kan, C., Pauli, V., Egervari, K., Lobrinus, J.A., Landis, B.N., Carleton, A., and Rodriguez, I. (2020). SARS-CoV-2 Receptors and Entry Genes Are Expressed in the Human Olfactory Neuroepithelium and Brain. iScience *23*, 101839. https://doi.org/10.1016/j.isci.2020.101839.

10. Khan, M., Yoo, S.-J., Clijsters, M., Backaert, W., Vanstapel, A., Speleman, K., Lietaer, C., Choi, S., Hether, T.D., Marcelis, L., et al. (2021). Visualizing in deceased COVID-19 patients how SARS-CoV-2 attacks the respiratory and olfactory mucosae but spares the olfactory bulb. Cell *184*, 5932–5949.e15. https://doi.org/10.1016/j.cell.2021.10.027.

11. Durante, M.A., Kurtenbach, S., Sargi, Z.B., Harbour, J.W., Choi, R., Kurtenbach, S., Goss, G.M., Matsunami, H., and Goldstein, B.J. (2020). Single-cell analysis of olfactory neurogenesis and differentiation in adult humans. Nat. Neurosci. *23*, 323–326. https://doi.org/10.1038/s41593-020-0587-9.

12. Morrison, E.E., and Costanzo, R.M. (1992). Morphology of olfactory epithelium in humans and other vertebrates. Microsc. Res. Tech. *23*, 49–61. https://doi.org/10.1002/jemt.1070230105.

13. Holbrook, E.H., Wu, E., Curry, W.T., Lin, D.T., and Schwob, J.E. (2011). Immunohistochemical characterization of human olfactory tissue. Laryngoscope *121*, 1687–1701. https://doi.org/10.1002/lary.21856.

14. Morrison, E.E., and Costanzo, R.M. (1990). Morphology of the human olfactory epithelium. J. Comp. Neurol. *297*, 1–13. https://doi.org/10.1002/cne.902970102.

15. Hernandez-Clavijo, A., Gonzalez-Velandia, K.Y., Rangaswamy, U., Guarneri, G., Boscolo-Rizzo, P., Tofanelli, M., Gardenal, N., Sanges, R., Dibattista, M., Tirelli, G., and Menini, A. (2022). Supporting Cells of the Human Olfactory Epithelium Co-Express the Lipid Scramblase TMEM16F and ACE2 and May Cause Smell Loss by SARS-CoV-2 Spike-Induced Syncytia. Cell. Physiol. Biochem. *56*, 254–269. https://doi.org/10.33594/000000531.

16. Moran, D.T., Rowley, J.C., Jafek, B.W., and Lovell, M.A. (1982). The fine structure of the olfactory mucosa in man. J. Neurocytol. *11*, 721–746. https://doi.org/10.1007/BF01153516.

17. Graziadei, P.P., and Graziadei, G.A. (1979). Neurogenesis and neuron regeneration in the olfactory system of mammals. I. Morphological aspects of differentiation and structural organization of the olfactory sensory neurons. J. Neurocytol. *8*, 1–18. https://doi.org/10.1007/BF01206454.

18. Zazhytska, M., Kodra, A., Hoagland, D.A., Frere, J., Fullard, J.F., Shayya, H., McArthur, N.G., Moeller, R., Uhl, S., Omer, A.D., et al. (2022). Non-cell-autonomous disruption of nuclear architecture as a potential cause of COVID-19-induced anosmia. Cell *185*, 1052–1064.e12. https://doi.org/10.1016/j.cell.2022.01.024.

19. Finlay, J.B., Brann, D.H., Abi Hachem, R., Jang, D.W., Oliva, A.D., Ko, T., Gupta, R., Wellford, S.A., Moseman, E.A., Jang, S.S., et al. (2022). Persistent post–COVID-19 smell loss is associated with immune cell infiltration and altered gene expression in olfactory epithelium. Sci. Transl. Med. *14*, eadd0484. https://doi.org/10.1126/scitranslmed.add0484.

20. Kleene, S.J. (2008). The electrochemical basis of odor transduction in vertebrate olfactory cilia. Chem. Senses *33*, 839–859. https://doi.org/10.1093/chemse/bjn048.

21. Pifferi, S., Menini, A., and Kurahashi, T. (2010). Signal Transduction in Vertebrate Olfactory Cilia. In The Neurobiology of Olfaction Frontiers in Neuroscience, A. Menini, ed. (CRC Press/Taylor & Francis).

22. Boccaccio, A., Menini, A., and Pifferi, S. (2021). The cyclic AMP signaling pathway in the rodent main olfactory system. Cell Tissue Res. *383*, 429–443. https://doi.org/10.1007/s00441-020-03391-7.

23. Genovese, F., Reisert, J., and Kefalov, V.J. (2021). Sensory Transduction in Photoreceptors and Olfactory Sensory Neurons: Common Features and Distinct

Characteristics. Front. Cell. Neurosci. *15*, 761416. https://doi.org/10.3389/fncel.2021.761416.

24. Kaupp, U.B. (2010). Olfactory signalling in vertebrates and insects: differences and commonalities. Nat. Rev. Neurosci. *11*, 188–200. https://doi.org/10.1038/nrn2789.

25. Nakamura, T., and Gold, G.H. (1987). A cyclic nucleotide-gated conductance in olfactory receptor cilia. Nature *325*, 442–444. https://doi.org/10.1038/325442a0.

26. Kurahashi, T. (1990). The response induced by intracellular cyclic AMP in isolated olfactory receptor cells of the newt. J. Physiol. *430*, 355–371. https://doi.org/10.1113/jphysiol.1990.sp018295.

27. Zufall, F., Firestein, S., and Shepherd, G.M. (1994). Cyclic nucleotide-gated ion channels and sensory transduction in olfactory receptor neurons. Annu. Rev. Biophys. Biomol. Struct. *23*, 577–607. https://doi.org/10.1146/annurev.bb.23.060194.003045.

28. Pifferi, S., Boccaccio, A., and Menini, A. (2006). Cyclic nucleotide-gated ion channels in sensory transduction. FEBS Lett. *580*, 2853–2859. https://doi.org/10.1016/j.febslet.2006.03.086.

29. Kleene, S.J., and Gesteland, R.C. (1991). Calcium-activated chloride conductance in frog olfactory cilia. J. Neurosci. *11*, 3624–3629. https://doi.org/10.1523/JNEUROSCI.11-11-03624.1991.

30. Kurahashi, T., and Yau, K.W. (1993). Co-existence of cationic and chloride components in odorant-induced current of vertebrate olfactory receptor cells. Nature *363*, 71–74. https://doi.org/10.1038/363071a0.

31. Stephan, A.B., Shum, E.Y., Hirsh, S., Cygnar, K.D., Reisert, J., and Zhao, H. (2009). ANO2 is the cilial calcium-activated chloride channel that may mediate olfactory amplification. Proc. Natl. Acad. Sci. USA *106*, 11776–11781. https://doi.org/10.1073/pnas.0903304106.

32. Pifferi, S., Dibattista, M., and Menini, A. (2009). TMEM16B induces chloride currents activated by calcium in mammalian cells. Pflügers Archiv *458*, 1023–1038. https://doi.org/10.1007/s00424-009-0684-9.

33. Pifferi, S., Cenedese, V., and Menini, A. (2012). Anoctamin 2/TMEM16B: a calcium-activated chloride channel in olfactory transduction: Anoctamin 2/TMEM16B in olfactory transduction. Exp. Physiol. *97*, 193–199. https://doi.org/10.1113/expphysiol.2011.058230.

34. Pietra, G., Dibattista, M., Menini, A., Reisert, J., and Boccaccio, A. (2016). The Ca2+-activated Cl- channel TMEM16B regulates action potential firing and axonal targeting in olfactory sensory neurons. J. Gen. Physiol. *148*, 293–311. https://doi.org/10.1085/jgp.201611622.

35. Dibattista, M., Pifferi, S., Boccaccio, A., Menini, A., and Reisert, J. (2017). The long tale of the calcium activated Cl^- channels in olfactory transduction. Channels *11*, 399–414. https://doi.org/10.1080/19336950.2017.1307489.

36. Firestein, S., and Werblin, F.S. (1987). Gated currents in isolated olfactory receptor neurons of the larval tiger salamander. Proc. Natl. Acad. Sci. USA *84*, 6292–6296. https://doi.org/10.1073/pnas.84.17.6292.

37. Kurahashi, T., and Shibuya, T. (1990). Ca2(+)-dependent adaptive properties in the solitary olfactory receptor cell of the newt. Brain Res. *515*, 261–268. https://doi.org/10.1016/0006-8993(90)90605-b.

38. Kawai, F., Kurahashi, T., and Kaneko, A. (1996). T-type Ca2+ channel lowers the threshold of spike generation in the newt olfactory receptor cell. J. Gen. Physiol. *108*, 525–535. https://doi.org/10.1085/jgp.108.6.525.

39. Borisy, F.F., Ronnett, G.V., Cunningham, A.M., Juilfs, D., Beavo, J., and Snyder, S.H. (1992). Calcium/calmodulin-activated phosphodiesterase expressed in olfactory receptor neurons. J. Neurosci. *12*, 915–923. https://doi.org/10.1523/JNEUROSCI.12-03-00915.1992.

40. Yan, C., Zhao, A.Z., Bentley, J.K., Loughney, K., Ferguson, K., and Beavo, J.A. (1995). Molecular cloning and characterization of a calmodulin-dependent phosphodiesterase enriched in olfactory sensory neurons. Proc. Natl. Acad. Sci. USA *92*, 9677–9681. https://doi.org/10.1073/pnas.92.21.9677.

41. Frings, S., and Lindemann, B. (1991). Current recording from sensory cilia of olfactory receptor cells in situ. I. The neuronal response to cyclic nucleotides. J. Gen. Physiol. *97*, 1–16. https://doi.org/10.1085/jgp.97.1.1.

42. Firestein, S., Darrow, B., and Shepherd, G.M. (1991). Activation of the sensory current in salamander olfactory receptor neurons depends on a G protein-mediated cAMP second messenger system. Neuron *6*, 825–835. https://doi.org/10.1016/0896-6273(91)90178-3.

43. Lowe, G., and Gold, G.H. (1995). Olfactory transduction is intrinsically noisy. Proc. Natl. Acad. Sci. USA *92*, 7864–7868. https://doi.org/10.1073/pnas.92.17.7864.

44. Reisert, J. (2010). Origin of basal activity in mammalian olfactory receptor neurons. J. Gen. Physiol. *136*, 529–540. https://doi.org/10.1085/jgp.201010528.

45. Connelly, T., Savigner, A., and Ma, M. (2013). Spontaneous and sensory-evoked activity in mouse olfactory sensory neurons with defined odorant receptors. J. Neurophysiol. *110*, 55–62. https://doi.org/10.1152/jn.00910.2012.

46. Dibattista, M., and Reisert, J. (2016). The Odorant Receptor-Dependent Role of Olfactory Marker Protein in Olfactory Receptor Neurons. J. Neurosci. *36*, 2995–3006. https://doi.org/10.1523/JNEUROSCI.4209-15.2016.

47. Margolis, F.L. (1972). A brain protein unique to the olfactory bulb. Proc. Natl. Acad. Sci. USA *69*, 1221–1224. https://doi.org/10.1073/pnas.69.5.1221.

48. Dibattista, M., Al Koborssy, D., Genovese, F., and Reisert, J. (2021). The functional relevance of olfactory marker protein in the vertebrate olfactory system: a never-ending story. Cell Tissue Res. *383*, 409–427. https://doi.org/10.1007/s00441-020-03349-9.

49. Malnic, B. (2007). Searching for the ligands of odorant receptors. Mol. Neurobiol. *35*, 175–181. https://doi.org/10.1007/s12035-007-0013-2.

50. Olender, T., Keydar, I., Pinto, J.M., Tatarskyy, P., Alkelai, A., Chien, M.-S., Fishilevich, S., Restrepo, D., Matsunami, H., Gilad, Y., and Lancet, D. (2016). The human olfactory transcriptome. BMC Genom. *17*, 619. https://doi.org/10.1186/s12864-016-2960-3.

51. Restrepo, D., Okada, Y., Teeter, J.H., Lowry, L.D., Cowart, B., and Brand, J.G. (1993). Human olfactory neurons respond to odor stimuli with an increase in cytoplasmic Ca2+. Biophys. J. *64*, 1961–1966. https://doi.org/10.1016/S0006-3495(93)81565-0.

52. Rawson, N.E., Gomez, G., Cowart, B., Brand, J.G., Lowry, L.D., Pribitkin, E.A., and Restrepo, D. (1997). Selectivity and Response Characteristics of Human Olfactory Neurons. J. Neurophysiol. *77*, 1606–1613. https://doi.org/10.1152/jn.1997.77.3.1606.

53. Rawson, N.E., Gomez, G., Cowart, B.J., Kriete, A., Pribitkin, E., and Restrepo, D. (2012). Age-associated loss of selectivity in human olfactory sensory neurons. Neurobiol. Aging *33*, 1913–1919. https://doi.org/10.1016/j.neurobiolaging.2011.09.036.

54. Tareilus, E., Noé, J., and Breer, H. (1995). Calcium signals in olfactory neurons. Biochim. Biophys. Acta *1269*, 129–138. https://doi.org/10.1016/0167-4889(95)00105-2.

55. Leinders-Zufall, T., Rand, M.N., Shepherd, G.M., Greer, C.A., and Zufall, F. (1997). Calcium entry through cyclic nucleotide-gated channels in individual cilia of olfactory receptor cells: spatiotemporal dynamics. J. Neurosci. *17*, 4136–4148. https://doi.org/10.1523/JNEUROSCI.17-11-04136.1997.

56. Leinders-Zufall, T., Greer, C.A., Shepherd, G.M., and Zufall, F. (1998). Imaging odor-induced calcium transients in single olfactory cilia: specificity of activation and role in transduction. J. Neurosci. *18*, 5630–5639. https://doi.org/10.1523/JNEUROSCI.18-15-05630.1998.

57. Gomez, G., Rawson, N.E., Cowart, B., Lowry, L.D., Pribitkin, E.A., and Restrepo, D. (2000). Modulation of odor-induced increases in [Ca(2+)](i) by inhibitors of protein kinases A and C in rat and human olfactory receptor neurons. Neuroscience *98*, 181–189. https://doi.org/10.1016/s0306-4522(00)00112-3.

58. Thüraüf, N., Gjuric, M., Kobal, G., and Hatt, H. (1996). Cyclic nucleotide-gated channels in identified human olfactory receptor neurons. Eur. J. Neurosci. *8*, 2080–2089. https://doi.org/10.1111/j.1460-9568.1996.tb00729.x.

59. Tamari, K., Takeuchi, H., Kobayashi, M., Takeuchi, K., Kurahashi, T., and Yamamoto, T. (2019). Electrical properties of cells from human olfactory epithelium. Auris Nasus Larynx *46*, 734–741. https://doi.org/10.1016/j.anl.2019.01.006.

60. Schild, D., and Restrepo, D. (1998). Transduction mechanisms in vertebrate olfactory receptor cells. Physiol. Rev. *78*, 429–466. https://doi.org/10.1152/physrev.1998.78.2.429.

61. Vogalis, F., Hegg, C.C., and Lucero, M.T. (2005). Ionic conductances in sustentacular cells of the mouse olfactory epithelium. J. Physiol. *562*, 785–799. https://doi.org/10.1113/jphysiol.2004.079228.

62. Henriques, T., Agostinelli, E., Hernandez-Clavijo, A., Maurya, D.K., Rock, J.R., Harfe, B.D., Menini, A., and Pifferi, S. (2019). TMEM16A calcium-activated chloride currents in supporting cells of the mouse olfactory epithelium. J. Gen. Physiol. *151*, 954–966. https://doi.org/10.1085/jgp.201812310.

63. Madrid, R., Sanhueza, M., Alvarez, O., and Bacigalupo, J. (2003). Tonic and phasic receptor neurons in the vertebrate olfactory epithelium. Biophys. J. *84*, 4167–4181. https://doi.org/10.1016/S0006-3495(03)75141-8.

64. Tomaru, A., and Kurahashi, T. (2005). Mechanisms determining the dynamic range of the bullfrog olfactory receptor cell. J. Neurophysiol. *93*, 1880–1888. https://doi.org/10.1152/jn.00303.2004.

65. Zhang, C., Finger, T.E., and Restrepo, D. (2000). Mature olfactory receptor neurons express connexin 43. J. Comp. Neurol. *426*, 1–12. https://doi.org/10.1002/1096-9861(20001009)426:1<1::AID-CNE1>3.0.CO;2-Y.

66. Rash, J.E., Davidson, K.G.V., Kamasawa, N., Yasumura, T., Kamasawa, M., Zhang, C., Michaels, R., Restrepo, D., Ottersen, O.P., Olson, C.O., and Nagy, J.I. (2005). Ultrastructural localization of connexins (Cx36, Cx43, Cx45), glutamate receptors and aquaporin-4 in rodent olfactory mucosa, olfactory nerve and olfactory bulb. J. Neurocytol. *34*, 307–341. https://doi.org/10.1007/s11068-005-8360-2.

67. Spray, D.C. (1996). Physiological Properties of Gap Junction Channels in the Nervous System. In Gap Junctions in the Nervous System Neuroscience Intelligence Unit, D.C. Spray and R. Dermietzel, eds. (Springer), pp. 39–59. https://doi.org/10.1007/978-3-662-21935-5_3.

68. Henkel, B., Drose, D.R., Ackels, T., Oberland, S., Spehr, M., and Neuhaus, E.M. (2015). Co-expression of anoctamins in cilia of olfactory sensory neurons. Chem. Senses *40*, 73–87. https://doi.org/10.1093/chemse/bju061.

69. Yu, C.R., Power, J., Barnea, G., O'Donnell, S., Brown, H.E.V., Osborne, J., Axel, R., and Gogos, J.A. (2004). Spontaneous neural activity is required for the establishment and maintenance of the olfactory sensory map. Neuron *42*, 553–566. https://doi.org/10.1016/s0896-6273(04)00224-7.

70. Imai, T., Suzuki, M., and Sakano, H. (2006). Odorant receptor-derived cAMP signals direct axonal targeting. Science *314*, 657–661. https://doi.org/10.1126/science.1131794.

71. Lorenzon, P., Redolfi, N., Podolsky, M.J., Zamparo, I., Franchi, S.A., Pietra, G., Boccaccio, A., Menini, A., Murthy, V.N., and Lodovichi, C. (2015). Circuit formation and function in the olfactory bulb of mice with reduced spontaneous afferent activity. J. Neurosci. *35*, 146–160. https://doi.org/10.1523/JNEUROSCI.0613-14.2015.

72. Chatelain, P., Veithen, A., Wilkin, F., and Philippeau, M. (2014). Deorphanization and Characterization of Human Olfactory Receptors in Heterologous Cells. Chem. Biodivers. *11*, 1764–1781. https://doi.org/10.1002/cbdv.201400083.

73. Gonzalez-Kristeller, D.C., do Nascimento, J.B.P., Galante, P.A.F., and Malnic, B. (2015). Identification of agonists for a group of human odorant receptors. Front. Pharmacol. *6*, 35. https://doi.org/10.3389/fphar.2015.00035.

74. Haag, F., Di Pizio, A., and Krautwurst, D. (2022). The key food odorant receptive range of broadly tuned receptor OR2W1. Food Chem. *375*, 131680. https://doi.org/10.1016/j.foodchem.2021.131680.

75. Braga, L., Ali, H., Secco, I., Chiavacci, E., Neves, G., Goldhill, D., Penn, R., Jimenez-Guardeño, J.M., Ortega-Prieto, A.M., Bussani, R., et al. (2021). Drugs that inhibit TMEM16 proteins block SARS-CoV-2 spike-induced syncytia. Nature *594*, 88–93. https://doi.org/10.1038/s41586-021-03491-6.

76. Aigouy, B., and Mirouse, V. (2013). ScientiFig: a tool to build publication-ready scientific figures. Nat. Methods *10*, 1048. https://doi.org/10.1038/nmeth.2692.

77. Shimazaki, R., Boccaccio, A., Mazzatenta, A., Pinato, G., Migliore, M., and Menini, A. (2006). Electrophysiological properties and modeling of murine vomeronasal sensory neurons in acute slice preparations. Chem. Senses *31*, 425–435. https://doi.org/10.1093/chemse/bjj047.

78. Dibattista, M., Mazzatenta, A., Grassi, F., Tirindelli, R., and Menini, A. (2008). Hyperpolarization-Activated Cyclic Nucleotide-Gated Channels in Mouse Vomeronasal Sensory Neurons. J. Neurophysiol. *100*, 576–586. https://doi.org/10.1152/jn.90263.2008.

79. Wong, W.M., Nagel, M., Hernandez-Clavijo, A., Pifferi, S., Menini, A., Spehr, M., and Meeks, J.P. (2018). Sensory Adaptation to Chemical Cues by Vomeronasal Sensory Neurons. eNeuro *5*. ENEURO.0223-18.2018. https://doi.org/10.1523/ENEURO.0223-18.2018.

80. Sarno, N., Hernandez-Clavijo, A., Boccaccio, A., Menini, A., and Pifferi, S. (2022). Slow Inactivation of Sodium Channels Contributes to Short-Term Adaptation in Vomeronasal Sensory Neurons. eneuro *9*. ENEURO.0471-21.2022. https://doi.org/10.1523/ENEURO.0471-21.2022.

81. Agostinelli, E., Gonzalez-Velandia, K.Y., Hernandez-Clavijo, A., Kumar Maurya, D., Xerxa, E., Lewin, G.R., Dibattista, M., Menini, A., and Pifferi, S. (2021). A Role for STOML3 in Olfactory Sensory Transduction. eNeuro *8*. ENEURO.0565-20.2021. https://doi.org/10.1523/ENEURO.0565-20.2021.

STAR★METHODS

KEY RESOURCES TABLE

REAGENT or RESOURCE	SOURCE	IDENTIFIER
Antibodies		
Polyclonal goat anti-OMP	Wako	Cat# 019–22291; RRID:AB_664696
Monoclonal mouse anti-β Tubulin III	BioLegend	Cat# 801202; RRID:AB_10063408
Polyclonal rabbit anti-ERMN	Novus	Cat# NBP1-84802; RRID:AB_11039928
Polyclonal rabbit anti-AC3	Santa Cruz	Cat# sc-588; RRID:AB_630839
Polyclonal rabbit anti-TMEM16B	Novus	Cat# NBP1-90739; RRID:AB_11033237
Donkey anti-rabbit Alexa Fluor Plus 594	Life Technologies	Cat# A32754; RRID:AB_2762827
Donkey anti-rabbit Alexa Fluor 488	Life Technologies	Cat# A21206; RRID:AB_2535792
Donkey anti-goat Alexa Fluor 647	Life Technologies	Cat# A32849; RRID:AB_2762840
Donkey anti-mouse Alexa Fluor 594	Life Technologies	Cat# A-21203; RRID:AB_141633
Donkey anti-mouse Alexa Fluor 488	Life Technologies	Cat# A32766; RRID:AB_2762823
Chemicals, peptides, and recombinant proteins		
3-isobutyl-1-methylxanthine (IBMX)	Sigma Aldrich	Cat# I5879
Acetophenone	Sigma Aldrich	Cat# A10701
Cineole	Sigma Aldrich	Cat# C8144
Eugenol	Sigma Aldrich	Cat# E51791
Heptaldehyde	Sigma Aldrich	Cat# H2120
Isoamyl acetate	Sigma Aldrich	Cat# 112674
(R)-(−)-carvone	Sigma Aldrich	Cat# 124931
(S)-(+)-carvone	Sigma Aldrich	Cat# 435759
Geraniol	Sigma Aldrich	Cat# 163333
Hexanal	Sigma Aldrich	Cat# 115606
7-hydroxycitronellal	Sigma Aldrich	Cat# 82934
(R)-(+)-limonene	Sigma Aldrich	Cat# 183164
Octanal	Sigma Aldrich	Cat# O5608
Software and algorithms		
ImageJ	National Institute of Health https://imagej.net/ij/index.html	RRID:SCR_003070
Micromanager	University of California at San Francisco https://micro-manager.org/	RRID:SCR_016865
NIS-Elements Nikon	Nikon https://www.microscope.healthcare.nikon.com/en_EU/products/software	RRID:SCR_014329
pClamp 10.6 PC software	Molecular Devices https://www.moleculardevices.com/products	RRID:SCR_011323
Clampfit 10.6	Molecular Devices https://www.moleculardevices.com/products	RRID:SCR_011323
Igor Pro 8 software	WaveMetrics https://www.wavemetrics.com/	RRID:SCR_000325

RESOURCE AVAILABILITY

Lead contact

Further information and requests for resources should be directed to and will be fulfilled by the lead contact, Anna Menini (anna.menini@sissa.it).

Materials availability

This study did not generate new unique reagents.

Data and code availability

- All data reported in this paper will be shared by the lead contact upon request.
- This paper does not report original code.
- Any additional information required to reanalyze the data reported in this paper is available from the lead contact upon request.

EXPERIMENTAL MODEL AND STUDY PARTICIPANT DETAILS

Human nasal tissue

Samples from human nasal tissue were obtained at the Section of Otolaryngology of the Department of Medical, Surgical and Health Sciences, University of Trieste, Trieste, Italy. The study was approved by the Ethics Committee on Clinical Investigation of the University of Trieste (nr 232/2016 and 110/2021), Friuli Venezia Giulia Region (CEUR-17236), each patient provided written informed consent and all experiments conform to the regulatory standards.

Biopsies were performed in the operating room from patients under general anesthesia at the end of the scheduled endoscopic sinonasal surgery. Two-three biopsy specimens were obtained from one nostril from the superior septum within the olfactory cleft and adjacent to the middle turbinate using a sickle knife and Blakesley forceps or cupped forceps. Once collected, biopsy specimens to be used for electrophysiology were immediately immersed in ice-cold artificial cerebrospinal fluid (ACSF) containing (in mM): 120 NaCl, 25 $NaHCO_3$, 5 KCl, 1 $CaCl_2$, 1 $MgSO_4$, 10 HEPES, 10 glucose, pH 7.4, while those to be used for immunohistochemistry were immersed in paraformaldehyde (PFA) at 4% in PBS. Samples containing olfactory epithelium were obtained from 9 Caucasian patients (5 males and 4 females, age between 24 and 70 years).

METHOD DETAILS

Immunohistochemistry

Human tissue samples used for immunohistochemistry were fixed in paraformaldehyde (PFA) at 4% in PBS pH 7.4 for 4 to 10 h at 4°C. After fixation, the tissue was kept in PBS pH 7.4 at 4°C, typically from 2 to 24 h. For cryoprotection of biopsies, the tissue was equilibrated overnight in 30% (w/v) sucrose in PBS at 4°C. Then, the tissue was embedded in cryostat embedding medium (BioOptica) and immediately frozen at −80°C. 16 μm sections were cut on a cryostat and mounted on Superfrost Plus Adhesion Microscope Slides (ThermoFisher Scientific). Sections were air-dried for 3 h and used the same day or stored at −20°C for later use. Cryostat embedding medium was removed from the tissue by incubating the slices in PBS for 15 min. The tissue was treated for 15 min with 0.5% (w/v) sodium dodecyl sulfate (SDS) in PBS for antigen retrieval, then washed and incubated in blocking solution (5% normal donkey serum, 0.2% Triton X-100 in PBS) for 90 min and finally incubated overnight at 4°C with the primary antibodies diluted in blocking solution. In the following day, the unbound primary antibodies were removed with PBS washes, then sections were incubated with Alexa Fluor conjugated secondary antibodies (1:500 dilution) in TPBS (0.2% Tween 20 in PBS) for 2 h at room temperature, washed and mounted with Vectashield (Vector Laboratories) or FluoromontG (ThermoFisher). DAPI (5 mg/mL) was added to the solution containing secondary antibody to stain the nuclei.

The following primary antibodies (dilution; catalog number, company) were used: polyclonal goat anti-OMP (1:1000; 019-22291, Wako), monoclonal mouse anti-β Tubulin III (TUJ1) (1:200; 801202, BioLegend), polyclonal rabbit anti-ERMN (1:200; NBP1-84802, Novus). Polyclonal rabbit anti-AC3 (1:100; sc-588, Santa Cruz) and polyclonal rabbit anti-TMEM16B (1:200, NBP1-90739, Novus). The following secondary antibodies were used: donkey anti-rabbit Alexa Fluor Plus 594 (1:500; A32754, Life Technologies), donkey anti-rabbit Alexa Fluor 488 (1:500; A21206, Life Technologies), donkey anti-goat Alexa Fluor 647 (1:500; A32849, Life Technologies), donkey anti-mouse Alexa Fluor 594 (1:500, A-21203, Life Technologies), donkey anti-mouse Alexa Fluor 488 (1:500, A32766, Life Technologies).

Control experiments, excluding primary antibodies, were performed for each immunolocalization. We performed at least 2 independent human tissue replicates for each antibody tested. All attempts at replication were successful.

Z-stack images were acquired using NIS-Elements Nikon software at 1024 × 1024 pixels resolution of each single image and analyzed with ImageJ software (National Institute of Health, USA). Max projections of Z-stacks or individual images within the stacks were used to display results. Figure assembly was performed on ImageJ (National Institutes of Health) using ScientiFig plugin.[76] No image modification was performed other than brightness and contrast adjustment.

Preparation of acute slices of human nasal tissue

Acute slices of human nasal epithelium used for electrophysiological experiments were prepared following a similar protocol to the one used for mouse olfactory and vomeronasal epithelium.[15,62,77–81] Within about 30 min from the biopsy, the human nasal epithelium was embedded in 3% Type I-A agarose (Sigma) prepared in ACSF once the agar had cooled to 38°C. Upon solidification, the agar block was fixed in a glass Petri dish and sliced with a vibratome (Vibratome 1000 Plus, Sectioning System) at 200 to 250 μm thickness in oxygenated ACSF solution. Slices were then left to recover for >30 min in chilled and oxygenated ACSF before electrophysiological experiments were initiated.

Electrophysiological recordings

Slices were transferred to a recording chamber and continuously perfused with oxygenated (95% O2, and 5% CO2) ACSF by gravity flow. Each slice was anchored to the base of the recording chamber using a homemade U-shaped silver wire, holding down the agar support without touching the slice itself. Slices were viewed with an upright microscope (Olympus BX51WI) by infrared differential contrast optics with water immersion 20X or 60X objectives. The olfactory epithelium was easily distinguished from the respiratory one because the first had no moving cilia while the second had long beating cilia.

Whole-cell recordings were performed by patching the soma of the cells. Patch pipettes pulled from borosilicate capillaries (WPI) with a PC-10 puller (Narishige) had a resistance of 3–6 MΩ. The intracellular solution filling the patch pipette contained (in mM) 80 K-Gluconate, 60 KCl, 2 Mg-ATP, 10 HEPES, and 1 EGTA, adjusted to pH 7.2 with KOH. To visualize the morphology of the cell, 0.01 mg/ml Alexa Fluor 594 carboxylic acid (Thermo Fisher, A33082) was dissolved in the patch pipette solution, diffused into the cell and the fluorescence image of the cell was observed under red fluorescence filter. Olfactory sensory neurons and supporting cells were clearly identified by their morphology (Figures 2A and 2D). Recordings in the whole-cell voltage- or current-clamp configurations were obtained with a Multiclamp 700B amplifier controlled by Clampex 10 via a Digidata 1440 (Molecular Devices). Data were low-pass filtered at 2 kHz and sampled at 10 kHz.

Experiments were performed at room temperature (20–25°C)

Responses of olfactory sensory neurons to stimuli were tested with 1 mM 3-isobutyl-1-methylxanthine (IBMX) and two odorant mixtures. Mix 1 was composed of acetophenone, cineole, eugenol, heptaldehyde, isoamyl acetate, while mix 2 was composed of (R)-(−)-carvone, (S)-(+)-carvone, geraniol, hexanal, 7-hydroxycitronellal, (R)-(+)-limonene, octanal. Each odorant was present at 100 μM. For each experiment, the response to high K^+ stimulation was used to evaluate the viability of the neuron and the time of stimulus application. Only olfactory sensory neurons that responded to high K^+ solution were included in the analysis.

1 mM IBMX was prepared weekly by directly dissolving it in ACSF solution. For odorant mixtures, each odorant was dissolved in dimethyl sulfoxide (DMSO) to prepare stock solutions at 5 M and mixtures were prepared by diluting each odorant at a final concentration of 100 μM in ACSF on the day of the experiment.

Stimuli were focally delivered to the neuron through an 8-into-1 multibarrel perfusion pencil connected to a ValveLink8.2 pinch valve perfusion system (AutoMate Scientific). The tip of the perfusion head, with a diameter of 360 μm, was placed ~500 μm away from the slice. To avoid mechanical artifacts, the slice was continuously perfused with ACSF and the flow out of the pipette was switched between ACSF and stimulus solutions.

All chemicals were purchased from Sigma-Aldrich unless otherwise stated.

QUANTIFICATION AND STATISTICAL ANALYSIS

Igor Pro 8 software (WaveMetrics, Lake Oswego, OR, USA) was used for data analysis and figure preparation. All averaged data from individual experiments in different cells are presented as mean ± standard error of the mean (SEM) and number of cells (n). These data were normally distributed (Shapiro-Wilk test).

3.2 Immature olfactory sensory neurons are intrinsically excitable and show maturation-dependent changes in voltage-gated Na^+ and K^+ currents

Chiara Ricci[1*], Cesar Adolfo Sánchez Triviño[1*], Uday Rangaswamy[1], Lorenza Tortella[1], Remo Sanges[1], Anna Boccaccio[2#] and Anna Menini[1#]

[1] Neuroscience Area, SISSA, Scuola Internazionale Superiore di Studi Avanzati, 34136 Trieste, Italy

[2] Institute of Biophysics, CNR, National Research Council, 16149 Genova, Italy

[*]These authors equally contributed

[#]Corresponding authors

Manuscript under revision.

Immature olfactory sensory neurons are intrinsically excitable and show maturation-dependent changes in voltage-gated Na^+ and K^+ currents

Chiara Ricci[1*], Cesar Adolfo Sánchez Triviño[1*], Uday Rangaswamy[1], Lorenza Tortella[1], Remo Sanges[1], Anna Boccaccio[2] and Anna Menini[1]

[1] Neuroscience Area, SISSA, Scuola Internazionale Superiore di Studi Avanzati, 34136 Trieste, Italy

[2] Institute of Biphysics, CNR, National Research Council, 16149 Genova, Italy

[*]These authors equally contributed

corresponding author: Anna Menini (menini@sissa.it), Anna Boccaccio (anna.boccaccio@ibf.cnr.it)

Running title: Immature olfactory sensory neurons

ABSTRACT

Olfactory sensory neurons (OSNs) detect odorants and send electrical signals to glomeruli in the olfactory bulb. Unlike most neurons, OSNs are continuously regenerated throughout life and immature neurons contribute to odorant-evoked responses in glomeruli. However, their intrinsic excitability properties are largely unknown. Here, we used acute slices of the olfactory epithelium from neonatal OMP-GFP mice to visually identify mature and immature OSNs and performed patch-clamp recordings to investigate their functional properties. Loose-patch recordings showed that immature OSNs display spontaneous firing at lower frequency than mature neurons. Whole-cell recordings showed that immature OSNs have more depolarized resting potentials, higher input resistance, fire only with phasic patterns, and generate slower action potentials with more depolarized thresholds. Instead, mature OSNs exhibited both phasic and tonic repetitive firing and faster spike kinetics. Voltage-clamp experiments showed that voltage-gated Na^+ currents in immature OSNs were almost entirely TTX-sensitive, whereas mature OSNs had both TTX-sensitive and TTX-resistant components whose availability depends on membrane potential. Voltage-gated K^+ currents also differed with maturation: immature OSNs lacked a transient component and had only a sustained K^+ current, whereas mature OSNs displayed both a transient component and an increased sustained current. Analysis of single-cell transcriptomic data identified upregulation of some Na^+ and K^+ channel genes during OSN maturation, consistent with the functional changes. Together, these results provide insights into the intrinsic excitability of immature OSNs and show how intrinsic properties change as OSNs mature, providing a foundation for future studies on the role of immature OSNs in sensory processing.

INTRODUCTION

Olfactory sensory neurons (OSNs) in the olfactory epithelium detect odorant molecules from the environment and transduce their binding to odorant receptors (ORs) into action potentials that are transmitted to the olfactory bulb (OB). OSNs are bipolar neurons that extend an axon to OB glomeruli and a dendrite toward the epithelial surface, with several cilia emerging from the apical part of the dendrite. Airborne odorants interact with ORs on these cilia and initiate a well-characterized transduction cascade. The binding of odorants to ORs activates adenylyl cyclase 3 (AC3) via the G protein G_{olf}, leading to a rise in cAMP concentration and the opening of cyclic nucleotide-gated

(CNG) channels that allow Ca^{2+} influx. The increase in intracellular Ca^{2+} concentration activates the Ca^{2+}-activated Cl^- channel TMEM16B (ANO2), generating an inward current that amplifies the CNG current. The resulting depolarization triggers action potentials that are transmitted to the OB [4, 12, 18, 35, 55].

The strategic localization of OSNs at the interface with the external environment enables highly efficient odorant detection, but also makes OSNs particularly vulnerable to environmental stress and damage. However, under physiological conditions, OSNs are continuously replaced throughout life and can also be regenerated after injury. Their lifespan typically ranges from 1 to 3 months, although survival is variable and influenced by both intrinsic and extrinsic factors [17, 28, 34, 39, 41, 45, 48].

Neurogenesis in the olfactory epithelium is sustained by basal stem cells, located near the basal lamina. As newly generated OSNs differentiate, they undergo sequential molecular and morphological changes, with immature OSNs initially expressing the growth-associated protein 43 (Gap43) and the G-protein γ-subunit 8 (Gγ8). Over the course of 7-10 days, these markers are downregulated and mature neurons express the olfactory marker protein (OMP), their well-established marker [24, 33, 39, 50, 60, 63, 69, 72]. Immature OSNs express multiple low-level OR transcripts and components of the cAMP transduction cascade, whereas mature OSNs are well known to express only a single type of OR allele from about 1,000 functional ORs [24, 30, 54, 60]. From a morphological point of view, immature OSNs have short dendrites and their soma are located more basally than those of mature OSNs [20, 21, 48, 49, 67].

At the functional level, mature OSNs have been extensively characterized [32, 47, 66], but little is known about immature OSNs [8, 29]. Cheetham et al. (2016) have shown that immature OSNs can already form functional synapses in the OB and optogenetic photoactivation of their axons elicit robust firing in OB neurons. Moreover, two-photon Ca^{2+} imaging of glomeruli innervated by immature OSNs showed odorant-evoked responses, indicating that these neurons respond to odorants. The response properties of glomeruli innervated by both immature and mature OSNs differed, suggesting that the two neuron populations provide complementary odorant information to individual glomeruli and highlighting the functional relevance of immature OSNs in odorant-evoked responses [29].

Despite their functional relevance, the spontaneous activity and intrinsic excitability properties of immature OSNs remain largely unknown, leaving a gap in our understanding of how these developing neurons contribute to early sensory processing. To address this, we performed patch-clamp recordings in acute slices from neonatal OMP-GFP mice to identify and characterize immature OSNs and compare their properties with those of mature OSNs. We found that immature OSNs are capable of spontaneous firing, though at a lower frequency than mature neurons and have reduced intrinsic excitability. Voltage-gated Na^+ currents showed maturation-dependent changes in activation and TTX sensitivity, while transient A-type K^+ currents were observed only in mature neurons. Analysis of publicly available single-cell transcriptomic data further confirmed differential expression of voltage-gated Na^+ and K^+ channel genes during OSN maturation.

MATERIALS AND METHODS

Ethical approval

Mice were handled in accordance with the guidelines of the Italian Animal Welfare Act and European Union guidelines on animal research, under a protocol approved by the SISSA Animal Care Committee. All experiments were performed on tissues from OMP-GFP mice [56] at postnatal days P0-P4. Every effort was made to minimize the number of animals used.

Acute slices of mouse olfactory epithelium

To obtain acute coronal slices of the olfactory epithelium, P0-P4 mice were decapitated and the heads, after skin removal, were dissected. The method was similar to that previously described [1, 26, 58]. The nose was embedded in 3% Type I-A Agarose prepared in artificial cerebrospinal fluid (ACSF) solution, once the agar had reached a temperature of 37 °C. The ACSF contained (in mM): 120 NaCl, 25 $NaHCO_3$, 5 KCl, 1 $MgSO_4$, 1 $CaCl_2$, 10 HEPES and 10 glucose, pH 7.4. Once solidified, the agar block was fixed in a metal chamber filled with cold, oxygenated ACSF. Coronal slices 300 µm thick were cut using a vibratome (Vibratome 1000 Plus Sectioning System) and kept in cold oxygenated ACSF until use.

Confocal imaging

Imaging was performed on acute coronal slices cut with the vibratome. Slices were fixed in 4% paraformaldehyde (PFA) in phosphate-buffered saline solution (PBS) for 1 hour at 4 °C. After washing in PBS, slices were stained with DAPI (2.5 µg/ml) in 0.2% Tween-20 in PBS for 2 hours at room temperature to label cell nuclei. After additional wash in PBS, slices were mounted with Fluoromount-G (Thermofisher). Images were acquired using a Nikon A1R confocal microscope equipped with a 40X objective. Z-stack images were acquired at a resolution of 1024 x 1024 pixels with a 2X zoom using NIS Elements software (Nikon) and further analyzed with ImageJ 1.54f software (NIH) to merge the different channels. Projections of 18 µm optical sections at maximal intensity were displayed.

Electrophysiological recordings

Acute coronal slices were anchored to the recording chamber using a custom-made U-shaped silver wire and continuously perfused with oxygenated ACSF. All the experiments were performed at room temperature (20-25 °C). The tissue was visualized with an upright microscope (BX51WI Olympus) equipped with a 40x water-immersion objective. Fluorescent neurons were identified using a mercury lamp (U-LH100HG Olympus) and a GFP filter set for GFP-expressing neurons or a red fluorescence filter for Alexa Fluor 594-labelled cells.

Extracellular solutions were delivered through an eight-in-one multibarrel perfusion pencil connected to a ValveLink 8.2 pinch-valve perfusion system (Automate Scientific). The perfusion pencil, with a tip diameter of 360 µm, was positioned approximately 0.5 mm from the slice.

Loose-patch recordings were obtained with patch pipettes of 2-4 MΩ filled with filtered ACSF. Seal resistances of 15-50 MΩ were established on the soma of OSNs to obtain the loose-patch configuration. Spontaneous activity was recorded in voltage-clamp mode with a holding potential of 0 mV.

Whole-cell recordings were performed from the soma of OSNs. For current- and voltage-clamp recordings, patch pipettes of 4-6 MΩ were filled with an intracellular solution containing (in mM): 80 KGluconate, 60 KCl, 2 MgATP, 1 EGTA and 10 HEPES, adjusted to pH 7.2 with KOH. The same solution was used to isolate K^+ currents in voltage-clamp experiments. For Na^+ current isolation, a Cs^+-based intracellular solution was used, containing: 135 CsCl, 5 NaCl, 5 EGTA and 10 HEPES, adjusted to pH 7.2 with NaOH. All intracellular solutions included Alexa Fluor-594 (1 µg/ml) to allow fluorescent visualization of cells (Fig. 1).

Resting membrane potential was measured in current-clamp mode without current injection and input resistance was evaluated in voltage-clamp mode by holding the cell at -80 mV and applying a 10 mV hyperpolarizing pulse.

Voltage-clamp recordings were repeated at least twice and only stable recordings were considered.

Electrophysiological recordings were performed using a Multiclamp 700B amplifier controlled by a Digidata 1550B via the Clampex 10.7 software (Molecular Devices). Data were low-pass filtered at 2 kHz and sampled at 10 or 20 kHz. Patch pipettes were pulled from borosilicate capillaries (WPI) using a PC-10 puller (Narishige).

The following chemicals were prepared as stock solutions as indicated and diluted in ACSF to the final concentrations on the day of the experiment: 1 mM tetrodotoxin citrate (TTX) (Latoxan) and 0.5 M 4-aminopyridine (4-AP) stored at -20 °C; 1 M $CdCl_2$ stored at 4 °C.

All chemicals were obtained from Sigma-Aldrich, unless otherwise specified.

Data analysis and statistics

Data analysis and figure preparation were performed using IgorPro software (Wavemetrics) or ImageJ 1.54f (NIH).

Epifluorescence images taken during electrophysiological experiments were pseudocolored in ImageJ to enhance the visualization of OSNs. The area corresponding to the immature OSN (Fig. 1) was extracted and relocalized using the Intelligent Scissors and Interactive Boundaries tools in GIMP 2.10.28.

All data from different OSNs (n) are presented as mean ± standard deviation (SD). In voltage-clamp experiments, capacitive transients were cut off from figures for clarity.

Loose-patch recordings were filtered with a bandwith from 5 to1500 Hz. Spikes were detected using a custom procedure based on an arbitrary threshold and verified by visual inspection of individual spike shapes. Mean firing frequency was calculated as the total number of spikes divided by 180 s recording duration. The interspike interval (ISI) was defined as the time interval between consecutive spikes, and the instantaneous frequency as the reciprocal of the ISI.

Voltage-gated activation curves were fitted with the Boltzmann equation: $G/G_{max} = 1/\{1+ \exp[(V_{1/2} -V)/k]\}$ where G is the conductance, G_{max} is the maximal conductance, $V_{1/2}$ is the membrane potential at which G is half of G_{max}, V is the membrane potential and k is the slope factor. Statistical analysis was performed using Prism 8 (GraphPad) or IgorPro (Wavemetrics) software. Normal distribution of the data was assessed with the Shapiro-Wilk test and equality of variances with the F test. For normally distributed data with equal variances, an unpaired t-test was used to determine statistical significance. When variances were different, Welch's correction was applied. Not normally distributed data were analyzed with the Mann-Whitney test. For multiple comparisons, one-way ANOVA followed by Tukey's post-hoc test was performed. In the case of not normally distributed data, a Kruskal-Wallis followed by Dunn's post-hoc test was used. For the I-V curves, statistical significance was assessed using a mixed model two-way ANOVA followed by Bonferroni correction.

Cumulative distributions were compared with the Kolmogorov-Smirnov test. P values < 0.05 were considered statistically significant. In the Figures, * indicates $P < 0.05$, ** $P < 0.001$, *** $P < 0.0001$.

Single-cell RNA seq analysis

Single-cell RNA seq analysis was performed on a published dataset of whole olfactory mucosa from five adult male C57BL/6 mice (8-12 weeks old) [7]. Analysis was performed in R (version 4.4.3) using the Seurat (version 5.3.0) [25] package. The raw count matrix and metadata were downloaded from the Gene Expression Omnibus (GEO) under accession number GSE151346. A seurat object was created using the CreateSeuratObject() function from this data. The dataset had been pre-processed for quality control metrics including total RNA counts (nCount_RNA), number of detected genes (nFeature_RNA), mitochondrial gene percentage (percent_mito), and doublet scores. Data were normalized using NormalizeData(), and the top 2000 variable features were identified with FindVariableFeatures(). These features were then scaled using ScaleData(). Principal component analysis was run on the scaled data with RunPCA(), and the first 30 principal components were used to generate a UMAP embedding with the RunUMAP() function.

Cell type refinement and differential expression analysis

To investigate the molecular profiles of mature and immature OSNs in a manner consistent with OSN identification in our electrophysiological experiments, we refined the original annotations of the OSN population. Cells were classified as immature OSNs (iOSNs) if they were negative for *Omp* detection while being positive for either *Gap43* or *Gng8*. All cells positive for *Omp* were classified as mature OSNs (mOSNs). Differential gene expression analysis between these two populations was performed using the FindMarkers() function with default parameters. Genes were considered significantly differentially expressed if they had an adjusted p-value < 0.05, an absolute $\log_2$ fold change > 0.25, and were expressed in at least 5% of cells in either population. Results were visualized using a volcano plot generated with the IgorPro (Wavemetrics) software.

RESULTS

To visually identify immature and mature OSNs, we used OMP-GFP mice, in which GFP fluorescence selectively labels mature OSNs. In olfactory epithelium slices, mature OSNs were easily identified by their GFP signal, whereas immature OSNs were non-fluorescent (Fig. 1A). Among the non-fluorescent cells, immature OSNs were identified based on their bipolar morphology and the location of their soma below the layer of GFP-positive neurons, toward the basal region of the olfactory epithelium. Figure 1B shows the typical bipolar morphology and soma location of an immature OSNs. The image was obtained in the whole-cell configuration, in which a fluorescent dye contained in the intracellular solution diffused into the neuron through the patch pipette, showing its morphology. The soma of the immature, GFP-negative OSN, is located more basally than that of GFP-positive mature OSNs.

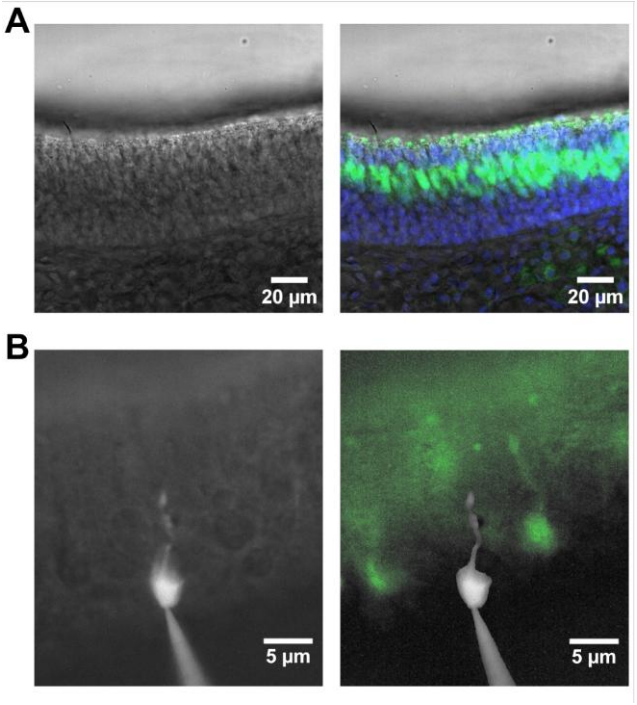

Fig. 1. Imaging of immature and mature OSNs

(A) Confocal images of a 300 µm coronal slice of the olfactory epithelium from a P2 OMP-GFP mouse, cut with a vibratome. Left: brightfield image. Right: merged brightfield and fluorescence images showing DAPI-stained nuclei (blue) and GFP-positive mature OSNs (green). (B) Epifluorescence image of an immature, GFP-negative OSN, filled with Alexa Fluor-594 (shown in white) via the patch pipette in a coronal slice of the olfactory epithelium. Left: overlay of Alexa Fluor-594 fluorescence with the brightfield image, showing the bipolar morphology of the immature neuron. Right: fluorescence image of the same slice showing GFP-positive mature OSNs (green), with the image of the immature neuron extracted from the left panel and superimposed to indicate its relative location.

Immature OSNs display spontaneous activity

Although the basal firing activity of mature OSNs in the absence of odorant stimulation is well established, the spontaneous firing activity of immature OSNs has remained uncharacterized. Using loose-patch recordings from the soma of OSNs in acute slices of the olfactory epithelium, we found that immature OSNs do have spontaneous firing in the absence of external stimuli, showing a wide range of firing patterns with frequencies ranging from 0.20 to 1.81 Hz (Fig. 2A, B, E). In comparison, mature OSNs had frequencies varying from 0.19 to 3.87 Hz (Fig. 2C, D, E). On average, immature OSNs fired at 0.78 ± 0.49 Hz (n = 16), whereas mature OSNs had a significantly higher mean firing frequency of 1.69 ± 0.98 Hz (n = 21; Fig. 2F).

To further analyze these firing patterns, we calculated the interspike interval (ISI) distributions, which describe the probability of occurrence of time intervals between consecutive spikes. Immature OSNs displayed a broad ISI distribution that lacked the prominent peak at short intervals observed in mature neurons (Fig. 2F). This difference is further supported by the instantaneous firing frequency analysis, calculated as the inverse of ISI: the cumulative fraction of events for mature OSNs was significantly shifted to the right compared to that of immature OSNs (Fig. 2G).

Taken together, these results demonstrate that immature OSNs exhibit spontaneous firing activity, characterized by lower firing rates and distinct firing patterns compared to mature OSNs. These findings suggest that neuronal excitability undergoes significant functional changes during OSN maturation.

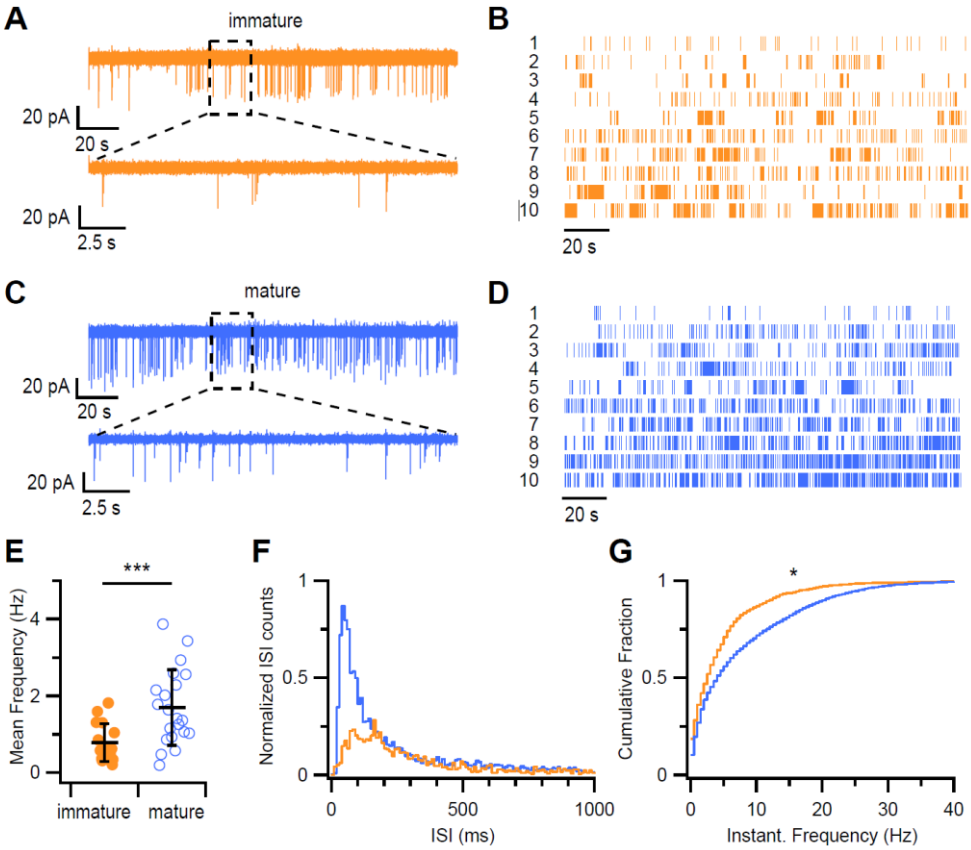

Fig. 2. Spontaneous firing activity differs between immature and mature OSNs
(A, C) Representative loose-patch recordings showing 180 s of spontaneous spiking activity from an immature (A) and a mature (C) OSN. Insets below each trace show regions indicated by the dashed boxes at an expanded time scale. (B, D) Raster plots of spontaneous activity from 10 representative immature (B) and mature (D) OSNs. Each row corresponds to the activity of a single neuron. (E) Scatter plots with averages ± SD of mean spontaneous firing frequencies from immature (n = 16) and mature (n = 21) OSNs (p = 0.0009, one-tailed t-test). (F) Normalized interspike interval (ISI) distributions (bin = 10 ms) for all recorded immature (orange) and mature (blue) OSNs. (G) Cumulative distribution of instantaneous firing frequencies (bin = 0.5 Hz) showing a rightward shift in mature compared to immature OSNs (p = 0.02, Kolmogorov–Smirnov test).

Maturation-dependent changes in evoked firing and membrane properties of OSNs

To further investigate maturation-dependent changes in functional properties, we recorded OSN responses to depolarizing current injections in the whole-cell current-clamp configuration. The membrane potential was held near –65 mV by applying a small holding current when needed, and depolarizing current steps, ranging from 2 to 12 pA, were delivered in 2 pA increments from this baseline.

Immature OSNs responded to current injections with phasic firing patterns, generating one or a few action potentials followed by a sustained depolarized plateau (Fig. 3A). Mature OSNs, instead, had greater heterogeneity in their firing behavior, showing either phasic or tonic firing, with tonic firing characterized by repetitive action potentials throughout the depolarizing step (Fig. 3B, C). No spontaneous activity was observed in immature neurons, whereas some mature neurons (19%, 6 out of 32) fired spontaneously.

Current injections of 2 or 4 pA were sufficient to elicit firing in several immature and mature neurons. Since most neurons fired in response to a 4 pA current step, we selected this amplitude for quantitative analysis. At 4 pA, 57% of immature OSNs (8 out of 14) fired action potentials, while the remaining neurons required a higher current injection of 6 pA. At each current step that elicited firing, immature OSNs responded exclusively with a phasic firing pattern.

In mature OSNs, a 4 pA step evoked firing in 81% of neurons (26 out of 32), with 37% (12 out of 32) showing phasic firing and 44% (14 out of 32) tonic firing, whereas 19% (6 out of 32), did not fire at 4 pA but responded only to higher current injections (6-12 pA).

To compare excitability parameters, we examined the first action potential evoked by the 4 pA step (Fig. 3D-F) and analyzed some of its properties with phase-plot analysis. Immature OSNs had a more depolarized action potential threshold (-40.4 ± 4.8, n = 8) than both phasic (-50.1 ± 6.5 mV, n = 12) and tonic (-55.5 ± 5 mV, n = 14) mature neurons (Fig. 3G). The maximal depolarization and repolarization rates were smaller in immature compared with tonic mature neurons but did not differ significantly from phasic mature neurons (Fig 3H, I). These slower kinetics are consistent with the broader action potential half-width calculated in immature (21.2 ± 9 ms, n = 8) compared with tonic (3.9 ± 2.5 ms, n = 14) and phasic mature neurons (8.5 ± 7.3 ms, n = 12; Fig. 3J).

Passive membrane properties also differed between groups. The resting membrane potential, measured at 0 pA holding current, was more depolarized in immature (–40.7 ± 12 mV, n = 8) than in both phasic (–62 ± 12.8 mV, n = 12) and tonic (–66.4 ± 6.7 mV, n = 14) mature OSNs (Fig. 3K). The input resistance was higher in immature (6.6 ± 2.9 GΩ, n = 8) than in tonic (1.2 ± 0.9 GΩ, n = 14) mature OSNs. A difference was also seen between immature neurons and phasic firing mature neurons (2.7 ± 1.6 GΩ, n = 12), which however did not reach statistical significance (Fig. 3L). Taken together, these results show that OSN maturation is associated with changes in both passive and active membrane properties. Immature neurons had a more depolarized resting potential and higher input resistance compared with mature OSNs. Immature neurons fired only with phasic patterns and had slower action potentials with a more depolarized threshold, whereas mature OSNs showed a diverse excitability profile and the emergence of tonic repetitive firing.

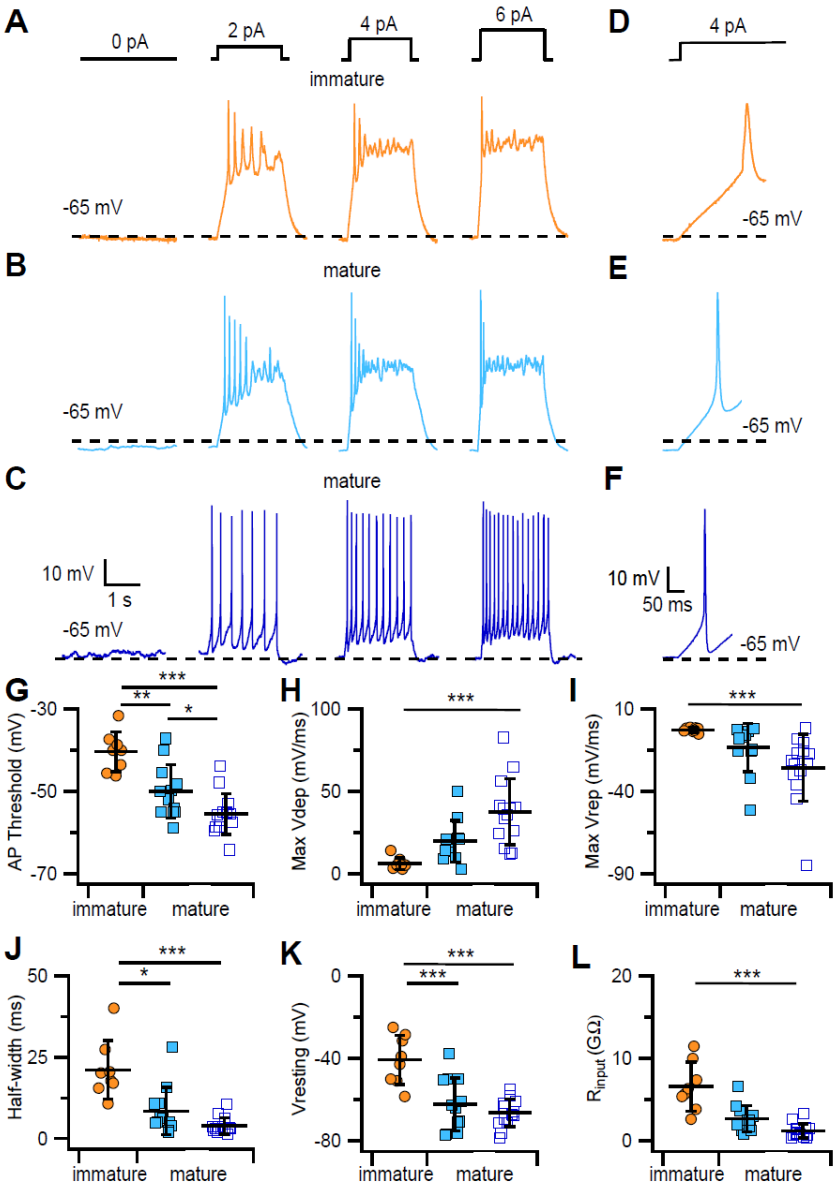

Fig. 3. Evoked firing activity in immature and mature OSNs shows differences in excitability

(A–C) Representative whole-cell current-clamp recordings from immature (A) and mature OSNs (B, C) in response to 2 s current injections of 0, 2, 4, or 6 pA. The immature OSN in (A) displayed a phasic firing pattern, whereas mature OSNs exhibited either phasic (B) or tonic (C) firing patterns. The black dashed lines indicate –65 mV. (D-F) Expanded view of the first action potential evoked by 4 pA current injection from recordings in (A-C). (G–L) Scatter plots with averages ± SD for the indicated properties in immature (orange circles, n = 8), phasic firing (blue filled squares, n = 12) and tonic firing mature OSNs (open squares, n = 14). (G-I) Action potential threshold, maximum depolarization rate (Max Vdep) and maximum repolarization rate (Max Vrep) calculated at 4 pA from phase-plot analysis. (J) Action potential half-width duration at 4 pA. (K) Resting membrane potential. (L) Input resistance. Statistical analysis: data in G and K were analyzed using one-way ANOVA followed by Tukey's post-hoc test, and data in panels H, I, J, and L were analyzed using Kruskal–Wallis test followed by Dunn's post-hoc test. Comparisons showed that immature neurons differed significantly from phasic firing mature neurons (G, $p = 0.002$; K, $p = 2.53 \times 10^{-4}$; H, $p = 0.06$; I, $p = 0.07$; J, $p = 0.048$; L, $p = 0.06$) and from tonic firing mature neurons (G, $p = 2.24 \times 10^{-6}$; K, $p = 1.35 \times 10^{-5}$; H, $p = 7.06 \times 10^{-5}$; I, $p = 2.20 \times 10^{-4}$; J, $p = 5.90 \times 10^{-5}$; L, $p = 3.34 \times 10^{-5}$). Phasic and tonic firing mature neurons did not differ significantly in most panels: G, $p = 0.05$; K, $p = 0.58$; H, $p = 0.11$; I, $p = 0.19$; J, $p = 0.13$; L, $p = 0.08$.

Maturation-dependent changes in voltage-gated currents of OSNs

To investigate the ionic mechanisms underlying differences in excitability, we recorded voltage-gated currents from the same immature and mature OSNs characterized in current-clamp experiments. Currents were measured from a holding potential of -80 mV using 200 ms voltage steps ranging from –90 mV to +50 mV in 10 mV increments. Depolarizing voltage steps elicited transient inward currents followed by outward currents in immature and mature neurons (Fig. 4A-C).

The average current-voltage relationship indicates some differences between immature and mature neurons. For example, the onset of inward currents in immature neurons occurred at about -50 mV, a more depolarized potential compared with the range between -70 mV and -60 mV measured in phasic and tonic firing mature OSNs. Peak inward currents occurred between –20 and -10 mV in immature neurons and at about -30 mV in both phasic and tonic firing mature OSNs (Fig. 4D). Furthermore, outward currents in immature neurons were mainly sustained, whereas mature neurons showed an additional transient peak current at the beginning of the voltage step (Fig. 4A-C, E, F). The average current-voltage relationship indicates that outward current activation occurred at about -10 mV in immature OSNs and between -30 mV and -20 mV in mature neurons (Fig. 4E). Immature neurons had smaller inward and outward current amplitudes compared with tonic firing mature neurons, whereas only outward currents were reduced relative to phasic mature neurons. These observations indicate maturation-dependent changes in voltage-gated currents in OSNs.

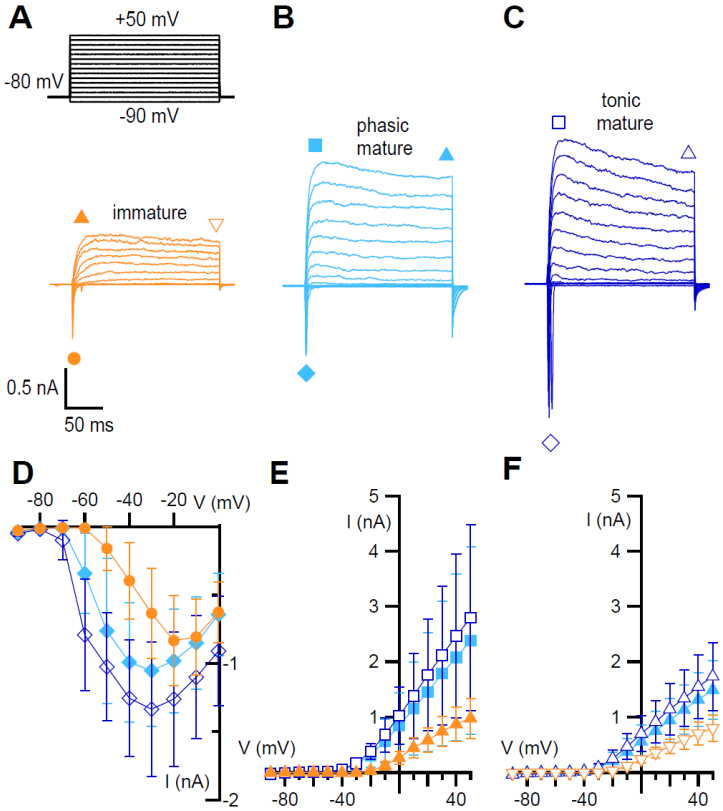

Fig. 4. Current-voltage relationships of immature and mature OSNs

(A-C) Representative whole-cell voltage-clamp recordings from immature (A), phasic firing mature (B), and tonic firing mature (C) OSNs. Voltage steps of 200 ms duration were given from a holding potential of -80 mV to voltages between -90 and +50 mV in 10 mV steps. (D-F) Average ± SD current-voltage relationship for (D) peak inward currents and for outward currents measured at the beginning (E) or at the end (F) of the voltage steps. Recordings were obtained from the same OSNs analyzed in Fig. 3G-L: immature, n = 8; phasic firing mature, n = 12; tonic firing mature, n = 14. Statistical comparisons performed using two-way ANOVA. Immature vs tonic firing mature: D, p = 0.002; E, p = 0.002; F, p = 5.72 x 10^{-4}. Immature vs phasic firing

mature: D, p = 0.44; E, p = 0.02; F, p = 0.004. Phasic firing mature vs tonic firing mature: D, p = 0.01; E, p = 0.48; F, p = 0.29.

To better characterize inward and outward current components, we performed experiments under conditions that selectively isolated voltage-gated Na^+ or K^+ currents (Figs. 5, 6).

To examine how voltage-gated Na^+ currents change during maturation, we used a Cs^+-based intracellular solution to block voltage-gated K^+ channels and, in some experiments, added 100 µM $CdCl_2$, a blocker of voltage-gated Ca^{2+} channels. To investigate whether different Na^+ channel subtypes are functionally expressed in immature and mature OSNs, we took advantage of biophysical and pharmacological differences, such as inactivation properties and sensitivity to TTX. Therefore, we applied prepulses to different potentials (-80 mV vs -110 mV) to modify the availability of Na^+ channels and tested whether Na^+ currents were TTX-sensitive or TTX-resistant (Fig. 5).

In immature OSNs, hyperpolarization of the prepulse from -80 mV to -110 mV produced a small increase in peak current amplitude (-0.63 ± 0.27 nA vs -0.89 ± 0.34 nA, n = 11), indicating that a small fraction of channels were inactivated at -80 mV and hyperpolarization to -110 mV allowed recruitment of additional channels (Fig. 5A, B, E). Activation curves obtained by plotting the normalized conductance versus the step voltages were well fitted by a Boltzmann equation. Hyperpolarizing the prepulse from -80 to -110 mV did not modify either the voltage dependence of activation or the slope factor ($V_{1/2}$: -36.2 ± 6 mV vs -37.2 ± 8.3 mV; k: 6.0 ± 2.3 mV vs 6.0 ± 2.2 mV, n=11; Fig. 5C, D). Application of 200 nM TTX almost completely blocked the current at both prepulse potentials, with an average current block of 89 ± 15 % (n = 4) at – 80 mV and 87 ± 14 % (n = 6) at -110 mV prepulse, indicating that all or the majority of Na^+ currents in immature OSNs are TTX-sensitive (Fig. 5A, B, F).

In mature OSNs, currents showed a stronger dependence on the prepulse potential. Hyperpolarizing the prepulse from -80 mV to -110 mV doubled the average peak current amplitude from -0.70 ± 0.34 nA to -1.40 ± 0.31 nA (n = 10), shifted the voltage dependence of activation to more negative potentials, from $V_{1/2}$ of -40.8 ± 8.6 mV to -54.0 ± 11.4 mV, and increased the slope factor (3.9 ± 2.0 mV vs 4.9 ± 1.9 mV; n = 6) (Fig. 5G-K). Application of 200 nM TTX blocked most of the current at a prepulse of -80 mV (84 ± 12 %, n = 6) but only partially at -110 mV (44 ± 11 %, n = 6), revealing a substantial TTX-resistant component (Fig. 5G, H, L).

In a set of experiments designed to evaluate the possible contribution of Ca^{2+} channels, we added 100 µM $CdCl_2$ to the extracellular solution to block voltage-gated Ca^{2+} channels. The activation curves from a prepulse of -110 mV in the presence of Cd^{2+} were similar to those measured in its absence, showing that voltage-gated Ca^{2+} channels did not significantly contribute to inward currents. In immature OSNs, $V_{1/2}$ and the slope factor were -35.9 ± 5.1 mV and 7.9 ± 2.9 mV (n = 7) in the presence of Cd^{2+}, not significantly different from -37.2 ± 8.3 mV and 6.0 ± 2.2 mV (n=11) measured in the absence of Cd^{2+} (p = 0.72 for $V_{1/2}$; p = 0.14 for k, unpaired t-test). In mature OSNs, the activation parameters were also unaffected by Cd^{2+}: $V_{1/2}$ and the slope factor were -47.8 ± 10.2 mV and 7.2 ± 3.0 mV (n = 15) with Cd^{2+}, compared with -54.0 ± 11.4 mV and 4.9 ± 1.9 mV (n=6) without Cd^{2+} (p = 0.24 for $V_{1/2}$, unpaired t-test; p = 0.13 for k, Mann-Whitney test).

The quantitative comparison of voltage-gated Na^+ currents shows that currents in immature OSNs are mainly carried by TTX-sensitive channels, whereas in mature OSNs both TTX-sensitive and TTX-resistant channels contribute to the total current, with channel availability strongly dependent on prepulse potential, indicating that different Na^+ channel subtypes are functionally expressed during maturation.

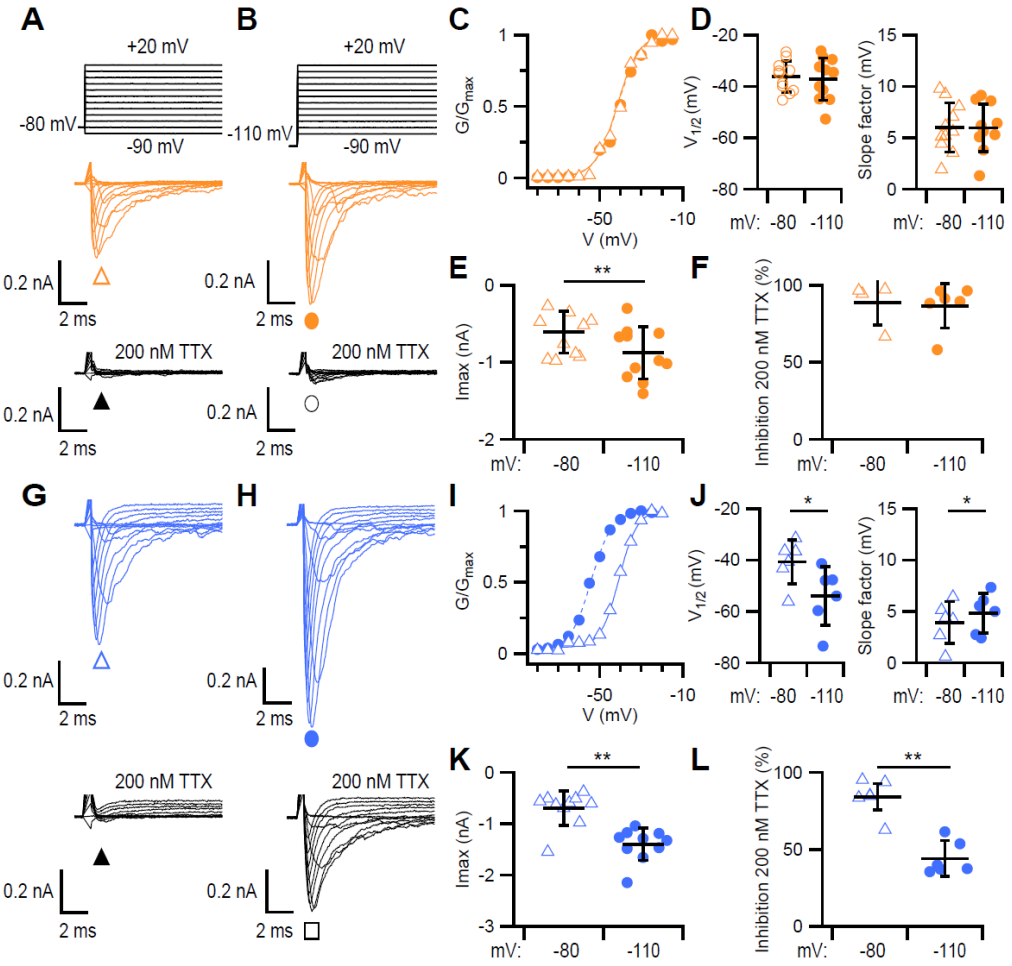

Fig. 5. Changes in Na^+ channel activation and TTX sensitivity across OSN maturation
Representative whole-cell voltage-clamp recordings obtained with a Cs^+-based intracellular solution from immature (A, B) and mature (G, H) OSNs. Voltage steps of 200 ms duration were given from a holding potential of -80 mV to voltages between -90 and +20 mV in 5 mV steps, or from a 100 ms prepulse to –110 mV in control conditions or after application of 200 nM TTX. For clarity, only recordings every 10 mV are shown and capacitive transients were cut off. (C, I) Normalized conductance–voltage relationships for the representative immature (A, B) and mature (G, H) OSNs. Lines are fits to the Boltzmann equation. (D, J) $V_{1/2}$ and k values from Boltzmann fits. Immature OSNs (D): p = 0.34 for $V_{1/2}$; p = 0.83 for k, (paired t-test, n = 11); mature OSNs (J): p = 0.03 for $V_{1/2}$; p = 0.03 for k (Wilcoxon test, n = 6). (E, K) Maximal peak inward currents from prepulses of -80 or -110 mV. Immature OSNs (E): p = 0.001 (paired t-test, n = 11); mature OSNs (K), p = 0.002 (Wilcoxon test, n=10). (F, L) Percentage of maximal current inhibited by 200 nM TTX from prepulse of -80 or -110 mV. Immature OSNs (F), p = 0.35, n = 4 at -80 mV and n = 6 at -110 mV; mature OSNs (L), p = 0.002, n = 6 at -80 mV and -110 mV (Mann-Whitney test). (D-F, J-L) Data are presented as scatter plots with averages ± SD.

To isolate voltage-gated K^+ currents, we recorded from a holding potential of -80 mV and blocked voltage-gated Na^+ and Ca^{2+} channels with 1 µM TTX and 100 µM $CdCl_2$. Currents were recorded in response to 600 ms depolarizing steps ranging from -50 mV to + 50 mV in 10 mV increments (Fig. 6A). Consistent with data shown in Fig. 4, outward currents in immature neurons were mainly sustained, whereas mature neurons showed both transient and sustained components. These differences are more evident in Fig. 6A and B, where isolation of K^+ currents and the longer step duration (600 ms instead of 200 ms) allow the distinct kinetic components to be more clearly

resolved. In immature neurons, the current-voltage relationship measured at the onset and at the end of the voltage steps were nearly identical, indicating the absence of a transient component (Fig. 6 B, C). In mature neurons, instead, currents were larger at the beginning than at the end of the voltage step over the -20 and +50 mV range, reflecting the presence of a transient component (Fig. 6A, C). Furthermore, the amplitude of outward currents was higher in mature compared to immature OSNs (Fig. 6C).

To further characterize the outward current components in mature OSNs, we combined biophysical and pharmacological approaches. First, we applied the same series of depolarizing steps either from a holding potential of -80 mV or after a depolarizing prepulse to +20 mV designed to inactivate the transient current (Fig. 6A, D). Subtracting the prepulse-inactivated current from the total current revealed a clear transient current followed by a plateau (Fig. 6E). We next examined the pharmacological sensitivity of the outward currents using 4-aminopyridine (4-AP), a well-established blocker of transient K^+ currents [22, 61, 62]. Both application of 5 mM 4-AP abolished the transient component and subtraction of the 4-AP-resistant current from the total current gave current kinetics similar to those obtained with the prepulse protocol (Fig. 6F, G). On average, both experimental procedures produced similar current-voltage relationships for the transient current, as well as comparable amplitudes of the remaining plateau currents, indicating that the two approaches isolated the same current components (Fig. 6H, I).

The comparison of voltage-gated K^+ currents shows the absence of a transient component in immature OSNs, whereas mature OSNs have a prominent transient, 4-AP–sensitive K^+ current, indicating a maturation-dependent change in voltage-gated K^+ channels.

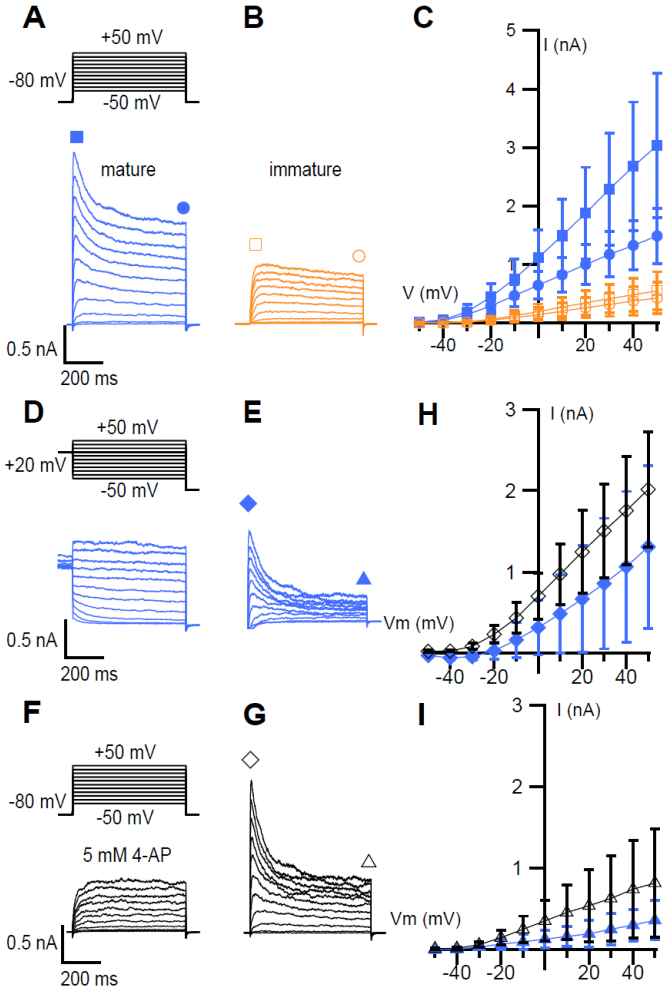

Fig. 6. Voltage-gated K^+ current components differ between immature and mature OSNs

(A) Representative whole-cell voltage-clamp recordings obtained from mature (A) or immature (B) OSNs using a K^+-based intracellular solution. The extracellular solution contained 1 μM TTX and 100 μM $CdCl_2$. Voltage-gated K^+ currents were elicited by 800 ms voltage steps from a holding potential of -80 mV to voltages between -50 and +50 mV in 10 mV steps. (C) Average ± SD current-voltage relationship measured at the beginning (squares) or end (circles) of the voltage steps in immature (orange, n = 13) and mature (blue, n = 28). Statistical comparisons by two-way ANOVA: mature beginning vs end, $p = 1.33 \times 10^{-6}$; immature beginning vs end, p = 0.28; mature vs immature at beginning: $p = 2.72 \times 10^{-8}$, mature vs immature at end, $p = 5.14 \times 10^{-9}$. (D) Representative currents from mature OSN elicited from an 800 ms prepulse potential of +20 mV to inactivate transient currents. (E) Difference current obtained by subtracting the prepulse-inactivated current in (D) from the total current in (A). (F) Block of the transient current component following application of 5 mM 4-AP. (G) Difference current obtained by subtracting the 4-AP blocked current in (F) from the total current in (A). (H, I) Average ± SD current-voltage relationships for the subtracted currents measured at the beginning (diamonds) or at the end (triangles) of the voltage steps in mature OSNs (H: p = 0.1; I: p = 0.1, two-way ANOVA, n = 6)

Public scRNA-seq data analysis suggests a maturation-linked transcriptional shift related to voltage-gated Na^+ and K^+ channels

To investigate the molecular basis underlying the electrophysiological differences in voltage-gated currents between immature and mature OSNs, we analyzed their transcriptional profiles using a published single-cell RNA sequencing dataset of the whole olfactory mucosa from C57BL/6 mice [7]**.** The original study assigned cell types to 29,585 cells based on canonical marker gene enrichment within unsupervised clusters. We further refined the annotation of OSNs by classifying as immature cells lacking *Omp* expression but expressing *Gap43* or *Gng8*, whereas cells expressing *Omp* were classified as mature OSNs (Fig. 7A) [24]. We then performed differential gene expression analysis between mature and immature OSNs (Supplementary Table1) and specifically examined genes encoding voltage-gated Ca^{2+} α subunits, Na^+ α and b subunits, and K^+ channels of the *Shaker-, Shab-, Shaw-,* and *Shal*-related families (Fig. 7B) [22]. However, while no genes related to voltage-gated Ca^{2+} channels resulted upregulated, several Na^+ channel genes were upregulated in mature OSNs, including *Scn5a*, *Scn8a* and *Scn9a*, which encode the $Na_v1.5$, $Na_v1.6$ and $Na_v1.7$ α-subunits, respectively, as well as *Scn3b* and *Scn4b*, which encode the β3 and β4 auxiliary subunits (Fig. 7B). $Na_v1.6$ and $Na_v1.7$ are TTX-sensitive channels, whereas $Na_v1.5$ is TTX-resistant [19].

Voltage-gated K^+ channel genes were also upregulated in mature OSNs, including *Kcnc2*, *Kcna4*, *Kcna5*, *Kcna6* and *Kcnb1*, with *Kcnc4* showing the highest statistical significance (Fig. 7B). These genes encode the $K_v1.2$, $K_v3.4$, $K_v1.5$, $K_v1.6$ and $K_v2.1$ channels, respectively. $K_v3.4$ channels primarily mediate fast-inactivating A-type K^+ currents, whereas $K_v1.2$, $K_v1.5$, $K_v1.6$ and $K_v2.1$ channels mainly contribute to non-inactivating or slowly inactivating delayed rectifier K^+ currents [22].

No genes related to the examined voltage-gated channel families were significantly downregulated.

These transcriptional differences indicate an upregulation of some Na^+ and K^+ channel genes during OSN maturation, consistent with the functional diversification of voltage-gated currents measured in immature and mature OSNs.

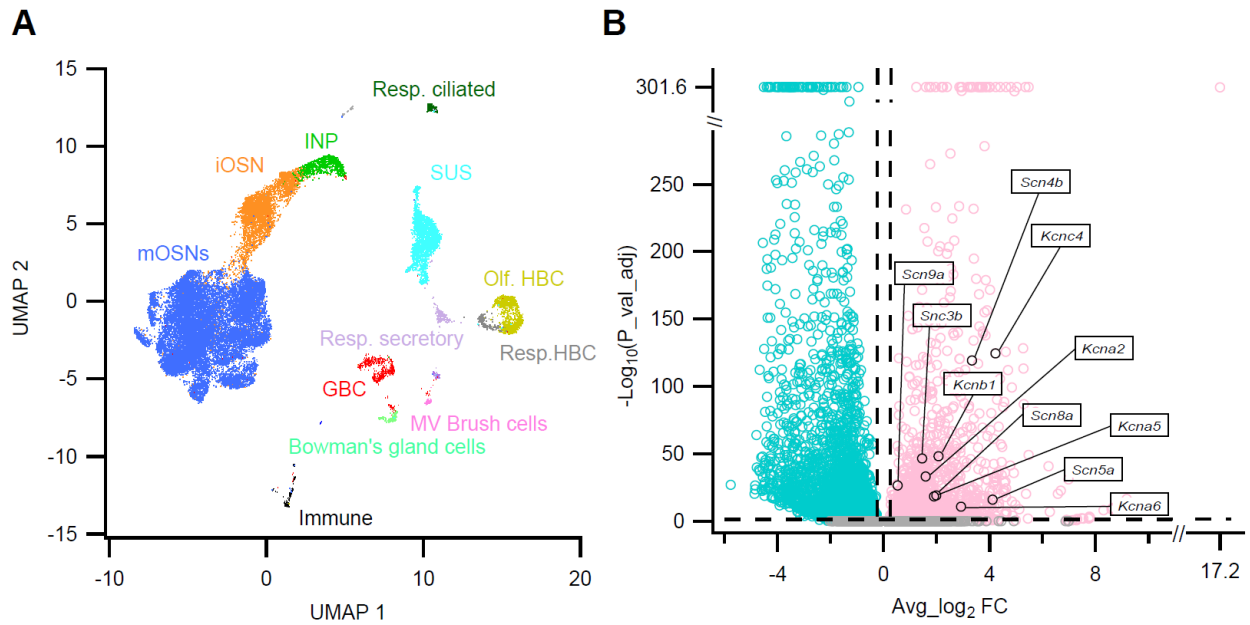

Fig. 7. scRNA-seq analysis reveals differential expression of voltage-gated channel genes in mature and immature OSNs

(A) Uniform Manifold Approximation and Projection (UMAP) plot from the whole olfactory mucosa dataset from Brann et al., 2020. Mature OSNs (mOSNs, blue) are *Omp*+ and immature OSNs (iOSNs, orange) are *Omp*$^{-}$ and *Gap43*$^{+}$ or *Gng8*$^{+}$. (B) Volcano plot of differentially expressed genes between mOSNs and iOSNs. Genes encoding voltage-gated Na^{+} and K^{+} channel subunits are highlighted. Dashed vertical lines indicate $\log_2$ fold-change thresholds at ±0.25, and the dashed horizontal line marks the adjusted P-value cutoff at 0.05. Upregulated Na^{+} channel genes in mOSNs include *Scn5a*, *Scna8* and *Scn9a* (α subunits) and *Scn3b* and *Scn4b* (β subunits); upregulated K^{+} channel genes in mOSNs include *Kcna2*, *Kcnc4*, *Kcna5*, *Kcna6* and *Kcnb1*.

DISCUSSION

In this study, we investigated maturation-dependent functional properties of OSNs from neonatal OMP-GFP mice. While mature OSNs have been extensively characterized electrophysiologically, no information is available on immature neurons. Our results show maturation-dependent changes in spontaneous activity, intrinsic excitability and the expression of voltage-gated channels.

Using loose-patch recordings, we found that immature OSNs fire spontaneously, showing that they are functionally active before completing maturation. Their firing activity is characterized by lower firing rates and distinct firing patterns compared with mature OSNs, indicating that neuronal excitability undergoes significant functional changes during OSN maturation. Since spontaneous activity is crucial for the establishment and refinement of synaptic connections within the OB [42, 74], intrinsic firing in immature OSNs may play an essential role to initiate and stabilize appropriate synaptic contacts in the OB [8].

Mature OSNs express only a single type of OR and their spontaneous activity primarily is triggered by the stochastic activation of that OR and the downstream cAMP-dependent transduction cascade. It has been shown that firing frequency depends on the specific OR expressed by each neuron [10, 51, 52, 57]. Instead, immature OSNs can express multiple OR transcripts and some components of the transduction cascade [24, 65, 68], suggesting that more than one OR may contribute to their spontaneous activity. Differences in spontaneous firing between immature and mature OSNs are therefore likely to arise from multiple factors, including OR expression, variation in the maturation

of the transduction cascade, as well as from intrinsic excitability properties. In this context, our data showed that immature OSNs are less intrinsically excitable than mature ones, as we will discuss later.

The use of OMP-GFP mice, in which GFP replaces the OMP coding sequence and OMP is therefore absent in both mature and immature OSNs, not only allows the visualization of mature OSNs but also ensures that spontaneous activity is independent of OMP. OMP has long been established as a marker for mature OSNs and plays a role in their responsiveness to odorants [11]. Recently, it has been shown that OMP regulates odorant response kinetics by modulating cAMP sequestration [13, 38, 53, 59]. Since basal OR activity contributes to regulate basal cAMP levels [57], modulation of cAMP dynamics by OMP can influence OSN spontaneous firing patterns [13, 53]. Although OMP knockout and heterozygous mice have similar mean firing rates, their firing pattern distributions differ [53]. Furthermore, OMP deletion particularly reduces spontaneous activity in OSNs expressing high basal activity ORs, such as M71, with weaker effects on low basal activity ORs, such as mOR-EG [13]. Thus, using the OMP-GFP line ensures that the observed differences in spontaneous firing between immature and mature OSNs cannot be attributed to OMP, which is absent in both groups.

To address the lack of information on the intrinsic membrane properties of immature OSNs, we performed whole-cell current-clamp and voltage-clamp recordings and found that OSN maturation is accompanied by pronounced changes in both passive and active membrane properties. Immature neurons had a more depolarized resting potential, higher input resistance, a more depolarized action potential threshold, and slower action potential kinetics compared with mature OSNs. Immature OSNs fired only with phasic patterns, whereas mature OSNs showed a broader range of excitability and were capable of tonic repetitive firing. Thus, whole-cell patch-clamp recordings provide direct evidence that immature OSNs are intrinsically less excitable than mature neurons, and this reduced intrinsic excitability likely contributes to the lower spontaneous firing activity measured in loose-patch recordings.

Regarding passive properties, the combination of a depolarized resting potential and high input resistance likely contribute to the reduced excitability of immature OSNs: although higher input resistance would amplify depolarizing inputs, the more depolarized resting potential cause inactivation of a fraction of voltage-gated Na^+ channels, reducing action potential generation.

Comparison with previous studies in adult animals shows that the resting membrane potential, input resistance and the presence of both phasic and tonic firing patterns in mature OSNs measured in our study are in general agreement with previous reports across multiple species, including humans [15, 27, 31, 37, 40, 44, 46, 58, 66, 70], whereas recordings from immature OSNs have not previously been reported.

To investigate the ion channels underlying maturation-dependence differences in excitability, we performed voltage-clamp recordings. Our experiments showed clear changes in voltage-gated Na^+ and K^+ currents. In immature OSNs, Na^+ currents were almost entirely TTX-sensitive, whereas in mature OSNs we observed both TTX-sensitive and TTX-resistant components. Moreover, the strong dependence of channel availability on prepulse potential further indicates that the expression of Na^+ channel subtypes changes during maturation. These physiological differences are consistent with our analysis of single-cell RNA sequencing data [7], which shows that mature OSNs upregulate genes encoding $Na_v1.5$, $Na_v1.6$ and $Na_v1.7$ α-subunits, along with β3 and β4 auxiliary subunits of Na_v channels. Among these channels, $Na_v1.5$ is known to be TTX-resistant, whereas $Na_v1.6$ and $Na_v1.7$ are TTX-sensitive [19], strongly suggesting that $Na_v1.5$ is responsible for the TTX-resistant Na^+ current measured in mature OSNs.

Our results on mature OSNs are in agreement with previous studies: Frenz et al. (2014) recorded both TTX-sensitive and TTX-resistant Na^+ currents in dissociated OSNs from adult mice and showed that they contribute to spontaneous firing activity [14, 16]. Their RT-PCR and immunohistochemistry data identified $Na_v1.5$ as the only TTX-resistant channel, localized specifically to dendrites. In addition, another finding consistent with our results comes from microarray mRNA profiling in OMP-GFP mice, which demonstrated that $Na_v1.5$ is expressed in mature OSNs but not in immature neurons

[64]. Together, these findings suggest that the TTX-resistant $Na_v1.5$ is a characteristic feature of OSN maturation.

Regarding TTX-sensitive channels, RT-PCR in previous studies detected mRNA for multiple Na_v α-subunits, including $Na_v1.2$, $Na_v1.3$, $Na_v1.6$ and $Na_v1.7$, but immunohistochemistry showed that only $Na_v1.3$, and $Na_v1.7$ are expressed at the protein level in OSNs [2, 5, 16, 73]. Thus, although our analysis of single-cell RNA sequencing data [7] indicates upregulation of $Na_v1.6$ and $Na_v1.7$ in mature OSNs, protein expression appears limited to $Na_v1.7$. Together, these results indicate that the TTX-sensitive component is primarily mediated by $Na_v1.3$ and $Na_v1.7$, with Na_v 1.7 expression increasing in mature OSNs.

Among the β-subunits, we observed upregulation β3 and β4, which modulate neuronal excitability by interacting with α-subunits and modifying channel gating [6]. For example, the β4 subunit has been linked to negative shifts in the activation curve of several Na_v subtypes [9, 75]. Therefore, differences in Na^+ current properties during OSN maturation may arise not only from the differential expression of expression of α-subunits but also from modulatory β subunits. In addition, post-translational modifications, such as phosphorylation or glycosylation, may further influence the kinetics and voltage-dependence of Na_v channels [36, 77].

Also voltage-gated K^+ currents showed pronounced maturation-dependent differences. Mature OSNs had a transient, 4-AP–sensitive K^+ current, whereas immature OSNs lacked a transient component. Both immature and mature neurons showed a sustained K^+ current, likely mediated by delayed rectifiers, but the amplitude of this sustained current was much larger in mature OSNs. From analysis of single-cell RNA sequencing data [7], we found that mature OSNs upregulate multiple voltage-gated K^+ channel genes, including $K_v1.2$, $K_v1.5$, $K_v1.6$, $K_v2.1$ and $K_v3.4$. Among these, $K_v3.4$ is known to mediate fast-inactivating A-type K^+ currents [22], suggesting it is the primary contributor to the transient component observed in mature OSNs. The other upregulated K_v channels mainly generate non-inactivating or slowly inactivating delayed rectifier K^+ currents [22], consistent with the larger amplitude of the sustained K^+ current in mature compared with immature OSNs.

Our results, showing both transient and sustained K^+ current components in mature OSNs, are in agreement with previous reports in several species [3, 15, 23, 37, 43, 44, 71, 76]. In addition, our transcriptional analysis identified $K_v3.4$ as a likely mediator of the transient A-type K^+ current in mature OSNs, in agreement with microarray mRNA profiling in OMP-GFP mice showing $K_v3.4$ expression in mature but not in immature OSNs [64]. Although other genes associated with A-type K^+ currents, $K_V1.4$, $K_v4.2$ and $K_v4.3$, have been reported in adult mouse OSNs (Han & Lucero, 2006), our analysis did not detect their differential expression, further indicating the specific role of $K_v3.4$ in OSN maturation.

In summary, our data provide a previously uncharacterized functional profile for immature OSNs, defined by a reduced excitability, the absence of TTX-resistant Na^+ currents, reduced sustained K^+ currents, and the lack of A-type K^+ currents, compared with mature OSNs. The progressive changes during maturation produce increased excitability, broader firing patterns, and faster action potential kinetics of mature OSNs. Transcriptomic analysis identified upregulation of some Na^+ and K^+ channel genes during OSN maturation, further supporting the functional diversification of voltage-gated currents during the transition from immature to mature OSNs.

REFERENCES

1. Agostinelli E, Gonzalez-Velandia KY, Hernandez-Clavijo A, Maurya DK, Xerxa E, Lewin GR, Dibattista M, Menini A, Pifferi S (2021) A Role for STOML3 in Olfactory Sensory Transduction. eNeuro 8. doi: 10.1523/ENEURO.0565-20.2021

2. Ahn H-S, Black JA, Zhao P, Tyrrell L, Waxman SG, Dib-Hajj SD (2011) Nav1.7 is the predominant sodium channel in rodent olfactory sensory neurons. Mol Pain 7:32. doi: 10.1186/1744-8069-7-32

3. Boccaccio A (2018) Patch-Clamp Recordings from Mouse Olfactory Sensory Neurons. Methods Mol Biol 1820:113–122. doi: 10.1007/978-1-4939-8609-5_9

4. Boccaccio A, Menini A, Pifferi S (2021) The cyclic AMP signaling pathway in the rodent main olfactory system. Cell Tissue Res 383:429–443. doi: 10.1007/s00441-020-03391-7

5. Bolz F, Kasper S, Bufe B, Zufall F, Pyrski M (2017) Organization and Plasticity of Sodium Channel Expression in the Mouse Olfactory and Vomeronasal Epithelia. Front Neuroanat 11:28. doi: 10.3389/fnana.2017.00028

6. Brackenbury WJ, Isom LL (2011) Na Channel β Subunits: Overachievers of the Ion Channel Family. Front Pharmacol 2:53. doi: 10.3389/fphar.2011.00053

7. Brann DH, Tsukahara T, Weinreb C, Lipovsek M, Van den Berge K, Gong B, Chance R, Macaulay IC, Chou H-J, Fletcher RB, Das D, Street K, de Bezieux HR, Choi Y-G, Risso D, Dudoit S, Purdom E, Mill J, Hachem RA, Matsunami H, Logan DW, Goldstein BJ, Grubb MS, Ngai J, Datta SR (2020) Non-neuronal expression of SARS-CoV-2 entry genes in the olfactory system suggests mechanisms underlying COVID-19-associated anosmia. Sci Adv 6:eabc5801. doi: 10.1126/sciadv.abc5801

8. Cheetham CEJ, Park U, Belluscio L (2016) Rapid and continuous activity-dependent plasticity of olfactory sensory input. Nat Commun 7:10729. doi: 10.1038/ncomms10729

9. Chen Y, Yu FH, Sharp EM, Beacham D, Scheuer T, Catterall WA (2008) Functional properties and differential neuromodulation of Na(v)1.6 channels. Mol Cell Neurosci 38:607–615. doi: 10.1016/j.mcn.2008.05.009

10. Connelly T, Savigner A, Ma M (2013) Spontaneous and sensory-evoked activity in mouse olfactory sensory neurons with defined odorant receptors. Journal of Neurophysiology 110:55–62. doi: 10.1152/jn.00910.2012

11. Dibattista M, Al Koborssy D, Genovese F, Reisert J (2021) The functional relevance of olfactory marker protein in the vertebrate olfactory system: a never-ending story. Cell Tissue Res 383:409–427. doi: 10.1007/s00441-020-03349-9

12. Dibattista M, Pifferi S, Boccaccio A, Menini A, Reisert J (2017) The long tale of the calcium activated Cl^- channels in olfactory transduction. Channels 11:399–414. doi: 10.1080/19336950.2017.1307489

13. Dibattista M, Reisert J (2016) The Odorant Receptor-Dependent Role of Olfactory Marker Protein in Olfactory Receptor Neurons. J Neurosci 36:2995–3006. doi: 10.1523/JNEUROSCI.4209-15.2016

14. Dionne VE (2016) Spontaneously active NaV1.5 sodium channels may underlie odor sensitivity. J Neurophysiol 116:776–783. doi: 10.1152/jn.00114.2016

15. Firestein S, Werblin FS (1987) Gated currents in isolated olfactory receptor neurons of the larval tiger salamander. Proc Natl Acad Sci U S A 84:6292–6296. doi: 10.1073/pnas.84.17.6292

16. Frenz CT, Hansen A, Dupuis ND, Shultz N, Levinson SR, Finger TE, Dionne VE (2014) NaV1.5 sodium channel window currents contribute to spontaneous firing in olfactory sensory neurons. J Neurophysiol 112:1091–1104. doi: 10.1152/jn.00154.2014

17. Gaun V, Martens JR, Schwob JE (2022) Lifespan of mature olfactory sensory neurons varies with location in the mouse olfactory epithelium and age of the animal. J Comp Neurol 530:2238–2251. doi: 10.1002/cne.25330

18. Genovese F, Reisert J, Kefalov VJ (2021) Sensory Transduction in Photoreceptors and Olfactory Sensory Neurons: Common Features and Distinct Characteristics. Front Cell Neurosci 15:761416. doi: 10.3389/fncel.2021.761416

19. Goldin AL, Barchi RL, Caldwell JH, Hofmann F, Howe JR, Hunter JC, Kallen RG, Mandel G, Meisler MH, Netter YB, Noda M, Tamkun MM, Waxman SG, Wood JN, Catterall WA (2000) Nomenclature of Voltage-Gated Sodium Channels. Neuron 28:365–368. doi: 10.1016/S0896-6273(00)00116-1

20. Graziadei PPC, Graziadei GAM (1979) Neurogenesis and neuron regeneration in the olfactory system of mammals. I. Morphological aspects of differentiation and structural organization of the olfactory sensory neurons. J Neurocytol 8:1–18. doi: 10.1007/BF01206454

21. Gregory JD, Kunkhyen T, Sweat SC, Huang JS, Brechbill TR, Cheetham CEJ (2025) New Neurons in the Postnatal Olfactory System: Functions in the Healthy and Regenerating Brain. Brain Sciences 15:597. doi: 10.3390/brainsci15060597

22. Gutman GA, Chandy KG, Grissmer S, Lazdunski M, McKinnon D, Pardo LA, Robertson GA, Rudy B, Sanguinetti MC, Stühmer W, Wang X (2005) International Union of Pharmacology. LIII. Nomenclature and molecular relationships of voltage-gated potassium channels. Pharmacol Rev 57:473–508. doi: 10.1124/pr.57.4.10

23. Han P, Lucero MT (2005) Pituitary adenylate cyclase activating polypeptide reduces A-type K+ currents and caspase activity in cultured adult mouse olfactory neurons. Neuroscience 134:745–756. doi: 10.1016/j.neuroscience.2005.05.007

24. Hanchate NK, Kondoh K, Lu Z, Kuang D, Ye X, Qiu X, Pachter L, Trapnell C, Buck LB (2015) Single-cell transcriptomics reveals receptor transformations during olfactory neurogenesis. Science 350:1251–1255. doi: 10.1126/science.aad2456

25. Hao Y, Stuart T, Kowalski M, Choudhary S, Hoffman P, Hartman A, Srivastava A, Molla G, Madad S, Fernandez-Granda C, Satija R (2024) Dictionary learning for integrative, multimodal, and massively scalable single-cell analysis. Nat Biotechnol 42:293–304. doi: 10.1038/s41587-023-01767-y

26. Henriques T, Agostinelli E, Hernandez-Clavijo A, Maurya DK, Rock JR, Harfe BD, Menini A, Pifferi S (2019) TMEM16A calcium-activated chloride currents in supporting cells of the mouse olfactory epithelium. Journal of General Physiology 151:954–966. doi: 10.1085/jgp.201812310

27. Hernandez-Clavijo A, Triviño CAS, Guarneri G, Ricci C, Mantilla-Esparza FA, Gonzalez-Velandia KY, Boscolo-Rizzo P, Tofanelli M, Bonini P, Dibattista M, Tirelli G, Menini A (2023) Shedding light on human olfaction: Electrophysiological recordings from sensory neurons in acute slices of olfactory epithelium. iScience 26. doi: https://doi.org/10.1016/j.isci.2023.107186

668 28. Holl A-M (2018) Survival of mature mouse olfactory sensory neurons labeled genetically
669 perinatally. Mol Cell Neurosci 88:258–269. doi: 10.1016/j.mcn.2018.02.005

670 29. Huang JS, Kunkhyen T, Rangel AN, Brechbill TR, Gregory JD, Winson-Bushby ED, Liu B, Avon JT,
671 Muggleton RJ, Cheetham CEJ (2022) Immature olfactory sensory neurons provide behaviourally
672 relevant sensory input to the olfactory bulb. Nat Commun 13:6194. doi: 10.1038/s41467-022-
673 33967-6

674 30. Iwema CL, Schwob JE (2003) Odorant receptor expression as a function of neuronal maturity in the
675 adult rodent olfactory system. Journal of Comparative Neurology 459:209–222. doi:
676 10.1002/cne.10583

677 31. Kawai F (2002) Ca2+-Activated K+ Currents Regulate Odor Adaptation by Modulating Spike
678 Encoding of Olfactory Receptor Cells. Biophysical Journal 82:2005–2015. doi: 10.1016/S0006-
679 3495(02)75549-5

680 32. Kawai F (2024) Somatic ion channels and action potentials in olfactory receptor cells and
681 vomeronasal receptor cells. J Neurophysiol 131:455–471. doi: 10.1152/jn.00137.2023

682 33. Keller A, Margolis FL (1975) Immunological studies of the rat olfactory marker protein. J
683 Neurochem 24:1101–1106. doi: 10.1111/j.1471-4159.1975.tb03883.x

684 34. Kikuta S, Sakamoto T, Nagayama S, Kanaya K, Kinoshita M, Kondo K, Tsunoda K, Mori K, Yamasoba
685 T (2015) Sensory deprivation disrupts homeostatic regeneration of newly generated olfactory
686 sensory neurons after injury in adult mice. J Neurosci 35:2657–2673. doi:
687 10.1523/JNEUROSCI.2484-14.2015

688 35. Kleene SJ (2008) The electrochemical basis of odor transduction in vertebrate olfactory cilia. Chem
689 Senses 33:839–859. doi: 10.1093/chemse/bjn048

690 36. Laedermann CJ, Syam N, Pertin M, Decosterd I, Abriel H (2013) β1- and β3- voltage-gated sodium
691 channel subunits modulate cell surface expression and glycosylation of Nav1.7 in HEK293 cells.
692 Front Cell Neurosci 7:137. doi: 10.3389/fncel.2013.00137

693 37. Lagostena L, Menini A (2003) Whole-cell recordings and photolysis of caged compounds in
694 olfactory sensory neurons isolated from the mouse. Chem Senses 28:705–716. doi:
695 10.1093/chemse/bjg063

696 38. Lee AC, He J, Ma M (2011) Olfactory Marker Protein Is Critical for Functional Maturation of Olfactory
697 Sensory Neurons and Development of Mother Preference. J Neurosci 31:2974–2982. doi:
698 10.1523/JNEUROSCI.5067-10.2011

699 39. Liberia T, Martin-Lopez E, Meller SJ, Greer CA (2019) Sequential Maturation of Olfactory Sensory
700 Neurons in the Mature Olfactory Epithelium. eNeuro 6:ENEURO.0266-19.2019. doi:
701 10.1523/ENEURO.0266-19.2019

702 40. Liman ER, Corey DP (1996) Electrophysiological characterization of chemosensory neurons from
703 the mouse vomeronasal organ. J Neurosci 16:4625–4637. doi: 10.1523/JNEUROSCI.16-15-
704 04625.1996

705 41. Loo AT, Youngentob SL, Kent PF, Schwob JE (1996) The aging olfactory epithelium: neurogenesis,
706 response to damage, and odorant-induced activity. Int J Dev Neurosci 14:881–900. doi:
707 10.1016/s0736-5748(96)00046-9

42. Lorenzon P, Redolfi N, Podolsky MJ, Zamparo I, Franchi SA, Pietra G, Boccaccio A, Menini A, Murthy VN, Lodovichi C (2015) Circuit formation and function in the olfactory bulb of mice with reduced spontaneous afferent activity. J Neurosci 35:146–160. doi: 10.1523/JNEUROSCI.0613-14.2015

43. Lynch JW, Barry PH (1991) Properties of transient K+ currents and underlying single K+ channels in rat olfactory receptor neurons. J Gen Physiol 97:1043–1072. doi: 10.1085/jgp.97.5.1043

44. Ma M, Chen WR, Shepherd GM (1999) Electrophysiological characterization of rat and mouse olfactory receptor neurons from an intact epithelial preparation. Journal of Neuroscience Methods 92:31–40. doi: 10.1016/S0165-0270(99)00089-8

45. Mackay-Sim A, Kittel PW (1991) On the Life Span of Olfactory Receptor Neurons. Eur J Neurosci 3:209–215. doi: 10.1111/j.1460-9568.1991.tb00081.x

46. Madrid R, Sanhueza M, Alvarez O, Bacigalupo J (2003) Tonic and phasic receptor neurons in the vertebrate olfactory epithelium. Biophys J 84:4167–4181. doi: 10.1016/S0006-3495(03)75141-8

47. Manzini I, Schild D, Di Natale C (2022) Principles of odor coding in vertebrates and artificial chemosensory systems. Physiological Reviews 102:61–154. doi: 10.1152/physrev.00036.2020

48. McClintock TS, Khan N, Xie C, Martens JR (2020) Maturation of the Olfactory Sensory Neuron and Its Cilia. Chem Senses 45:805–822. doi: 10.1093/chemse/bjaa070

49. McIntyre JC, Titlow WB, McClintock TS (2010) Axon Growth and Guidance Genes Identify Nascent, Immature, and Mature Olfactory Sensory Neurons. J Neurosci Res 88:3243–3256. doi: 10.1002/jnr.22497

50. Miragall F, Graziadei GAM (1982) Experimental studies on the olfactory marker protein. II. Appearance of the olfactory marker protein during differentiation of the olfactory sensory neurons of mouse: an immunohistochemical and autoradiographic study. Brain Research 239:245–250. doi: 10.1016/0006-8993(82)90846-0

51. Nakashima A, Ihara N, Shigeta M, Kiyonari H, Ikegaya Y, Takeuchi H (2019) Structured spike series specify gene expression patterns for olfactory circuit formation. Science 365:eaaw5030. doi: 10.1126/science.aaw5030

52. Nakashima A, Takeuchi H, Imai T, Saito H, Kiyonari H, Abe T, Chen M, Weinstein LS, Yu CR, Storm DR, Nishizumi H, Sakano H (2013) Agonist-Independent GPCR Activity Regulates Anterior-Posterior Targeting of Olfactory Sensory Neurons. Cell 154:1314. doi: 10.1016/j.cell.2013.08.033

53. Nakashima N, Nakashima K, Taura A, Takaku-Nakashima A, Ohmori H, Takano M (2020) Olfactory marker protein directly buffers cAMP to avoid depolarization-induced silencing of olfactory receptor neurons. Nat Commun 11:2188. doi: 10.1038/s41467-020-15917-2

54. Nickell MD, Breheny P, Stromberg AJ, McClintock TS (2012) Genomics of Mature and Immature Olfactory Sensory Neurons. J Comp Neurol 520:2608–2629. doi: 10.1002/cne.23052

55. Pifferi S, Menini A, Kurahashi T (2010) Signal Transduction in Vertebrate Olfactory Cilia. In: Menini A (ed) The Neurobiology of Olfaction. CRC Press/Taylor & Francis, Boca Raton (FL)

56. Potter SM, Zheng C, Koos DS, Feinstein P, Fraser SE, Mombaerts P (2001) Structure and Emergence of Specific Olfactory Glomeruli in the Mouse. J Neurosci 21:9713–9723. doi: 10.1523/JNEUROSCI.21-24-09713.2001

57. Reisert J (2010) Origin of basal activity in mammalian olfactory receptor neurons. The Journal of general physiology 136:529–40. doi: 10.1085/jgp.201010528

58. Reisert J, Pifferi S, Guarneri G, Ricci C, Menini A, Dibattista M (2024) The Ca2+-activated Cl– channel TMEM16B shapes the response time course of olfactory sensory neurons. The Journal of Physiology 602:4889–4905. doi: 10.1113/JP286959

59. Reisert J, Yau K-W, Margolis FL (2007) Olfactory marker protein modulates the cAMP kinetics of the odour-induced response in cilia of mouse olfactory receptor neurons. The Journal of Physiology 585:731–740. doi: 10.1113/jphysiol.2007.142471

60. Rodriguez-Gil DJ, Bartel DL, Jaspers AW, Mobley AS, Imamura F, Greer CA (2015) Odorant receptors regulate the final glomerular coalescence of olfactory sensory neuron axons. Proceedings of the National Academy of Sciences 112:5821–5826. doi: 10.1073/pnas.1417955112

61. Rogawski MA (1985) The A-current: how ubiquitous a feature of excitable cells is it? Trends in Neurosciences 8:214–219. doi: 10.1016/0166-2236(85)90082-7

62. Rudy B (1988) Diversity and ubiquity of K channels. Neuroscience 25:729–749. doi: 10.1016/0306-4522(88)90033-4

63. Ryba NJ, Tirindelli R (1995) A novel GTP-binding protein gamma-subunit, G gamma 8, is expressed during neurogenesis in the olfactory and vomeronasal neuroepithelia. J Biol Chem 270:6757–6767. doi: 10.1074/jbc.270.12.6757

64. Sammeta N, Yu T-T, Bose SC, McClintock TS (2007) Mouse olfactory sensory neurons express 10,000 genes. J Comp Neurol 502:1138–1156. doi: 10.1002/cne.21365

65. Saraiva LR, Ibarra-Soria X, Khan M, Omura M, Scialdone A, Mombaerts P, Marioni JC, Logan DW (2015) Hierarchical deconstruction of mouse olfactory sensory neurons: from whole mucosa to single-cell RNA-seq. Sci Rep 5:18178. doi: 10.1038/srep18178

66. Schild D, Restrepo D (1998) Transduction mechanisms in vertebrate olfactory receptor cells. Physiol Rev 78:429–466. doi: 10.1152/physrev.1998.78.2.429

67. Schwob JE, Szumowski KE, Stasky AA (1992) Olfactory sensory neurons are trophically dependent on the olfactory bulb for their prolonged survival. J Neurosci 12:3896–3919. doi: 10.1523/JNEUROSCI.12-10-03896.1992

68. Tan L, Li Q, Xie XS (2015) Olfactory sensory neurons transiently express multiple olfactory receptors during development. Mol Syst Biol 11:844. doi: 10.15252/msb.20156639

69. Tirindelli R, Ryba NJP (1996) The G-protein γ-subunit Gy8 is Expressed in the Developing Axons of Olfactory and Vomeronasal Neurons. European Journal of Neuroscience 8:2388–2398. doi: 10.1111/j.1460-9568.1996.tb01202.x

70. Tomaru A, Kurahashi T (2005) Mechanisms determining the dynamic range of the bullfrog olfactory receptor cell. J Neurophysiol 93:1880–1888. doi: 10.1152/jn.00303.2004

71. Trotier D (1986) A patch-clamp analysis of membrane currents in salamander olfactory receptor cells. Pflugers Arch 407:589–595. doi: 10.1007/BF00582636

72. Verhaagen J, Oestreicher AB, Gispen WH, Margolis FL (1989) The expression of the growth associated protein B50/GAP43 in the olfactory system of neonatal and adult rats. J Neurosci 9:683–691. doi: 10.1523/JNEUROSCI.09-02-00683.1989

73. Weiss J, Pyrski M, Jacobi E, Bufe B, Willnecker V, Schick B, Zizzari P, Gossage SJ, Greer CA, Leinders-Zufall T, Woods CG, Wood JN, Zufall F (2011) Loss-of-function mutations in sodium channel Nav1.7 cause anosmia. Nature 472:186–190. doi: 10.1038/nature09975

74. Yu CR, Power J, Barnea G, O'Donnell S, Brown HEV, Osborne J, Axel R, Gogos JA (2004) Spontaneous neural activity is required for the establishment and maintenance of the olfactory sensory map. Neuron 42:553–566. doi: 10.1016/s0896-6273(04)00224-7

75. Zhao J, O'Leary ME, Chahine M (2011) Regulation of Nav1.6 and Nav1.8 peripheral nerve Na+ channels by auxiliary β-subunits. J Neurophysiol 106:608–619. doi: 10.1152/jn.00107.2011

76. Zufall F, Stengl M, Franke C, Hildebrand JG, Hatt H (1991) Ionic currents of cultured olfactory receptor neurons from antennae of male Manduca sexta. J Neurosci 11:956–965. doi: 10.1523/JNEUROSCI.11-04-00956.1991

77. Zybura AS, Baucum AJ, Rush AM, Cummins TR, Hudmon A (2020) CaMKII enhances voltage-gated sodium channel Nav1.6 activity and neuronal excitability. J Biol Chem 295:11845–11865. doi: 10.1074/jbc.RA120.014062

Additional information

Data availability statement

The data that support findings of this study are available from the first and corresponding authors upon reasonable request.

Competing interests

None declared.

Author contributions

The study was conceptualized and designed by A.M., A.B., C.R. and C.A.S.T. Electrophysiological experiments and confocal imaging were performed and analyzed by C.R., C.A.S.T. and L.T. Single-cell transcriptomic data were analyzed by U. R. and R.S. The manuscript was written by A.M., A.B., C.R, C.A.S.T. and R.S. with comments and approval from all the authors.

Funding

The research was supported by PRIN grant 202297W2H3 (awarded by A. M.).

Acknowledgements

OMP-GFP mice were kindly provided by Dr. Peter Mombaerts.

Keywords

olfaction, neuronal excitability, development, voltage-gated channels

Supplementary Files

Supplementary Table1: Excel file including the differentially expressed genes.

Any gels or blots were performed.

Clinical Trial number

Any clinical trial was performed.

4. DISCUSSION

4.1 Acute slices as a model for human OSNs characterization

In the first part of the project, we demonstrated that acute slices provide a viable model for studying the characteristics of the human OE, preserving better physiological conditions compared to dissociated OSNs.

We found that human OSNs have passive properties similar to other vertebrates (Schild & Restrepo, 1998; Kawai, 2024). Our values obtained from OE slices are consistent with previous data collected from dissociated OSNs by Restrepo et al. (1993). Performing whole-cell voltage clamp experiments from OSNs, we recorded voltage-gated outward currents, as previously reported (Restrepo *et al.*, 1993*b*; Tamari *et al.*, 2019). We also detected transient voltage-gated inward currents, which have been observed only sporadically in human dissociated OSNs (Restrepo *et al.*, 1993*b*; Tamari *et al.*, 2019). The dissociation procedure may damage cells, limiting proper investigation, whereas our preparation preserves both the morphological and physiological features of the tissue. In contrast, our measurements of voltage-gated currents from supporting cells revealed only outward currents. This characteristic appears to be peculiar to human supporting cells, as transient inward currents have been reported in mice (Vogalis *et al.*, 2005; Henriques *et al.*, 2019). Moreover, mouse supporting cells display large leak currents, associated with the presence of gap junctions (Vogalis *et al.*, 2005; Henriques *et al.*, 2019). As we did not observe any leak current in humans, our results suggest that human supporting cells may possess a lower density of gap junctions, or different composition, which could influence the overall cellular metabolism and intercellular communication.

We were able to elicit action potentials in human OSNs, demonstrating that they exhibit diverse firing patterns, including both tonic and phasic behaviours. This feature is common across species and our experiments show that humans are not the exception (Firestein & Werblin, 1987; Liman & Corey, 1996; Ma *et al.*, 1999; Kawai, 2002; Madrid *et al.*, 2003; Tomaru & Kurahashi, 2005).

At the functional level, we investigated the capability of human OSNs from acute slices to respond to odorants. Through immunohistochemistry, we first verified the presence of some of the major components of the transduction pathway known from rodent OSNs (Kleene, 2008; Pifferi *et al.*, 2010; Boccaccio *et al.*, 2021). In particular, we localized ACIII and TMEM16B proteins in the ciliary region of human OSNs, while α and γ subunits of G protein have been already visualized in previous immunohistochemical studies (Holbrook *et al.*, 2011; Durante *et al.*, 2020). Stimulating with the phosphodiesterase inhibitor IBMX, we elicited inward currents and action potentials, providing evidence that also human OSNs rely on cAMP as a second

messenger. In rodents, OSNs display OR-dependent basal activity and consequently have different basal cAMP levels (Reisert, 2010). Since IBMX-evoked currents reflect the levels of basal activity, our results suggest that human OSNs may display varying levels of basal activity depending on the OR they express.

We finally directly stimulated human OSNs with two different odorant mixtures to increase the probability of response and we obtained the first electrophysiological responses from human samples. The selective response of neurons to the mixtures confirms that each OSN can be activated by a limited number of odorants, related to the expressed OR type. Being able to record odorant responses opens the possibility to expand this research to a larger panel of compounds, focusing on key food-related odorants, whose corresponding ORs have been shown to be enriched in human samples (Saraiva *et al.*, 2019). Exploring different chemical groups and a broader range of concentrations may help determine whether the heterogeneity in firing patterns observed in our study reflects distinct coding strategies. This approach may also allow unveiling the mechanisms underlying odorant detection and sensory adaptation.

4.2 Immature OSNs excitability and voltage-gated currents influence

In the second part of the thesis, we functionally characterized immature OSNs, using OMP-GFP mice, and demonstrated that these cells are intrinsically excitable. Loose-patch recordings revealed that immature OSNs generate spontaneous action potentials, though at lower frequency and different patterns compared to mature OSNs. In mature OSNs, spontaneous activity strictly depends on the basal activity of the expressed ORs (Reisert, 2010; Connelly *et al.*, 2013; Nakashima *et al.*, 2019). Multiple ORs, as well as some components of the transduction pathway, have been detected in immature OSNs (Hanchate *et al.*, 2015; Tan *et al.*, 2015; Saraiva *et al.*, 2015), suggesting a possible contribution of OR-driven activity at early maturation stages. Developmental changes in firing behaviour could therefore reflect differences in transduction mechanisms or in intrinsic properties.

The OMP-GFP mouse model was essential not only for clearly differentiating immature and mature OSNs, but also for understanding that the observed differences in firing cannot be attributed to OMP. Although OMP can modulate firing through regulation of intracellular cAMP concentration (Nakashima *et al.*, 2020; Dibattista *et al.*, 2021), in this model OSNs at both stages lack OMP, thus excluding OMP involvement in definition of firing of immature OSNs.

Through whole-cell current clamp experiments, we bypassed the transduction machinery, exploiting the intrinsic mechanisms shaping the immature OSNs excitability. Also in this experiment, these cells displayed a reduced excitability. They were characterized by phasic

firing behaviour, with the ability of generating just one or few spikes. Moreover, action potentials from immature OSNs exhibited a more depolarized threshold and slower kinetics. Analysis of passive properties revealed that cells at early maturation stages have a more depolarized resting potential and a higher R_{input}. Both features may reduce the availability of Na_v needed for action potential rising. Although elevated R_{input} can enhance depolarization, it can impede the recruitment of enough Na_v that would allow repetitive firing. Progressive hyperpolarization of the membrane and decrease of R_{input} along neuronal maturation have also been reported in other developing neuronal populations, such as granule cells in the OB (Carleton *et al.*, 2003) and hippocampal neurons (Spigelman *et al.*, 1992).

In contrast, mature OSNs exhibited a heterogeneous range of firing pattern, showing both a phasic and a tonic pattern, characterized by sustained firing. As previously observed, such variability has been consistently reported across species (Firestein & Werblin, 1987; Liman & Corey, 1996; Ma *et al.*, 1999; Kawai, 2002; Madrid *et al.*, 2003; Tomaru & Kurahashi, 2005; Hernandez-Clavijo *et al.*, 2023). This heterogeneity may reflect functional diversity among mature OSNs, as previously proposed (Madrid *et al.*, 2003; Connelly *et al.*, 2013), with some of them optimized for higher sensitivity (tonic firing) and others for rapid detection of changes in the environment (phasic firing), potentially contributing to a broader dynamic range in olfactory coding.

Differences in voltage-gated channels further support maturation-dependent changes in excitability. Isolating Na^+ currents, immature OSNs showed an activation curve shifted towards more depolarized potentials with respect to mature OSNs, which, on the other hand, showed a strong dependency on the prepulse potential. Changing the holding potential from -80 to -110 mV allowed the recruitment of more channels only in mature OSNs, reflecting differences in channel composition during development. Indeed, TTX application nearly abolished all Na^+ currents in immature OSNs, revealing that they are almost entirely TTX-sensitive, whereas a TTX-resistant component remained in mature cells. This residual current is characterized by a more hyperpolarized activation V_{half} and likely corresponds to the TTX-resistant $Na_v1.5$ subtype previously identified in mouse OSNs (Frenz *et al.*, 2014). Frenz and colleagues (2014) proposed that $Na_v1.5$ contributes to the hyperpolarized activation threshold and its blockade suppresses the spontaneous firing, demonstrating the important role of this channel in generating spontaneous activity. When analysing transcriptomics, we found an upregulation of $Na_v1.5$, $Na_v1.6$ and $Na_v1.7$ α subunits. Among them, $Na_v1.5$ is the only TTX-resistant component, while the others are TTX-sensitive (Goldin *et al.*, 2000). Previous studies also reported mRNA expression of $Na_v1.7$, as the most abundant, and additional isoforms at lower levels: $Na_v1.2$,

$Na_v1.3$, $Na_v1.5$ and $Na_v1.6$ (Weiss *et al.*, 2011; Ahn *et al.*, 2011; Frenz *et al.*, 2014; Bolz *et al.*, 2017). Consistent with our findings, mRNA profiling from OMP-GFP mice demonstrated that $Na_v1.5$ channel is detected in mature, but not immature OSNs (Sammeta *et al.*, 2007).

At the protein level $Na_v1.3$, $Na_v1.5$ and $Na_v1.7$ are the only ones that have been detected; with the $Na_v1.3$ and $Na_v1.7$ expressed in soma and axon bundles (Weiss *et al.*, 2011; Bolz *et al.*, 2017) and $Na_v1.5$ on dendrites (Frenz *et al.*, 2014) of OSNs.

Taken together, these observations suggest that channel expression and TTX-sensitivity changes along neuronal differentiation, with $Na_v1.5$ being particularly expressed in mature OSNs and $Na_v1.7$ protein expression increasing with maturation, thereby enhancing excitability in mature cells.

In addition, transcriptomic analysis revealed upregulation of β3 and β4, which modulate neuronal excitability through interactions with α subunits, influencing Na_v channel gating in a cell-type and subtype specific manner (Brackenbury & Isom, 2011). In particular, the β4 subunit has been linked to negative shifts in the activation curve of several α subunits (Yu *et al.*, 2003; Chen *et al.*, 2008; Zhao *et al.*, 2011), Therefore, altered kinetics in mature OSNs may also arise from changes in modulatory subunits. Moreover, we cannot exclude the possibility that additional post-translational modifications, such as phosphorylation or glycosylation, occur during OSN development, further influencing the kinetics and voltage-dependence of Na_v (Laedermann *et al.*, 2013; Zybura *et al.*, 2020).

On the contrary, involvement of voltage-gated Ca^{2+} currents to distinct inward current properties appears negligible, since differences between immature and immature OSNs remained significant even in the presence of the Ca_v blocker Cd^{2+}, and no differentially expressed genes related to Ca_v were detected.

Isolation of voltage-gated K^+ currents revealed the presence of a sustained component, consistently reported across multiple species including moths (Zufall *et al.*, 1991), salamanders (Trotier, 1986; Firestein & Werblin, 1987) and mice (Ma *et al.*, 1999; Lagostena & Menini, 2003; Boccaccio, 2018). Although present in both cell types, this current showed higher amplitudes in mature OSNs than immature ones. In accordance with this observation, we found upregulation of the $K_v1.2$, $K_v1.5$, $K_v1.6$ and $K_v2.1$ transcripts in mature OSNs. All these subtypes are associated to non-inactivating or slowly inactivating delayed rectifier K^+ currents (Gutman *et al.*, 2005).

In addition, mature OSNs exhibited a transient, 4-AP sensitive K^+ current, which was absent in immature OSNs. Our analysis on scRNA-seq revealed upregulation of $K_v3.4$ in mature OSNs. This K_v channel subtype generates fast-inactivating A-type K^+ currents, therefore can be a

potential candidate for mediating the transient current in mature OSNs (Gutman *et al.*, 2005). Our results are in agreement with microarray data showing that $K_v3.4$ expression is restricted to mature OSNs (Sammeta *et al.*, 2007). Other genes associated with the A-type current, in particular $K_v1.4$, $K_v4.2$ and $K_v4.3$, have been reported to be expressed in adult mouse OSNs (Han & Lucero, 2006). However, they do not appear among the differentially expressed genes, strengthening the importance of the $K_v3.4$ gene during maturation.

A-type K^+ currents were previously observed in mature OSNs, however we report a steady state component that persists after 600 ms, a feature previously unexplored (Han & Lucero, 2005). These discrepancies may arise from differences in experimental procedures. Indeed, Han and Lucero (2005) recorded from mouse dissociated cells after 24h in culture. Under this condition, temperature changes might affect K_v channels kinetics, which is highly temperature-sensitive (Ranjan *et al.*, 2019). Moreover, culturing OSNs might alter biophysical properties of ion channels (Ono *et al.*, 2012; Song *et al.*, 2018). By using acute slices, we aimed to preserve the most physiological conditions, thereby minimizing alterations in current properties and firing behaviour of OSNs.

Given the well-established role of the A-type K^+ current in shaping action potential waveforms and regulating firing frequency (Connor & Stevens, 1971; Rogawski, 1985; Rudy, 1988; Rudy *et al.*, 1999; Sonner & Stern, 2007), its absence in immature neurons likely contributes to the slower spike kinetics and reduced excitability of developing OSNs. On the other hand, the presence of A-type current in mature OSNs may facilitate faster and higher membrane repolarization during the falling phase of the action potential, thereby promoting more effective removal of Na_v channels inactivation and enabling higher firing capabilities.

Overall, our results uncover key functional and biophysical differences between immature and mature OSNs. Given the importance of ion channel expression and neuronal excitability in synaptic connections refinement (Yu *et al.*, 2004; Lorenzon *et al.*, 2015), their progressive tuning may be crucial for the establishment of newly generated OSNs within the OB, ensuring both regeneration and stability of sensory processing throughout life.

5. REFERENCES

Ahn H-S, Black JA, Zhao P, Tyrrell L, Waxman SG & Dib-Hajj SD (2011). Nav1.7 is the predominant sodium channel in rodent olfactory sensory neurons. *Mol Pain* **7,** 32.

Albeanu DF, Provost AC, Agarwal P, Soucy ER, Zak JD & Murthy VN (2018). Olfactory marker protein (OMP) regulates formation and refinement of the olfactory glomerular map. *Nat Commun* **9,** 5073.

Altman J (1969). Autoradiographic and histological studies of postnatal neurogenesis. IV. Cell proliferation and migration in the anterior forebrain, with special reference to persisting neurogenesis in the olfactory bulb. *Journal of Comparative Neurology* **137,** 433–457.

Altman J & Das GD (1965). Autoradiographic and histological evidence of postnatal hippocampal neurogenesis in rats. *Journal of Comparative Neurology* **124,** 319–335.

Alvites RD, Caseiro AR, Pedrosa SS, Branquinho ME, Varejão ASP & Maurício AC (2018). The Nasal Cavity of the Rat and Mouse-Source of Mesenchymal Stem Cells for Treatment of Peripheral Nerve Injury. *Anat Rec (Hoboken)* **301,** 1678–1689.

Attali B, Chandy KG, Giese MH, Grissmer S, Gutman GA, Jan LY, Lazdunski M, Mckinnon D, Nerbonne J, Pardo LA, Robertson GA, Rudy B, Sanguinetti MC, Stühmer W, Trimmer JS & Wang X (2023). Voltage-gated potassium channels (K_v) in GtoPdb v.2023.1. *GtoPdb CITE*.

Axel R (2005). Scents and Sensibility: A Molecular Logic of Olfactory Perception (Nobel Lecture). *Angewandte Chemie International Edition* **44,** 6110–6127.

Bannister LH & Dodson HC (1992). Endocytic pathways in the olfactory and vomeronasal epithelia of the mouse: Ultrastructure and uptake of tracers. *Microscopy Research and Technique* **23,** 128–141.

Barnes IHA, Ibarra-Soria X, Fitzgerald S, Gonzalez JM, Davidson C, Hardy MP, Manthravadi D, Van Gerven L, Jorissen M, Zeng Z, Khan M, Mombaerts P, Harrow J, Logan DW & Frankish A (2020). Expert curation of the human and mouse olfactory receptor gene repertoires identifies conserved coding regions split across two exons. *BMC Genomics* **21,** 196.

Bean BP (2007). The action potential in mammalian central neurons. *Nat Rev Neurosci* **8,** 451–465.

Belluscio L, Gold GH, Nemes A & Axel R (1998). Mice deficient in G(olf) are anosmic. *Neuron* **20,** 69–81.

Billig GM, Pál B, Fidzinski P & Jentsch TJ (2011). Ca2+-activated Cl− currents are dispensable for olfaction. *Nat Neurosci* **14,** 763–769.

Boccaccio A (2018). Patch-Clamp Recordings from Mouse Olfactory Sensory Neurons. *Methods Mol Biol* **1820,** 113–122.

Boccaccio A, Lagostena L, Hagen V & Menini A (2006). Fast Adaptation in Mouse Olfactory Sensory Neurons Does Not Require the Activity of Phosphodiesterase. *J Gen Physiol* **128,** 171–184.

Boccaccio A & Menini A (2007). Temporal development of cyclic nucleotide-gated and Ca2+ -activated Cl- currents in isolated mouse olfactory sensory neurons. *J Neurophysiol* **98,** 153–160.

Boccaccio A, Menini A & Pifferi S (2021). The cyclic AMP signaling pathway in the rodent main olfactory system. *Cell Tissue Res* **383,** 429–443.

Bolz F, Kasper S, Bufe B, Zufall F & Pyrski M (2017). Organization and Plasticity of Sodium Channel Expression in the Mouse Olfactory and Vomeronasal Epithelia. *Front Neuroanat* **11,** 28.

Brackenbury WJ & Isom LL (2011). Na Channel β Subunits: Overachievers of the Ion Channel Family. *Front Pharmacol* **2,** 53.

Brann DH et al. (2020). Non-neuronal expression of SARS-CoV-2 entry genes in the olfactory system suggests mechanisms underlying COVID-19-associated anosmia. *Sci Adv* **6,** eabc5801.

Breipohl W, Laugwitz HJ & Bornfeld N (1974). Topological relations between the dendrites of olfactory sensory cells and sustentacular cells in different vertebrates. An ultrastructural study. *J Anat* **117,** 89–94.

Brunet LJ, Gold GH & Ngai J (1996). General Anosmia Caused by a Targeted Disruption of the Mouse Olfactory Cyclic Nucleotide–Gated Cation Channel. *Neuron* **17,** 681–693.

Bryche B, St Albin A, Murri S, Lacôte S, Pulido C, Ar Gouilh M, Lesellier S, Servat A, Wasniewski M, Picard-Meyer E, Monchatre-Leroy E, Volmer R, Rampin O, Le Goffic R, Marianneau P & Meunier N (2020). Massive transient damage of the olfactory epithelium associated with infection of sustentacular cells by SARS-CoV-2 in golden Syrian hamsters. *Brain Behav Immun* **89,** 579–586.

Buck L & Axel R (1991). A novel multigene family may encode odorant receptors: a molecular basis for odor recognition. *Cell* **65,** 175–187.

Buck LB (2005). Unraveling the Sense of Smell (Nobel Lecture). *Angewandte Chemie International Edition* **44,** 6128–6140.

Buiakova OI, Baker H, Scott JW, Farbman A, Kream R, Grillo M, Franzen L, Richman M, Davis LM, Abbondanzo S, Stewart CL & Margolis FL (1996). Olfactory marker protein

(OMP) gene deletion causes altered physiological activity of olfactory sensory neurons. *Proc Natl Acad Sci U S A* **93,** 9858–9863.

Carleton A, Petreanu LT, Lansford R, Alvarez-Buylla A & Lledo P-M (2003). Becoming a new neuron in the adult olfactory bulb. *Nat Neurosci* **6,** 507–518.

Carr VM, Farbman AI, Colletti LM & Morgan JI (1991). Identification of a new non-neuronal cell type in rat olfactory epithelium. *Neuroscience* **45,** 433–449.

Catterall WA (2000*a*). From Ionic Currents to Molecular Mechanisms: The Structure and Function of Voltage-Gated Sodium Channels. *Neuron* **26,** 13–25.

Catterall WA (2000*b*). Structure and regulation of voltage-gated Ca2+ channels. *Annu Rev Cell Dev Biol* **16,** 521–555.

Catterall WA, Perez-Reyes E, Snutch TP & Striessnig J (2005). International Union of Pharmacology. XLVIII. Nomenclature and Structure-Function Relationships of Voltage-Gated Calcium Channels. *Pharmacological Reviews* **57,** 411–425.

Cenedese V, Betto G, Celsi F, Cherian OL, Pifferi S & Menini A (2012). The voltage dependence of the TMEM16B/anoctamin2 calcium-activated chloride channel is modified by mutations in the first putative intracellular loop. *J Gen Physiol* **139,** 285–294.

Cheetham CE & Belluscio L (2014). An Olfactory Critical Period. *Science* **344,** 157–158.

Cheetham CEJ, Park U & Belluscio L (2016). Rapid and continuous activity-dependent plasticity of olfactory sensory input. *Nat Commun* **7,** 10729.

Chen Y, Yu FH, Sharp EM, Beacham D, Scheuer T & Catterall WA (2008). Functional properties and differential neuromodulation of Na(v)1.6 channels. *Mol Cell Neurosci* **38,** 607–615.

Cheng K-H, Cheng Y-S, Yeh H-C, Guilmette RA, Simpson SQ, Yang Y-H & Swift DL (1996). *In vivo* measurements of nasal airway dimensions and ultrafine aerosol deposition in the human nasal and oral airways. *Journal of Aerosol Science* **27,** 785–801.

Coetzee WA, Amarillo Y, Chiu J, Chow A, Lau D, McCormack T, Moreno H, Nadal MS, Ozaita A, Pountney D, Saganich M, Vega-Saenz de Miera E & Rudy B (1999). Molecular diversity of K+ channels. *Ann N Y Acad Sci* **868,** 233–285.

Connelly T, Savigner A & Ma M (2013). Spontaneous and sensory-evoked activity in mouse olfactory sensory neurons with defined odorant receptors. *Journal of Neurophysiology* **110,** 55–62.

Connor JA & Stevens CF (1971). Prediction of repetitive firing behaviour from voltage clamp data on an isolated neurone soma. *J Physiol* **213,** 31–53.

Dibattista M, Al Koborssy D, Genovese F & Reisert J (2021). The functional relevance of olfactory marker protein in the vertebrate olfactory system: a never-ending story. *Cell Tissue Res* **383,** 409–427.

Dibattista M, Pifferi S, Boccaccio A, Menini A & Reisert J (2017). The long tale of the calcium activated Cl^- channels in olfactory transduction. *Channels* **11,** 399–414.

Dibattista M, Pifferi S, Hernandez-Clavijo A & Menini A (2024). The physiological roles of anoctamin2/TMEM16B and anoctamin1/TMEM16A in chemical senses. *Cell Calcium* **120,** 102889.

Dibattista M & Reisert J (2016). The Odorant Receptor-Dependent Role of Olfactory Marker Protein in Olfactory Receptor Neurons. *J Neurosci* **36,** 2995–3006.

Doty RL ed. (2003). Morphology of the Mammalian Olfactory Epithelium: Form, Fine Structure, Function, and Pathology. In *Handbook of Olfaction and Gustation*, 0 edn., pp. 102–167. CRC Press.

Durante MA, Kurtenbach S, Sargi ZB, Harbour JW, Choi R, Kurtenbach S, Goss GM, Matsunami H & Goldstein BJ (2020). Single-cell analysis of olfactory neurogenesis and differentiation in adult humans. *Nat Neurosci* **23,** 323–326.

Enomoto T, Wakui K & Hirota J (2021). Bcl11b is required for proper odorant receptor expression in the mouse septal organ. *Cell Tissue Res* **384,** 643–653.

Erdélyi L & Such G (1988). The A-type potassium current: catechol-induced blockage in snail neurons. *Neurosci Lett* **92,** 46–51.

Fang A & Yu CR (2024). Activity-dependent formation of the topographic map and the critical period in the development of mammalian olfactory system. *genesis* **62,** e23586.

Ferrero DM & Liberles SD (2010). The secret codes of mammalian scents. *WIREs Systems Biology and Medicine* **2,** 23–33.

Firestein S (2001). How the olfactory system makes sense of scents. *Nature* **413,** 211–218.

Firestein S & Werblin FS (1987). Gated currents in isolated olfactory receptor neurons of the larval tiger salamander. *Proc Natl Acad Sci U S A* **84,** 6292–6296.

Fleischer J (2021). The Grueneberg ganglion: signal transduction and coding in an olfactory and thermosensory organ involved in the detection of alarm pheromones and predator-secreted kairomones. *Cell Tissue Res* **383,** 535–548.

Fletcher RB, Das D, Gadye L, Street KN, Baudhuin A, Wagner A, Cole MB, Flores Q, Choi YG, Yosef N, Purdom E, Dudoit S, Risso D & Ngai J (2017). Deconstructing Olfactory Stem Cell Trajectories at Single Cell Resolution. *Cell Stem Cell* **20,** 817-830.e8.

Fluegge D, Moeller LM, Cichy A, Gorin M, Weth A, Veitinger S, Cainarca S, Lohmer S, Corazza S, Neuhaus EM, Baumgartner W, Spehr J & Spehr M (2012). Mitochondrial Ca2+ mobilization is a key element in olfactory signaling. *Nat Neurosci* **15,** 754–762.

Fodoulian L, Tuberosa J, Rossier D, Boillat M, Kan C, Pauli V, Egervari K, Lobrinus JA, Landis BN, Carleton A & Rodriguez I (2020). SARS-CoV-2 Receptors and Entry Genes Are Expressed in the Human Olfactory Neuroepithelium and Brain. *iScience* **23,** 101839.

Frenz CT, Hansen A, Dupuis ND, Shultz N, Levinson SR, Finger TE & Dionne VE (2014). NaV1.5 sodium channel window currents contribute to spontaneous firing in olfactory sensory neurons. *J Neurophysiol* **112,** 1091–1104.

Gaun V, Martens JR & Schwob JE (2022). Lifespan of mature olfactory sensory neurons varies with location in the mouse olfactory epithelium and age of the animal. *J Comp Neurol* **530,** 2238–2251.

Gautam SH, Otsuguro K-I, Ito S, Saito T & Habara Y (2007). T-type Ca2+ channels mediate propagation of odor-induced Ca2+ transients in rat olfactory receptor neurons. *Neuroscience* **144,** 702–713.

Genovese F & Tizzano M (2018). Microvillous cells in the olfactory epithelium express elements of the solitary chemosensory cell transduction signaling cascade. *PLoS One* **13,** e0202754.

Gogos JA, Osborne J, Nemes A, Mendelsohn M & Axel R (2000). Genetic Ablation and Restoration of the Olfactory Topographic Map. *Cell* **103,** 609–620.

Goldin AL, Barchi RL, Caldwell JH, Hofmann F, Howe JR, Hunter JC, Kallen RG, Mandel G, Meisler MH, Netter YB, Noda M, Tamkun MM, Waxman SG, Wood JN & Catterall WA (2000). Nomenclature of Voltage-Gated Sodium Channels. *Neuron* **28,** 365–368.

Gomez G, Rawson NE, Cowart B, Lowry LD, Pribitkin EA & Restrepo D (2000). Modulation of odor-induced increases in [Ca(2+)](i) by inhibitors of protein kinases A and C in rat and human olfactory receptor neurons. *Neuroscience* **98,** 181–189.

González C, Baez-Nieto D, Valencia I, Oyarzún I, Rojas P, Naranjo D & Latorre R (2012). K(+) channels: function-structural overview. *Compr Physiol* **2,** 2087–2149.

Graziadei PPC & Monti Graziadei GA (1978). Continuous Nerve Cell Renewal in the Olfactory System. In *Development of Sensory Systems*, ed. Bate CM, Carr VMcM, Graziadei PPC, Hirsch HVB, Hughes A, Ingle D, Leventhal AG, Monti Graziadei GA, Rubel EW, Saxod R, Scheibel AB, Scheibel ME, Silver J & Jacobson M, pp. 55–83. Springer, Berlin, Heidelberg.

Gregory JD, Kunkhyen T, Sweat SC, Huang JS, Brechbill TR & Cheetham CEJ (2025). New Neurons in the Postnatal Olfactory System: Functions in the Healthy and Regenerating Brain. *Brain Sciences* **15,** 597.

Guarneri G, Pifferi S, Dibattista M, Reisert J & Menini A (2023). Paradoxical electro-olfactogram responses in TMEM16B knock-out mice. *Chem Senses* **48,** bjad003.

Gutierrez R & Simon SA (2021). Physiology of Taste Processing in the Tongue, Gut, and Brain. *Comprehensive Physiology* **11,** 2489–2523.

Gutman GA, Chandy KG, Grissmer S, Lazdunski M, McKinnon D, Pardo LA, Robertson GA, Rudy B, Sanguinetti MC, Stühmer W & Wang X (2005). International Union of Pharmacology. LIII. Nomenclature and molecular relationships of voltage-gated potassium channels. *Pharmacol Rev* **57,** 473–508.

Han P & Lucero MT (2005). Pituitary adenylate cyclase activating polypeptide reduces A-type K+ currents and caspase activity in cultured adult mouse olfactory neurons. *Neuroscience* **134,** 745–756.

Han P & Lucero MT (2006). Pituitary adenylate cyclase activating polypeptide reduces expression of Kv1.4 and Kv4.2 subunits underlying A-type K(+) current in adult mouse olfactory neuroepithelia. *Neuroscience* **138,** 411–419.

Hanchate NK, Kondoh K, Lu Z, Kuang D, Ye X, Qiu X, Pachter L, Trapnell C & Buck LB (2015). Single-cell transcriptomics reveals receptor transformations during olfactory neurogenesis. *Science* **350,** 1251–1255.

Harding J, Graziadei PP, Monti Graziadei GA & Margolis FL (1977). Denervation in the primary olfactory pathway of mice. IV. Biochemical and morphological evidence for neuronal replacement following nerve section. *Brain Res* **132,** 11–28.

Harkema JR, Carey SA & Wagner JG (2006). The nose revisited: a brief review of the comparative structure, function, and toxicologic pathology of the nasal epithelium. *Toxicol Pathol* **34,** 252–269.

Hayoz S, Jia C & Hegg C (2012). Mechanisms of constitutive and ATP-evoked ATP release in neonatal mouse olfactory epithelium. *BMC Neuroscience* **13,** 53.

Hegg CC, Irwin M & Lucero MT (2009). Calcium store-mediated signaling in sustentacular cells of the mouse olfactory epithelium. *Glia* **57,** 634–644.

Henriques T, Agostinelli E, Hernandez-Clavijo A, Maurya DK, Rock JR, Harfe BD, Menini A & Pifferi S (2019). TMEM16A calcium-activated chloride currents in supporting cells of the mouse olfactory epithelium. *Journal of General Physiology* **151,** 954–966.

Hernandez-Clavijo A, Gonzalez-Velandia KY, Rangaswamy U, Guarneri G, Boscolo-Rizzo P, Tofanelli M, Gardenal N, Sanges R, Dibattista M, Tirelli G & Menini A (2022). Supporting Cells of the Human Olfactory Epithelium Co-Express the Lipid Scramblase TMEM16F and ACE2 and May Cause Smell Loss by SARS-CoV-2 Spike-Induced Syncytia. *Cell Physiol Biochem* **56,** 254–269.

Hernandez-Clavijo A, Triviño CAS, Guarneri G, Ricci C, Mantilla-Esparza FA, Gonzalez-Velandia KY, Boscolo-Rizzo P, Tofanelli M, Bonini P, Dibattista M, Tirelli G & Menini A (2023). Shedding light on human olfaction: Electrophysiological recordings from sensory neurons in acute slices of olfactory epithelium. *iScience*; DOI: https://doi.org/10.1016/j.isci.2023.107186.

Hess D & El Manira A (2001). Characterization of a high-voltage-activated IA current with a role in spike timing and locomotor pattern generation. *Proceedings of the National Academy of Sciences* **98,** 5276–5281.

Hilliard TN, Zhu J, Farley R, Escudero-Garcia S, Wainwright BJ, Jeffery PK, Griesenbach U, Bush A, Davies JC & Alton EWFW (2008). Nasal Abnormalities in Cystic Fibrosis Mice Independent of Infection and Inflammation. *Am J Respir Cell Mol Biol* **39,** 19–25.

Holbrook EH, Wu E, Curry WT, Lin DT & Schwob JE (2011). Immunohistochemical characterization of human olfactory tissue. *Laryngoscope* **121,** 1687–1701.

Holl A-M (2018). Survival of mature mouse olfactory sensory neurons labeled genetically perinatally. *Mol Cell Neurosci* **88,** 258–269.

Huang JS, Kunkhyen T, Rangel AN, Brechbill TR, Gregory JD, Winson-Bushby ED, Liu B, Avon JT, Muggleton RJ & Cheetham CEJ (2022). Immature olfactory sensory neurons provide behaviourally relevant sensory input to the olfactory bulb. *Nat Commun* **13,** 6194.

Ito I & Maeno T (1986). Catechol: a potent and specific inhibitor of the fast potassium channel in frog primary afferent neurones. *J Physiol* **373,** 115–127.

Iwema CL & Schwob JE (2003). Odorant receptor expression as a function of neuronal maturity in the adult rodent olfactory system. *Journal of Comparative Neurology* **459,** 209–222.

Johnston J (2021). Pharmacology of A-Type K+ Channels. In *Pharmacology of Potassium Channels*, ed. Gamper N & Wang K, pp. 167–183. Springer International Publishing, Cham.

Jones DT & Reed RR (1989). Golf: an olfactory neuron specific-G protein involved in odorant signal transduction. *Science* **244,** 790–795.

Kaneko H, Putzier I, Frings S, Kaupp UB & Gensch T (2004). Chloride Accumulation in Mammalian Olfactory Sensory Neurons. *J Neurosci* **24,** 7931–7938.

Kawai F (2002). Ca2+-Activated K+ Currents Regulate Odor Adaptation by Modulating Spike Encoding of Olfactory Receptor Cells. *Biophysical Journal* **82,** 2005–2015.

Kawai F (2024). Somatic ion channels and action potentials in olfactory receptor cells and vomeronasal receptor cells. *J Neurophysiol* **131,** 455–471.

Kleene SJ (2008). The electrochemical basis of odor transduction in vertebrate olfactory cilia. *Chem Senses* **33,** 839–859.

Kurahashi T & Menini A (1997). Mechanism of odorant adaptation in the olfactory receptor cell. *Nature* **385,** 725–729.

Lacinová L (2004). Pharmacology of recombinant low-voltage activated calcium channels. *Curr Drug Targets CNS Neurol Disord* **3,** 105–111.

Lacroix M-C, Badonnel K, Meunier N, Tan F, Poupon CS-L, Durieux D, Monnerie R, Baly C, Congar P, Salesse R & Caillol M (2008). Expression of Insulin System in the Olfactory Epithelium: First Approaches to its Role and Regulation. *Journal of Neuroendocrinology* **20,** 1176–1190.

Laedermann CJ, Syam N, Pertin M, Decosterd I & Abriel H (2013). β1- and β3- voltage-gated sodium channel subunits modulate cell surface expression and glycosylation of Nav1.7 in HEK293 cells. *Front Cell Neurosci* **7,** 137.

Lagostena L & Menini A (2003). Whole-cell recordings and photolysis of caged compounds in olfactory sensory neurons isolated from the mouse. *Chem Senses* **28,** 705–716.

Laska M & Shepherd GM (2007). Olfactory discrimination ability of CD-1 mice for a large array of enantiomers. *Neuroscience* **144,** 295–301.

Li F, Ponissery-Saidu S, Yee KK, Wang H, Chen M-L, Iguchi N, Zhang G, Jiang P, Reisert J & Huang L (2013). Heterotrimeric G protein subunit Gγ13 is critical to olfaction. *J Neurosci* **33,** 7975–7984.

Liberia T, Martin-Lopez E, Meller SJ & Greer CA (2019). Sequential Maturation of Olfactory Sensory Neurons in the Mature Olfactory Epithelium. *eNeuro* **6,** ENEURO.0266-19.2019.

Liman ER & Corey DP (1996). Electrophysiological characterization of chemosensory neurons from the mouse vomeronasal organ. *J Neurosci* **16,** 4625–4637.

Lin W, Ezekwe EA, Zhao Z, Liman ER & Restrepo D (2008). TRPM5-expressing microvillous cells in the main olfactory epithelium. *BMC Neuroscience* **9,** 114.

Loo AT, Youngentob SL, Kent PF & Schwob JE (1996). The aging olfactory epithelium: neurogenesis, response to damage, and odorant-induced activity. *Int J Dev Neurosci* **14,** 881–900.

Lorenzon P, Redolfi N, Podolsky MJ, Zamparo I, Franchi SA, Pietra G, Boccaccio A, Menini A, Murthy VN & Lodovichi C (2015). Circuit formation and function in the olfactory bulb of mice with reduced spontaneous afferent activity. *J Neurosci* **35,** 146–160.

Low VF, Lin C, Su S, Osanlouy M, Khan M, Safaei S, Maso Talou G, Curtis MA & Mombaerts P (2024). Visualizing the human olfactory projection and ancillary structures in a 3D reconstruction. *Commun Biol* **7,** 1467.

Lowe G & Gold GH (1995). Olfactory transduction is intrinsically noisy. *Proc Natl Acad Sci U S A* **92,** 7864–7868.

Lynch JW & Barry PH (1989). Action potentials initiated by single channels opening in a small neuron (rat olfactory receptor). *Biophysical Journal* **55,** 755–768.

Lynch JW & Barry PH (1991). Properties of transient K+ currents and underlying single K+ channels in rat olfactory receptor neurons. *J Gen Physiol* **97,** 1043–1072.

Ma L, Wu Y, Qiu Q, Scheerer H, Moran A & Yu CR (2014). A Developmental Switch of Axon Targeting in the Continuously Regenerating Mouse Olfactory System. *Science* **344,** 194–197.

Ma M (2007). Encoding olfactory signals via multiple chemosensory systems. *Crit Rev Biochem Mol Biol* **42,** 463–480.

Ma M, Chen WR & Shepherd GM (1999). Electrophysiological characterization of rat and mouse olfactory receptor neurons from an intact epithelial preparation. *Journal of Neuroscience Methods* **92,** 31–40.

Mackay-Sim A & Kittel PW (1991). On the Life Span of Olfactory Receptor Neurons. *Eur J Neurosci* **3,** 209–215.

Madrid R, Sanhueza M, Alvarez O & Bacigalupo J (2003). Tonic and phasic receptor neurons in the vertebrate olfactory epithelium. *Biophys J* **84,** 4167–4181.

Malnic B, Gonzalez-Kristeller DC & Gutiyama LM (2010). Odorant Receptors. In *The Neurobiology of Olfaction*, ed. Menini A, Frontiers in Neuroscience. CRC Press/Taylor & Francis, Boca Raton (FL).

Manzini I, Schild D & Di Natale C (2022). Principles of odor coding in vertebrates and artificial chemosensory systems. *Physiological Reviews* **102,** 61–154.

Marcucci F, Maier-Balough E, Zou D-J & Firestein S (2011). Exuberant growth and synapse formation of olfactory sensory neuron axonal arborizations. *J Comp Neurol* **519,** 3713–3726.

Maresh A, Rodriguez Gil D, Whitman MC & Greer CA (2008). Principles of glomerular organization in the human olfactory bulb--implications for odor processing. *PLoS One* **3,** e2640.

Maue RA & Dionne VE (1987). Patch-clamp studies of isolated mouse olfactory receptor neurons. *J Gen Physiol* **90,** 95–125.

McClintock TS, Khan N, Xie C & Martens JR (2020). Maturation of the Olfactory Sensory Neuron and Its Cilia. *Chem Senses* **45,** 805–822.

Ménache MG, Hanna LM, Gross EA, Lou SR, Zinreich SJ, Leopold DA, Jarabek AM & Miller FJ (1997). Upper respiratory tract surface areas and volumes of laboratory animals and humans: considerations for dosimetry models. *J Toxicol Environ Health* **50,** 475–506.

Menco BP, Birrell GB, Fuller CM, Ezeh PI, Keeton DA & Benos DJ (1998). Ultrastructural localization of amiloride-sensitive sodium channels and Na+,K(+)-ATPase in the rat's olfactory epithelial surface. *Chem Senses* **23,** 137–149.

Menco BP & Jackson JE (1997). Cells resembling hair cells in developing rat olfactory and nasal respiratory epithelia. *Tissue Cell* **29,** 707–713.

Milho R, Frederico B, Efstathiou S & Stevenson PG (2012). A Heparan-Dependent Herpesvirus Targets the Olfactory Neuroepithelium for Host Entry. *PLOS Pathogens* **8,** e1002986.

Miragall F & Graziadei GAM (1982). Experimental studies on the olfactory marker protein. II. Appearance of the olfactory marker protein during differentiation of the olfactory sensory neurons of mouse: an immunohistochemical and autoradiographic study. *Brain Research* **239,** 245–250.

Mombaerts P (2004). Genes and ligands for odorant, vomeronasal and taste receptors. *Nat Rev Neurosci* **5,** 263–278.

Mombaerts P, Wang F, Dulac C, Chao SK, Nemes A, Mendelsohn M, Edmondson J & Axel R (1996). Visualizing an Olfactory Sensory Map. *Cell* **87,** 675–686.

Montani G, Tonelli S, Elsaesser R, Paysan J & Tirindelli R (2006). Neuropeptide Y in the olfactory microvillar cells. *Eur J Neurosci* **24,** 20–24.

Morrison EE & Costanzo RM (1990). Morphology of the human olfactory epithelium. *J Comp Neurol* **297,** 1–13.

Munger SD, Leinders-Zufall T & Zufall F (2009). Subsystem organization of the mammalian sense of smell. *Annu Rev Physiol* **71,** 115–140.

Nagayama S, Homma R & Imamura F (2014). Neuronal organization of olfactory bulb circuits. *Front Neural Circuits* **8,** 98.

Nakamura T & Gold GH (1987). A cyclic nucleotide-gated conductance in olfactory receptor cilia. *Nature* **325,** 442–444.

Nakashima A, Ihara N, Shigeta M, Kiyonari H, Ikegaya Y & Takeuchi H (2019). Structured spike series specify gene expression patterns for olfactory circuit formation. *Science* **365,** eaaw5030.

Nakashima A, Takeuchi H, Imai T, Saito H, Kiyonari H, Abe T, Chen M, Weinstein LS, Yu CR, Storm DR, Nishizumi H & Sakano H (2013). Agonist-Independent GPCR Activity Regulates Anterior-Posterior Targeting of Olfactory Sensory Neurons. *Cell* **154,** 1314.

Nakashima N, Nakashima K, Taura A, Takaku-Nakashima A, Ohmori H & Takano M (2020). Olfactory marker protein directly buffers cAMP to avoid depolarization-induced silencing of olfactory receptor neurons. *Nat Commun* **11,** 2188.

Neureither F, Stowasser N, Frings S & Möhrlen F (2017). Tracking of unfamiliar odors is facilitated by signal amplification through anoctamin 2 chloride channels in mouse olfactory receptor neurons. *Physiol Rep* **5,** e13373.

Nickell MD, Breheny P, Stromberg AJ & McClintock TS (2012). Genomics of Mature and Immature Olfactory Sensory Neurons. *J Comp Neurol* **520,** 2608–2629.

Ono K, Xu S, Hitomi S & Inenaga K (2012). Comparison of the electrophysiological and immunohistochemical properties of acutely dissociated and 1-day cultured rat trigeminal ganglion neurons. *Neurosci Lett* **523,** 162–166.

Pietra G, Dibattista M, Menini A, Reisert J & Boccaccio A (2016). The Ca2+-activated Cl- channel TMEM16B regulates action potential firing and axonal targeting in olfactory sensory neurons. *J Gen Physiol* **148,** 293–311.

Pifferi S (2017). Permeation Mechanisms in the TMEM16B Calcium-Activated Chloride Channels ed. Arreola J. *PLoS ONE* **12,** e0169572.

Pifferi S, Boccaccio A & Menini A (2006). Cyclic nucleotide-gated ion channels in sensory transduction. *FEBS Lett* **580,** 2853–2859.

Pifferi S, Cenedese V & Menini A (2012). Anoctamin 2/TMEM16B: a calcium-activated chloride channel in olfactory transduction: Anoctamin 2/TMEM16B in olfactory transduction. *Experimental Physiology* **97,** 193–199.

Pifferi S, Dibattista M & Menini A (2009). TMEM16B induces chloride currents activated by calcium in mammalian cells. *Pflugers Arch* **458,** 1023–1038.

Pifferi S, Menini A & Kurahashi T (2010). Signal Transduction in Vertebrate Olfactory Cilia. In *The Neurobiology of Olfaction*, ed. Menini A, Frontiers in Neuroscience. CRC Press/Taylor & Francis, Boca Raton (FL).

Potter SM, Zheng C, Koos DS, Feinstein P, Fraser SE & Mombaerts P (2001). Structure and Emergence of Specific Olfactory Glomeruli in the Mouse. *J Neurosci* **21,** 9713–9723.

Rajendra S, Lynch JW & Barry PH (1992). An analysis of Na+ currents in rat olfactory receptor neurons. *Pflugers Arch* **420,** 342–346.

Ranjan R, Logette E, Marani M, Herzog M, Tâche V, Scantamburlo E, Buchillier V & Markram H (2019). A Kinetic Map of the Homomeric Voltage-Gated Potassium Channel (Kv) Family. *Frontiers in Cellular Neuroscience*.

Redolfi N & Lodovichi C (2021). Spontaneous Afferent Activity Carves Olfactory Circuits. *Front Cell Neurosci*.

Reisert J (2010). Origin of basal activity in mammalian olfactory receptor neurons. *The Journal of general physiology* **136,** 529–540.

Reisert J, Lai J, Yau K-W & Bradley J (2005). Mechanism of the excitatory Cl- response in mouse olfactory receptor neurons. *Neuron* **45,** 553–561.

Reisert J, Pifferi S, Guarneri G, Ricci C, Menini A & Dibattista M (2024). The Ca2+-activated Cl− channel TMEM16B shapes the response time course of olfactory sensory neurons. *The Journal of Physiology* **602,** 4889–4905.

Reisert J, Yau K-W & Margolis FL (2007). Olfactory marker protein modulates the cAMP kinetics of the odour-induced response in cilia of mouse olfactory receptor neurons. *The Journal of Physiology* **585,** 731–740.

Ressler KJ, Sullivan SL & Buck LB (1993). A zonal organization of odorant receptor gene expression in the olfactory epithelium. *Cell* **73,** 597–609.

Restrepo D, Okada Y, Teeter JH, Lowry LD, Cowart B & Brand JG (1993*a*). Human olfactory neurons respond to odor stimuli with an increase in cytoplasmic Ca2+. *Biophysical Journal* **64,** 1961–1966.

Restrepo D, Okada Y, Teeter JH, Lowry LD, Cowart B & Brand JG (1993*b*). Human olfactory neurons respond to odor stimuli with an increase in cytoplasmic Ca2+. *Biophys J* **64,** 1961–1966.

Richard MB, Taylor SR & Greer CA (2010). Age-induced disruption of selective olfactory bulb synaptic circuits. *Proceedings of the National Academy of Sciences* **107,** 15613–15618.

Rodolfo-Masera T (1943). Su l'esistenza di un particolare organo olfattivo nel setto nasale della cavia e di altri roditori. *Arch Ital Anat Embryol* **48,** 157–212.

Rodriguez-Gil DJ, Bartel DL, Jaspers AW, Mobley AS, Imamura F & Greer CA (2015). Odorant receptors regulate the final glomerular coalescence of olfactory sensory neuron axons. *Proceedings of the National Academy of Sciences* **112,** 5821–5826.

Rogawski MA (1985). The A-current: how ubiquitous a feature of excitable cells is it? *Trends in Neurosciences* **8,** 214–219.

Rudy B (1988). Diversity and ubiquity of K channels. *Neuroscience* **25,** 729–749.

Rudy B, Chow A, Lau D, Amarillo Y, Ozaita A, Saganich M, Moreno H, Nadal MS, Hernandez-Pineda R, Hernandez-Cruz A, Erisir A, Leonard C & Vega-Saenz de Miera E (1999). Contributions of Kv3 channels to neuronal excitability. *Ann N Y Acad Sci* **868,** 304–343.

Ruiz Tejada Segura ML, Abou Moussa E, Garabello E, Nakahara TS, Makhlouf M, Mathew LS, Wang L, Valle F, Huang SSY, Mainland JD, Caselle M, Osella M, Lorenz S, Reisert J, Logan DW, Malnic B, Scialdone A & Saraiva LR (2022). A 3D transcriptomics atlas of the mouse nose sheds light on the anatomical logic of smell. *Cell Reports* **38,** 110547.

Ryba NJ & Tirindelli R (1995). A novel GTP-binding protein gamma-subunit, G gamma 8, is expressed during neurogenesis in the olfactory and vomeronasal neuroepithelia. *J Biol Chem* **270,** 6757–6767.

Sah P & McLachlan EM (1992). Potassium currents contributing to action potential repolarization and the afterhyperpolarization in rat vagal motoneurons. *J Neurophysiol* **68,** 1834–1841.

Sakano H (2020). Developmental regulation of olfactory circuit formation in mice. *Dev Growth Differ* **62,** 199–213.

Sammeta N, Yu T-T, Bose SC & McClintock TS (2007). Mouse olfactory sensory neurons express 10,000 genes. *J Comp Neurol* **502,** 1138–1156.

Santoro SW & Dulac C (2012). The activity-dependent histone variant H2BE modulates the life span of olfactory neurons. *Elife* **1,** e00070.

Saraiva LR, Ibarra-Soria X, Khan M, Omura M, Scialdone A, Mombaerts P, Marioni JC & Logan DW (2015). Hierarchical deconstruction of mouse olfactory sensory neurons: from whole mucosa to single-cell RNA-seq. *Sci Rep* **5,** 18178.

Saraiva LR, Riveros-McKay F, Mezzavilla M, Abou-Moussa EH, Arayata CJ, Makhlouf M, Trimmer C, Ibarra-Soria X, Khan M, Van Gerven L, Jorissen M, Gibbs M, O'Flynn C, McGrane S, Mombaerts P, Marioni JC, Mainland JD & Logan DW (2019). A transcriptomic atlas of mammalian olfactory mucosae reveals an evolutionary influence on food odor detection in humans. *Sci Adv* **5,** eaax0396.

Schild D & Restrepo D (1998). Transduction mechanisms in vertebrate olfactory receptor cells. *Physiol Rev* **78,** 429–466.

Sharma A, Kumar R, Aier I, Semwal R, Tyagi P & Varadwaj P (2019). Sense of Smell: Structural, Functional, Mechanistic Advancements and Challenges in Human Olfactory Research. *CN* **17,** 891–911.

Song Y, Zhang M, Tao X, Xu Z, Zheng Y, Zhu M, Zhang L, Qiao J & Gao L (2018). Difference of acute dissociation and 1-day culture on the electrophysiological properties of rat dorsal root ganglion neurons. *J Physiol Biochem* **74,** 207–221.

Sonner PM & Stern JE (2007). Functional role of A-type potassium currents in rat presympathetic PVN neurones. *J Physiol* **582,** 1219–1238.

Spigelman I, Zhang L & Carlen PL (1992). Patch-clamp study of postnatal development of CA1 neurons in rat hippocampal slices: membrane excitability and K+ currents. *Journal of Neurophysiology*; DOI: 10.1152/jn.1992.68.1.55.

Stephan AB, Shum EY, Hirsh S, Cygnar KD, Reisert J & Zhao H (2009). ANO2 is the cilial calcium-activated chloride channel that may mediate olfactory amplification. *Proc Natl Acad Sci USA* **106,** 11776–11781.

Stephan AB, Tobochnik S, Dibattista M, Wall CM, Reisert J & Zhao H (2012). The Na+/Ca2+ exchanger NCKX4 governs termination and adaptation of the mammalian olfactory response. *Nat Neurosci* **15,** 131–137.

Su C-Y, Menuz K & Carlson JR (2009). Olfactory Perception: Receptors, Cells, and Circuits. *Cell* **139,** 45–59.

Suzuki Y, Takeda M & Farbman AI (1996). Supporting cells as phagocytes in the olfactory epithelium after bulbectomy. *J Comp Neurol* **376,** 509–517.

Takeuchi H & Sakano H (2014). Neural map formation in the mouse olfactory system. *Cell Mol Life Sci* **71,** 3049–3057.

Tamari K, Takeuchi H, Kobayashi M, Takeuchi K, Kurahashi T & Yamamoto T (2019). Electrical properties of cells from human olfactory epithelium. *Auris Nasus Larynx* **46,** 734–741.

Tan L, Li Q & Xie XS (2015). Olfactory sensory neurons transiently express multiple olfactory receptors during development. *Mol Syst Biol* **11,** 844.

Tirindelli R, Dibattista M, Pifferi S & Menini A (2009). From Pheromones to Behavior. *Physiological Reviews* **89,** 921–956.

Tirindelli R & Ryba NJP (1996). The G-protein γ-subunit Gy8 is Expressed in the Developing Axons of Olfactory and Vomeronasal Neurons. *European Journal of Neuroscience* **8,** 2388–2398.

Tomaru A & Kurahashi T (2005). Mechanisms determining the dynamic range of the bullfrog olfactory receptor cell. *J Neurophysiol* **93,** 1880–1888.

Touhara K & Vosshall LB (2009). Sensing odorants and pheromones with chemosensory receptors. *Annu Rev Physiol* **71,** 307–332.

Traboulsie A, Chemin J, Chevalier M, Quignard J-F, Nargeot J & Lory P (2007). Subunit-specific modulation of T-type calcium channels by zinc. *J Physiol* **578,** 159–171.

Trombley PQ & Westbrook GL (1991). Voltage-gated currents in identified rat olfactory receptor neurons. *J Neurosci* **11,** 435–444.

Trotier D (1986). A patch-clamp analysis of membrane currents in salamander olfactory receptor cells. *Pflugers Arch* **407,** 589–595.

Vassar R, Ngai J & Axel R (1993). Spatial segregation of odorant receptor expression in the mammalian olfactory epithelium. *Cell* **74,** 309–318.

Verhaagen J, Oestreicher AB, Gispen WH & Margolis FL (1989). The expression of the growth associated protein B50/GAP43 in the olfactory system of neonatal and adult rats. *J Neurosci* **9,** 683–691.

Vogalis F, Hegg CC & Lucero MT (2005). Ionic conductances in sustentacular cells of the mouse olfactory epithelium. *J Physiol* **562,** 785–799.

Wang J, Ou S-W & Wang Y-J (2017). Distribution and function of voltage-gated sodium channels in the nervous system. *Channels* **11,** 534–554.

Watt WC, Sakano H, Lee Z-Y, Reusch JE, Trinh K & Storm DR (2004). Odorant stimulation enhances survival of olfactory sensory neurons via MAPK and CREB. *Neuron* **41,** 955–967.

Weiss J, Pyrski M, Jacobi E, Bufe B, Willnecker V, Schick B, Zizzari P, Gossage SJ, Greer CA, Leinders-Zufall T, Woods CG, Wood JN & Zufall F (2011). Loss-of-function mutations in sodium channel Nav1.7 cause anosmia. *Nature* **472,** 186–190.

Weiss L, Jungblut LD, Pozzi AG, Zielinski BS, O'Connell LA, Hassenklöver T & Manzini I (2020). Multi-glomerular projection of single olfactory receptor neurons is conserved among amphibians. *J Comp Neurol* **528,** 2239–2253.

Weng Y, Zapiec B, Paredes R & Mombaerts P (2025). Glomeruli of the Mouse Olfactory Bulb: Numbers, Sizes, Shapes. *Eur J Neurosci* **62,** e70327.

Xiao Y, Yang J, Ji W, He Q, Mao L & Shu Y (2021). A- and D-type potassium currents regulate axonal action potential repolarization in midbrain dopamine neurons. *Neuropharmacology* **185,** 108399.

Young JM, Friedman C, Williams EM, Ross JA, Tonnes-Priddy L & Trask BJ (2002). Different evolutionary processes shaped the mouse and human olfactory receptor gene families. *Hum Mol Genet* **11,** 535–546.

Yu CR, Power J, Barnea G, O'Donnell S, Brown HEV, Osborne J, Axel R & Gogos JA (2004). Spontaneous neural activity is required for the establishment and maintenance of the olfactory sensory map. *Neuron* **42,** 553–566.

Yu FH & Catterall WA (2003). Overview of the voltage-gated sodium channel family. *Genome Biology* **4,** 207.

Yu FH, Westenbroek RE, Silos-Santiago I, McCormick KA, Lawson D, Ge P, Ferriera H, Lilly J, DiStefano PS, Catterall WA, Scheuer T & Curtis R (2003). Sodium Channel β4, a New Disulfide-Linked Auxiliary Subunit with Similarity to β2. *The Journal of Neuroscience* **23,** 7577.

Yusuf N & Monahan K (2024). Epigenetic programming of stochastic olfactory receptor choice. *Genesis* **62,** e23593.

Zak JD, Grimaud J, Li R-C, Lin C-C & Murthy VN (2018). Calcium-activated chloride channels clamp odor-evoked spike activity in olfactory receptor neurons. *Sci Rep* **8,** 10600.

Zapiec B & Mombaerts P (2020). The Zonal Organization of Odorant Receptor Gene Choice in the Main Olfactory Epithelium of the Mouse. *Cell Reports* **30,** 4220-4234.e5.

Zhao J, O'Leary ME & Chahine M (2011). Regulation of Nav1.6 and Nav1.8 peripheral nerve Na+ channels by auxiliary β-subunits. *J Neurophysiol* **106,** 608–619.

Zufall F, Firestein S & Shepherd GM (1994). Cyclic nucleotide-gated ion channels and sensory transduction in olfactory receptor neurons. *Annu Rev Biophys Biomol Struct* **23,** 577–607.

Zufall F, Stengl M, Franke C, Hildebrand JG & Hatt H (1991). Ionic currents of cultured olfactory receptor neurons from antennae of male Manduca sexta. *J Neurosci* **11,** 956–965.

Zybura AS, Baucum AJ, Rush AM, Cummins TR & Hudmon A (2020). CaMKII enhances voltage-gated sodium channel Nav1.6 activity and neuronal excitability. *J Biol Chem* **295,** 11845–11865.